

THE ASTROPHYSICAL JOURNAL

An International Review of Spectroscopy and
Astronomical Physics

FOUNDED IN 1895 BY GEORGE E. HALE AND JAMES E. KEELER

EDITORS

W. W. MORGAN
Managing Editor

Yerkes Observatory of the University of Chicago

S. CHANDRASEKHAR

PAUL W. MERRILL
Mount Wilson Observatory of the
Carnegie Institution of Washington

HARLOW SHAPLEY
Harvard College Observatory
Cambridge, Massachusetts

N. U. MAYALL
Lick Observatory
University of California

With the Collaboration of the American Astronomical Society

COLLABORATING EDITORS

CECILIA H. PAYNE-GAPOSCHKIN, *Harvard College Observatory*; H. N. RUSSELL, *Princeton University*;
ANDREW MCKELLAR, *Dominion Astrophysical Observatory, Victoria*; C. S. BEALS, *Dominion
Astrophysical Observatory, Victoria*; LUIS E. ERRO, *Astrophysical Observatory, Tonan-
zintla*; O. C. WILSON, *Mount Wilson Observatory*; LYMAN SPITZER, JR., *Princeton
University Observatory*; A. N. VYSOTSKY, *Leander McCormick Observ-
atory*; ALBERT E. WHITFORD, *Washburn Observatory*

VOLUME 107

JANUARY-MAY 1948



THE UNIVERSITY OF CHICAGO PRESS
CHICAGO, ILLINOIS

CAMBRIDGE UNIVERSITY PRESS, LONDON

PUBLISHED JANUARY, MARCH, MAY, 1948

COMPOSED AND PRINTED BY THE UNIVERSITY OF CHICAGO PRESS
CHICAGO, ILLINOIS, U.S.A.

7A.

ON
TH
A T
ON
A F
SUN
Fe
SPE
T
NOT
A
N
T
T
T
A
REV
ANAL
an
RAD
THE
W
SPECT
ON TH
ON TH
an
SCATT
THE S

Astron. Obs.
Shaker

Astronomical
Observations

Q.B.

.A859

CONTENTS

NUMBER 1

ON NOISE ARISING FROM THE SOLAR GRANULATION. Martin Schwarzschild	1
THE TEMPERATURE OF INTERSTELLAR MATTER. I. Lyman Spitzer, Jr.	6
A THEORETICAL DISCUSSION OF THE ULTIMATE LIMITS OF ASTRONOMICAL PHOTOELECTRIC PHOTOMETERS. Harold L. Johnson	34
ON THE RADIATIVE EQUILIBRIUM OF A STELLAR ATMOSPHERE. XXII. S. Chandrasekhar	48
A PHOTOELECTRIC GUIDER FOR ASTRONOMICAL TELESCOPES. Horace W. Babcock	73
SUNSPOT GROUPS OF IRREGULAR MAGNETIC POLARITY. Robert S. Richardson	78
Fe II EMISSION LINES IN α HERCULIS AND α SCORPII. G. Herzberg	94
SPECTROGRAPHIC OBSERVATIONS OF THE ECLIPSING BINARIES OF THE W URSAE MAJORIS TYPE: AH VIRGINIS AND TZ BOOTIS. Y. C. Chang	96

NOTES

AN EXTENSION OF THE INTERSTELLAR ABSORPTION-CURVE. A. E. Whitford	102
NOVAE AND PLANETARY NEBULAE. R. Minkowski	106
THE PARALLAX OF SS CYGNI. K. Aa. Strand	106
THE CLASSIFICATION OF THE "METALLIC-LINE" STARS. Nancy G. Roman, W. W. Mor- gan, and Olin J. Eggen	107
THE HIGHER MEMBERS OF THE ($2^3P^0-n^3D$) SERIES OF He I IN THE SPECTRUM OF 55 CYGNI. O. Struve and H. Chun	109
ASTROPHYSICAL EVIDENCE FOR THE PROBABILITY OF A NUCLEAR REACTION. E. Schatz- man	110
REVIEWS	112

NUMBER 2

ANALYSIS OF THE MILKY WAY IN NORTHERN CASSIOPEIA AND CEPHEUS. Elaine Nantkes and Robert H. Baker	113
RADIAL VELOCITIES OF 204 STARS IN THE REGION OF THE HYADES. Ralph E. Wilson	119
THE STRUCTURE OF THE ATMOSPHERE OF THE K-TYPE COMPONENT OF ZETA AURIGAE. O. C. Wilson	126
SPECTROPHOTOMETRY OF THE F STARS AND OF τ URSAE MAJORIS. I. Jesse L. Greenstein	151
ON THE RADIATIVE EQUILIBRIUM OF A STELLAR ATMOSPHERE. XXII. S. Chandrasekhar	188
ON THE RADIATIVE EQUILIBRIUM OF A STELLAR ATMOSPHERE. XXIII. S. Chandrasekhar and Frances H. Breen	216
SCATTERING IN A PLANETARY ATMOSPHERE. H. C. van de Hulst	220
THE SCHUSTER PROBLEM FOR AN EXTENDED ATMOSPHERE. Anne B. Underhill	247

THE EFFECT OF NONGRAYNESS ON THE TEMPERATURE DISTRIBUTION OF THE SOLAR ATMOSPHERE. Guido Münch	265
COLOR INDICES OF PROPER-MOTION STARS. W. J. Luyten and P. D. Jose	269
NOTES	
THE VELOCITY-CURVE OF THE CLUSTER-TYPE VARIABLE UY BOOTIS. A. Virginia Farquhar	276
THE METHOD OF "COLOR-DIFFERENCE." W. Becker	278

NUMBER 3

SPECTROPHOTOMETRY OF THE WOLF-RAYET STAR HD 45166. F. J. Neubauer and Lawrence H. Aller	281
THE ULTRAVIOLET SOLAR SPECTRUM, $\lambda\lambda$ 2935-3060. Harold D. Babcock, Charlotte E. Moore, and Mary F. Coffeen	287
WAVE LENGTHS OF ATOMIC ABSORPTION LINES IN THE SPECTRA OF LONG-PERIOD VARIABLE STARS. Paul W. Merrill	303
THE SPECTRUM OF Z ANDROMEDAE IN 1946 AND 1947. Paul W. Merrill	317
J. S. PLASKETT'S STAR OF LARGE MASS, HD 47129. Otto Struve	327
THE SPECTRUM OF γ PEGASI. Anne B. Underhill	337
THE INTENSITIES AND PROFILES OF LINES IN SOME B-TYPE STARS. Anne B. Underhill	349
A POLARIGRAPHIC STUDY OF THE REFLECTION NEBULA NGC 6729. Walter T. Whitney and Edwin B. Weston	371
STARS IN DIFFUSE NEBULAE. Jesse L. Greenstein	375
SOME f -VALUES FOR IONIZED OXYGEN AND IONIZED SILICON. D. R. Bates and Agnete Damgaard	383
VIBRATIONAL ENERGY LEVELS OF THE CARBON DIOXIDE MOLECULE. Robert C. Herman	386
A NEW BAND SYSTEM OF THE C_2 MOLECULE. John G. Phillips	389
METHANE IN THE EARTH'S ATMOSPHERE. Marcel V. Migeotte	400
ANHARMONIC PULSATIONS OF THE CEPHEID VARIABLE. H. K. Sen	404
NOTES	
NOTE ON THE PECULIAR SPECTRUM OF HD 25878. W. P. Bidelman	413
LIGHT-CURVE OF A NEW VARIABLE OF R CORONAE BOREALIS TYPE. Chang Yuin	413
REPLY TO D. TER HAAR'S REMARKS ON MY PAPER, "THE PHYSICS OF COSMIC GRAINS." F. Cernuschi	417
A FAINT S-TYPE STAR IN THE CLEAR REGION IN CYGNUS. J. J. Nassau and G. B. van Albada	418
A NEW BAND IN THE INFRARED SPECTRA OF S-TYPE STARS. J. J. Nassau and G. B. van Albada	418
ON THE OCCURRENCE OF LANTHANUM OXIDE IN S-TYPE STARS. Philip C. Keenan	420
NOTICE CONCERNING Be STARS. Paul W. Merrill and Cora G. Burwell	421
REVIEWS	422
INDEX	425

VOLUME 107

MAR 9 1948

NUMBER 1

THE ASTROPHYSICAL JOURNAL

AN INTERNATIONAL REVIEW OF SPECTROSCOPY
AND ASTRONOMICAL PHYSICS

Founded in 1895 by GEORGE E. HALE and JAMES E. KEELER

Edited by

W. W. MORGAN

Managing Editor

Yerkes Observatory of the University of Chicago

S. CHANDRASEKHAR

PAUL W. MERRILL

Mount Wilson Observatory of the
Carnegie Institution of Washington

HARLOW SHAPLEY

Harvard College Observatory
Cambridge, Massachusetts

N. U. MAYALL

Lick Observatory
University of California

JANUARY 1948

ON NOISE ARISING FROM THE SOLAR GRANULATION . . .	<i>Martin Schwarzschild</i>	1
THE TEMPERATURE OF INTERSTELLAR MATTER. I . . .	<i>Lyman Spitzer, Jr.</i>	6
A THEORETICAL DISCUSSION OF THE ULTIMATE LIMITS OF ASTRONOMICAL PHOTOELECTRIC PHOTOMETERS . . .	<i>Harold L. Johnson</i>	34
ON THE RADIATIVE EQUILIBRIUM OF A STELLAR ATMOSPHERE. XXII . . .	<i>S. Chandrasekhar</i>	48
A PHOTOELECTRIC GUIDER FOR ASTRONOMICAL TELESCOPES . . .	<i>Herbert W. Belloc</i>	73
SUNSPOT GROUPS OF IRREGULAR MAGNETIC POLARITY . . .	<i>Robert S. Richardson</i>	78
F_{12} EMISSION LINES IN α HERCULIS AND α SCORPII . . .	<i>G. Herzberg</i>	94
SPECTROGRAPHIC OBSERVATIONS OF THE ECLIPSING BINARIES OF THE W URSAE MAJORIS TYPE: AH VIRGINIS AND TZ BOOTIS . . .	<i>T. C. Chang</i>	96
NOTES		
AN EXTENSION OF THE INTERSTELLAR ABSORPTION-CURVE . . .	<i>A. E. Whitford</i>	102
NOVAE AND PLANETARY NEBULAE . . .	<i>R. Minkowski</i>	106
THE PARALLAX OF SS CYGNI . . .	<i>E. An. Svanidze</i>	106
THE CLASSIFICATION OF THE "METALLIC-LINE" STARS . . .	<i>Nancy G. Roman, W. W. Morgan, and Otto J. Eggen</i>	107
THE HIGHER MEMBERS OF THE ($2P^{\circ}$ - $n^{\circ}D$) SERIES OF He I IN THE SPECTRUM OF 55 CYGNI . . .	<i>O. Struve and H. Chen</i>	109
ASTROPHYSICAL EVIDENCE FOR THE PROBABILITY OF A NUCLEAR REACTION . . .	<i>E. Salpeter</i>	110
REVIEWS . . .		112

THE UNIVERSITY OF CHICAGO PRESS
CHICAGO, ILLINOIS, U.S.A.

THE ASTROPHYSICAL JOURNAL

AN INTERNATIONAL REVIEW OF SPECTROSCOPY
AND ASTRONOMICAL PHYSICS

Edited by

W. W. MORGAN

Managing Editor

Yerkes Observatory of the University of Chicago

S. CHANDRASEKHAR

PAUL W. MERRILL

Mount Wilson Observatory of the
Carnegie Institution of Washington

HARLOW SHAPLEY

Harvard College Observatory
Cambridge, Massachusetts

N. U. MAYALL

Lick Observatory
University of California

With the Collaboration of the American Astronomical Society

Collaborating Editors:

1946-48

C. S. BEALS
Dominion Astrophysical Observa-
tory, Victoria

LUIS E. ERRO
Astrophysical Observatory,
Tonantzinla

O. C. WILSON
Mount Wilson Observatory

1947-49

LYMAN SPITZER, JR.
Princeton University Observatory

A. N. VYSSOTSKY
Leander McCormick Observatory

ALBERT E. WHITFORD
Washburn Observatory

1948-50

CECILIA H. PAYNE-GAPOSCHKIN
Harvard College Observatory

H. N. RUSSELL
Princeton University

ANDREW McKELLAR
Dominion Astrophysical Observa-
tory, Victoria

The Astrophysical Journal is published bimonthly by the University of Chicago at the University of Chicago Press, 5750 Ellis Avenue, Chicago, Illinois, during July, September, November, January, March, and May. The subscription price is \$12.00 a year; the price of single copies is \$3.00. Orders for service of less than a full year will be charged at the single-copy rate. Postage is prepaid by the publishers on all orders from the United States and its possessions, Argentina, Bolivia, Brazil, Chile, Colombia, Costa Rica, Cuba, Dominican Republic, Ecuador, Guatemala, Haiti, Republic of Honduras, Mexico, Morocco (Spanish Zone), Nicaragua, Panama, Paraguay, Peru, Rio de Oro, El Salvador, Spain (including Balearic Islands, Canary Islands, and the Spanish Offices in Northern Africa; Andorra), Spanish Guinea, Uruguay, and Venezuela. Postage is charged extra as follows: for Canada and Newfoundland, 42 cents on annual subscriptions (total \$12.42); on single copies, 7 cents (total \$3.07); for all other countries in the Postal Union, 96 cents on annual subscriptions (total \$12.96), on single copies 16 cents (total \$3.16). Patrons are requested to make all remittances payable to The University of Chicago Press, in United States currency or its equivalent by postal or express money orders or bank drafts.

The following are authorized agents:

For the British Empire, except North America, India, and Australasia: The Cambridge University Press, Bentley House, 200 Euston Road, London, N.W. 1, England. Prices of yearly subscriptions and of single copies may be had on application.

Claims for missing numbers should be made within the month following the regular month of publication. The publishers expect to supply missing numbers free only when losses have been sustained in transit, and when the reserve stock will permit.

Business correspondence should be addressed to The University of Chicago Press, Chicago 37, Illinois.

Communications for the editors and manuscripts should be addressed to: W. W. Morgan, Editor of THE ASTROPHYSICAL JOURNAL, Yerkes Observatory, Williams Bay, Wisconsin.

Line drawings and photographs should be made by the author, and all marginal notes such as co-ordinates, wave lengths, etc., should be included in the cuts. It will not be possible to set up such material in type.

One copy of the corrected galley proof should be returned as soon as possible to the editor, Yerkes Observatory, Williams Bay, Wisconsin. Authors should take notice that the manuscript will not be sent to them with the proof.

The cable address is "Observatory, Williamsbay, Wisconsin."

The articles in this journal are indexed in the *International Index to Periodicals*, New York, N.Y.

Applications for permission to quote from this journal should be addressed to: The University of Chicago Press, and will be freely granted.

Entered as second-class matter, July 21, 1940, at the Post-Office at Chicago, Ill., under the act of March 3, 1879. Acceptance for mailing at special rate of postage provided for in United States Postal Act of October 3, 1917, Section 1103, amended February 26, 1945.

[PRINTED
IN U.S.A.]

THE ASTROPHYSICAL JOURNAL

AN INTERNATIONAL REVIEW OF SPECTROSCOPY AND
ASTRONOMICAL PHYSICS

VOLUME 107

JANUARY 1948

NUMBER 1

ON NOISE ARISING FROM THE SOLAR GRANULATION

MARTIN SCHWARZSCHILD

Princeton University Observatory

Received September 15, 1947

ABSTRACT

It is shown that the mechanism which maintains the high temperature of the corona may consist of a stream of acoustical noise which is produced by the granulation and which transports mechanical energy into the corona.

I. ENERGY BALANCE IN THE CORONA

Until recently the main problem of the chromosphere and the corona was the question of their support. When for these outer layers of the solar atmosphere a temperature was assumed similar to that of the photosphere, it was found that the gas pressure was insufficient to explain the low density gradient and the large extent observed. Recently, however, it was found that the temperature of the chromosphere is of the order of $35,000^\circ$ and that of the corona of the order of $1,000,000^\circ$. These values were determined from the observed particle velocities,¹ further, from the high degree of ionization,² and, finally, from the radiation intensity in the 10-meter region.³ If these temperature values are introduced into the hydrostatic equation, the gas pressure is seen to be fully adequate to produce the low observed density gradients.⁴ Now, therefore, the main problem of the chromosphere and the corona (here considered as a unit and called "corona") has become the question of how the high temperature of the corona is maintained.

To maintain this temperature, the heat loss suffered by the corona has to be compensated for. Recently, the rate of this heat loss has been estimated by Biermann and ten Bruggencate.⁵ The process they find mainly responsible is the emission produced by

¹ For chromosphere: R. O. Redman, *M.N.*, **102**, 140, 1942; for corona: W. Grotrian, *Zs. f. Ap.*, **3**, 199, 1931.

² For chromosphere: Cillié and Menzel, *Harvard Circ.* 410, 1935; for corona: B. Edlén, *Zs. f. Ap.*, **22**, 62, 1943.

³ E. G. Bowen, cited by J. L. Greenstein, *Observatory*, **67**, 23, 1947.

⁴ For chromosphere: R. Wildt, *Ap. J.*, **105**, 36, 1946; for corona: Biermann and ten Bruggencate, *Göttingen Veröff.*, Vol. **83**, 1947. The temperatures given in the last paper referred to are reliable only until about $r = 1.5R$. Farther out, the temperatures have to be appreciably reduced, if one applies the corrections to the coronal density given by H. C. van de Hulst, *Ap. J.*, **105**, 487, 1947.

⁵ *Op. cit.*

free-free transitions of electrons in the fields of protons. For this process they obtain from Cillié's⁶ formula, with the help of Baumbach's⁷ densities, 10^3 ergs/sec per square centimeter of the photospheric surface. This gives for the rate of heat loss of the whole corona,

$$L_{\text{corona}} = 6 \times 10^{25} \text{ ergs/sec.}$$

(This energy flow is approximately one hundred times smaller than the observed brightness of the corona. The observed brightness, however, arises mostly from electron scattering, a process which does not enter into the heat balance of the corona.)

The mechanism which maintains the high temperature of the corona has to fulfil two conditions: first, it has to provide energy at a rate equal to that of the heat loss of the corona, and, second, it has to provide this energy in such a form that it can be delivered to the material of the corona at its high temperature.

In the following paragraphs a mechanism will be discussed for the heat supply of the corona consisting of a steady stream of acoustical waves which, first, originates in the turbulent motions of the granules, second, transports mechanical energy through the photospheric layers, and, lastly, dissipates its energy in the corona.

II. KINETIC ENERGY OF THE GRANULATION

The basic energy source of the mechanism here considered is the kinetic energy of the granules. In estimating the strength of this source, the following approximate data may be used:

Mean diameter of a rising granule:⁸ $d = 1000 \text{ km}$,

Mean velocity of rising granules:⁹ $v = 1 \text{ km/sec}$,

Mean density at top of convective zone:¹⁰ $\rho = 10^{-7}$,

Average lifetime of a granule:¹¹ $t = 200 \text{ sec}$,

Total number of granules at any one time:¹² $N = 10^6$.

These data correspond to a flow pattern for the convection at the upper boundary of the turbulent zone, in which approximately one-tenth of the surface is occupied by rising elements and the remaining nine-tenths are covered by slowly sinking material.

From these data the kinetic energy of one rising granule is found to be

$$E = \frac{\rho}{2} \frac{\pi}{6} d^3 v^2 = 2 \times 10^{26} \text{ ergs.}$$

From this, one obtains for the total kinetic energy which is brought up by the granules to the top of the convection zone each second,

$$L_{\text{granules}} = \frac{NE}{t} = 10^{30} \text{ ergs/sec.}$$

⁶ *M.N.*, **92**, 830, 1932.

⁷ *A.N.*, **263**, 121, 1937.

⁸ P. C. Keenan, *Ap. J.*, **88**, 360, 1938; ten Bruggencate and H. Müller, *Zs. f. Ap.*, **21**, 198, 1942.

⁹ A. Unsöld, *Physik der Sternatmosphären* (1938), p. 384.

¹⁰ B. Strömgren, *Festschrift für E. Strömgren* (1940), p. 218.

¹¹ Ten Bruggencate and W. Grotian, *Zs. f. Ap.*, **12**, 323, 1936.

¹² Keenan, *op. cit.*

The comparison of L_{granules} with L_{corona} as given in the first section shows that the basic energy source here considered is amply sufficient to cover the needs of the corona.

Since the convection of the granules does not occur in the form of semistationary cells but rather in the form of short-lived elements, it seems unlikely that the photospheric layers just above the convection zone could be in an unperturbed state. The perturbations transmitted by the granules into the layers above may, at least in part, take the form of acoustic waves. An upper limit to the energy transported by these waves may be obtained with the help of the following estimates. The material velocity, w , in a wave should be at most as large as the velocity of the rising granules; hence as an upper limit for the mean material velocity one may take

$$\bar{w} < \frac{1}{2} \text{ km/sec.}$$

Further, the sound velocity of isothermal waves in the photospheric layers is

$$V = \sqrt{\frac{R}{m} T} = 7 \text{ km/sec.}$$

From this we obtain for the energy transport in a wave,

$$F = \rho \bar{w}^2 V < 2 \times 10^8 \text{ ergs/sec/cm}^2.$$

Since at any one moment only one-tenth of the solar surface is occupied by rising granules and since only this surface fraction can act as a source of perturbations, we find as the upper limit for the energy transport of the stream of noise,

$$L_{\text{noise}} < F \frac{4\pi R^2}{10} < 10^{30} \text{ ergs/sec.}$$

Because this upper limit for L_{noise} comes out to be identical with L_{granules} , it follows that the maximum assumptions for the noise would correspond to a state in which the entire kinetic energy of the granules is transformed into noise energy.

Actually, however, the energy transport of the noise may be well below the above upper limit for the following reasons: (a) the mean material velocity, \bar{w} , produced by the motion of the granules may easily be as low as 0.1 km/sec;¹³ (b) a granule may be effective as a source of perturbations for only a fraction of its lifetime, so that, at any moment, appreciably less than one-tenth of the solar surface gives rise to perturbations; (c) a sizable component of the energy transport of the noise may be deflected into horizontal directions and hence not reach beyond the photospheric layers; and (d) the portion of the noise that is of low frequencies may be reflected back by the steep photospheric density gradient. However, in spite of these reducing factors, since there is a large safety factor available in the basic energy source, it appears likely that the energy stream in the noise produced by the turbulence of the granulation is sufficient in size to offset the heat loss of the corona.

III. ACOUSTICAL TRANSPORT OF THE ENERGY

Before the flow of the noise through the photospheric layers and into the corona can be investigated, the following crude consideration of the dissipation of the noise energy is necessary. If in an individual wave the material velocity, w , is much smaller than the

¹³ As far as the noise emission is concerned, one might consider a granule as equivalent to a vibrating solid sphere in a homogeneous compressible gas. Then, for the fraction of the kinetic energy of the granule emitted upward in the form of a wave during the time of retardation, one finds 1–30 per cent, depending on the exact ratio of the diameter of the granule to the wave length emitted (see H. Lamb, *The Dynamical Theory of Sound* [London, 1910], p. 228).

sound velocity, V , the dissipation of the wave energy may be negligible; however, if w is comparable to V , the dissipation may be rapid. (This will be particularly so if the dissipation process involves a degeneration of the wave into a shock wave.) We may then introduce for \bar{w} , the mean material velocity in the noise, a critical value defined by

$$\bar{w}_{\text{crit}}^2 = \beta V^2 = \beta \frac{k}{m} T,$$

where β is a fraction, say 0.1. If \bar{w} is smaller than this critical value, virtually none of the individual waves will suffer dissipation. However, if \bar{w} reaches the critical value, the strongest of the individual waves will be rapidly dissipated, and the energy transport of the noise as a whole will decrease.

An immediate consequence of the foregoing critical upper limit for the velocities in the noise is that these velocities will be in no layer dynamically important and, hence, that in the presence of the noise the ordinary hydrostatic equation may still be used.

Now the flow of the noise through the photospheric layers may be considered. At the top of the granulation, \bar{w} may be approximately 0.1 km/sec, whereas V there is 7 km/sec; therefore, the noise is well below the critical value and will proceed essentially without dissipation through the next layers above. The temperature in these layers will not be affected by the noise and consequently will stay approximately constant, while the density will decrease upward according to the hydrostatic law. Since the noise is not dissipated in these layers, its energy transport, F (with $F = \rho \bar{w}^2 V$), must remain constant; hence, to offset the decrease of the density ρ , the mean material velocity \bar{w} will increase throughout these layers. Finally, at a particular place, here called the "base of the corona," \bar{w} will reach the critical limit (approximately 2 km/sec corresponding to the photospheric temperature) beyond which the dissipation will start. Thus, from the top of the granulation to the base of the corona, \bar{w} increases by a factor of about 20, and therefore ρ decreases by a factor of 400. From the hydrostatic equation one finds that such a density drop occurs over a distance of about 800 km. Since this thick layer between the top of the granulation and the base of the corona will include the entire photospheric layers, it follows that the noise passes through the photosphere without any dynamic or thermodynamic effect on this layer. The absence of such effects is in agreement with observations.

In following the noise, finally, into the corona, one cannot derive theoretically the temperature reached in the corona as long as the rate of dissipation of the noise has not been investigated. However, if the maximum value for the temperature in the corona is taken from observation, we may estimate the steepness of the temperature increase in the lowest part of the corona as follows: In the corona the energy of the noise is transformed into heat energy. For the noise, this transformation has the consequence that the energy transport will decrease outward. It may be approximated by

$$F = \rho \bar{w}^2 V \propto \frac{1}{x^a} \quad \text{with} \quad x = \frac{R+h}{R},$$

where h is the height above the base of the corona and a is an unknown constant. For the temperature of the corona, the energy transformation has the consequence that at any place the temperature has a value close to that given by the critical relation for \bar{w} above. If, namely, at a particular point the temperature was well above this value, virtually no noise energy would be dissipated into heat, and the temperature would drop. On the other hand, if the temperature was too low, most of the noise energy would be dissipated right in this layer, and the temperature would rise. Therefore, the critical relation between \bar{w} and T may be taken to hold approximately throughout the lower part of the corona. If this relation is used to eliminate \bar{w} from the above fall-off law for F and if,

further, this law is introduced into the hydrostatic equation for the elimination of ρ , a differential equation for the temperature as a function of the height is obtained. The solution of this equation is found to be

$$T = \frac{2}{2\alpha - 1} \frac{GM}{R} \frac{m}{k} \left(\frac{1}{x} - \frac{1}{x^{2\alpha}} \right) + T_0 \frac{1}{x^{2\alpha}},$$

where T_0 is the temperature at the base of the corona. This solution gives a temperature maximum at

$$x = (2\alpha)^{1/2\alpha - 1},$$

with

$$T_{\max} = \frac{1}{\alpha} \frac{GM}{R} \frac{m}{k} = \frac{1.6 \cdot 10^7}{\alpha x},$$

where the molecular weight is taken to be 0.7. If the temperature maximum is to agree with the observational value of approximately $1,000,000^\circ$, then α has to be approximately 10. With this value for α , one finds from the above solution that $T = 35,000^\circ$ at $x = 1.001$, i.e., $h = 700$ km; and $T = 1,000,000^\circ$ at $x = 1.05$, i.e., $h = 35,000$ km. The steepness of the temperature increase in the lowest layers of the corona as represented by the two heights just computed is, in order of magnitude, in agreement with observations.⁴

IV. CONCLUSIONS

From the foregoing estimates the following conclusions can be drawn:

a) The flow of kinetic energy carried by the granules may be amply sufficient to provide the heat necessary for maintaining the high temperatures in the chromosphere and corona even if the stream of acoustical waves produced by the granules will carry only a small fraction of the energy of the granules into the higher layers.

b) The stream of noise produced by the granules will transport its mechanical energy across the photospheric layers without affecting the dynamical and thermodynamical equilibrium in this region, but the energy of the noise may be dissipated in the chromosphere and corona, thus acting as the heat source for these layers.

I should like to thank Dr. R. Wildt very much for the helpful discussions with him on the subject of this paper.

NOTE ADDED IN PROOF.—Recently a reprint was received of a paper by L. Biermann (*Naturwiss.*, **33**, 118, 1946) in which he discusses a mechanism for the heating of the chromosphere very similar to the mechanism here discussed for the heating of the entire corona.

THE TEMPERATURE OF INTERSTELLAR MATTER. I

LYMAN SPITZER, JR.

Yale University*

Received June 30, 1947

ABSTRACT

The processes which tend to increase the equilibrium kinetic temperature of interstellar matter are considered in detail. The equations for the energy gained by photoelectric ionization of H and other atoms, by the photodetachment of electrons from H^- , and by photoelectric emission from solid grains are put into a form suitable for numerical computation. Since the electrical charge on the grains enters into the problem, the various physical processes, such as the sticking probability of electrons, which determine the magnitude of the charge on a grain, are also discussed, and the quantitative physical information available on these processes is summarized. The kinetic energy transferred from cosmic rays to the much-less-energetic atoms and grains is treated briefly. The processes which tend to decrease the equilibrium kinetic temperature and the final equilibrium temperatures to be expected will be discussed in a subsequent paper.

Since thermodynamic equilibrium is not even remotely attained in interstellar space, there is no uniquely defined temperature which characterizes interstellar matter. It was pointed out by Eddington,¹ however, that the frequent elastic encounters between the interstellar particles would establish a Maxwellian velocity distribution, with equipartition of kinetic energy among the various interstellar atoms. Interactions between the atoms and the small solid grains² responsible for the extinction of starlight will bring³ the kinetic energy of the grains also into equipartition with the energy of the interstellar particles. The specific deviations from the Maxwellian distribution which may be expected have recently been investigated quantitatively.⁴ A numerical application of these general results shows that in interstellar space, as well as in the somewhat denser nebulae, such deviations are wholly negligible. Thus the distribution of particle velocities corresponds very closely to the distribution in thermodynamic equilibrium at some particular temperature, which may be called the "interstellar kinetic temperature."

The classic discussion of interstellar temperature is due to Eddington.^{1,5} He pointed out that electrons, when ejected from an atom by photoionization, have an average kinetic energy corresponding to the color temperature of the ionizing radiation—about $10,000^\circ$ – $20,000^\circ$ for the ultraviolet radiation capable of ionizing the atoms present. Since free-free transitions of electrons in the fields of the positive ions reduce the electron energy, a value of $10,000^\circ$ was suggested by Eddington as the kinetic temperature of interstellar matter.

A somewhat different result was obtained by Rosseland,⁶ who found that the kinetic temperature of an interstellar medium composed entirely of hydrogen was a smaller fraction—about one-sixth—of the color temperature of the exciting radiation. This result

* Now at the Princeton University Observatory, Princeton, N.J.

¹ *Proc. Roy. Soc. A*, **111**, 424, 1926 (Bakerian Lecture).

² In accordance with discussions among several workers in the field, the solid interstellar particles are referred to as "grains"; the terms "dust" and "smoke," which imply a certain type of origin for the interstellar grains, are not used here, but are reserved for discussions of the evolution of solid particles.

³ L. Spitzer, Jr., *Ap. J.*, **93**, 369, 1941.

⁴ D. Bohm and L. H. Aller, *Ap. J.*, **105**, 131, 1947.

⁵ *Internal Constitution of the Stars* (Cambridge: At the University Press, 1926), p. 371.

⁶ *Theoretical Astrophysics* (New York: Clarendon Press, 1936), p. 321.

depends in part on the assumption that the radiation emitted by the interstellar gas at each frequency may be found from Kirchhoff's law and is thus equal to the absorption coefficient at that frequency multiplied by the Planck function for black-body radiation at the kinetic temperature. While this assumption is justified in thermodynamic equilibrium, its validity in interstellar space is open to serious question. In particular, as compared with thermodynamic equilibrium, the ground state of an atom in interstellar space is enormously overpopulated relative to the ionized state. The absorption coefficient at frequencies beyond the ionization limit is proportional to the number of these neutral atoms, while the emission is proportional to the number of the ionized atoms and electrons. It follows that the intensity of radiation emitted by captures in the ground state is enormously less than that found from Kirchhoff's law. One may conclude that Rosseland's analysis is not directly relevant to the exact determination of interstellar kinetic temperatures.

In accordance with Eddington's results, a kinetic temperature of about $10,000^\circ$ has usually been assumed in most of the subsequent theoretical work on interstellar matter. The importance of this temperature is evidenced by the variety of papers in which the results depend critically on this assumption. Among the subjects discussed in these investigations are: the condensation of interstellar atoms to form grains;⁷ the ionization equilibrium of interstellar metallic atoms;^{8, 9} the ionization equilibrium of interstellar hydrogen;¹⁰ the dissociation equilibrium of interstellar molecules;^{11, 12, 13} the origin of short-wave radiation observed from the galactic center;^{14, 15} the charge on solid grains;^{3, 16} and the formation of concentrations of grains, which subsequently grow into stars.¹⁷ In some of these references no explicit discussion of the kinetic temperature is given, but it is implicitly assumed that this temperature is equal to the color temperature of the dilute ionizing radiation, which is taken equal to $10,000^\circ$ or $15,000^\circ$.

The possibility that collisions between electrons and molecules might seriously reduce the kinetic temperature in regions where the interstellar medium is relatively dense has been suggested¹⁸ in connection with a theory of accretion of interstellar matter by stars. The quantitative analysis of inelastic collisions between electrons and molecules will be discussed in the second paper of the present series. It has also been pointed out³ that collisions between interstellar atoms and grains tend to reduce the kinetic temperature. A detailed discussion of this mechanism has recently been given in an important paper by F. Hoyle.¹⁹ However, Hoyle's treatment is concerned primarily with the properties of a hypothetical interstellar medium whose density exceeds 5×10^{-22} gm/cm³; the analysis is presented in connection with the general structure of spiral galaxies. The present discussion concerns primarily the properties of interstellar matter in the neighborhood of the sun, to which Hoyle's analysis is not directly relevant.

In the steady state the kinetic temperature of matter is determined by the condition

⁷ B. Lindblad, *M.N.*, **95**, 20, 1934; *Nature*, **135**, 133, 1935; D. ter Haar, *B.A.N.*, No. 361, 1943 (*Ap. J.*, **100**, 288, 1944).

⁸ O. Struve, *Proc. Nat. Acad. Sci.*, **25**, 36, 1939.

⁹ T. H. Dunham, Jr., *Proc. Amer. Phil. Soc.*, **81**, 277, 1938.

¹⁰ B. Strömberg, *Ap. J.*, **89**, 526, 1939.

¹¹ A. McKellar, *Pub. A.S.P.*, **52**, 187, 1940.

¹² P. Swings, *Ap. J.*, **95**, 270, 1942.

¹³ H. A. Kramers and D. ter Haar, *B.A.N.*, No. 371, 1944.

¹⁴ L. G. Henyey and P. C. Keenan, *Ap. J.*, **91**, 625, 1940.

¹⁵ G. Reber and J. L. Greenstein, *Observatory*, **67**, 15, 1947.

¹⁶ B. Jung, *A.N.*, **263**, 425, 1937.

¹⁷ F. L. Whipple, *Ap. J.*, **104**, 1, 1946.

¹⁸ F. Hoyle and R. A. Lyttleton, *Proc. Cambridge Phil. Soc.*, **35**, 405, 1939; **36**, 424, 1940.

¹⁹ *M.N.*, **105**, 287, 1945.

that the kinetic energy gained per cubic centimeter per second must just equal the corresponding energy lost. Thus an investigation of the kinetic temperature must deal with two types of processes: those which convert other types of energy, chiefly radiant energy from the stars, into kinetic energy of random motion, and those which dissipate kinetic energy by converting it into other forms, chiefly the far-infrared radiation emitted by the grains and the visible radiation emitted as forbidden emission lines by the atoms. The present paper, the first of a series on interstellar kinetic temperatures, investigates the processes which contribute to the kinetic energy in the steady state. Collisions between interstellar clouds and similar time-dependent processes may also contribute to the kinetic energy; the discussion of such nonequilibrium effects is postponed to a subsequent paper.

The first section of the present paper treats in a general way the various processes which can convert radiant energy from the stars into kinetic energy of the interstellar particles. In all these processes a compound particle is disrupted, the absorbed energy being divided among the component particles. Since in a steady state as many compound particles are formed by encounters as are disrupted by photon absorption, it is convenient to regard these processes as superelastic collisions, i.e., two component particles collide, emit a quantum, and adhere together for a short time but subsequently dissociate with the absorption of a quantum, the final kinetic energy exceeding the initial energy. The following sections apply these general equations to a number of specific types of superelastic collisions—i.e., electron capture by protons, metallic ions, neutral hydrogen atoms, and solid grains and also capture of atoms by one another. Some of the processes which have been investigated are relatively unimportant in most of interstellar space but might become dominant under some conditions. In the section dealing with grains the factors affecting the electrical charge on the grain are also treated, since this charge affects the number of electrons captured by the grain. A final section analyzes the transfer of energy from cosmic rays to the interstellar medium. A second paper, now in preparation, discusses the various inelastic encounters which tend to dissipate the kinetic energy of the interstellar particles. In a subsequent discussion these various results will be used to determine the kinetic temperature of interstellar matter.

It should be emphasized that many of these results are quite preliminary. Adequate theoretical or experimental research is lacking on many of the important physical phenomena. For example, if the radiation from the brighter stars contains a very great excess of ultraviolet radiation, the kinetic temperature of interstellar space will obviously be effected. In addition, the unexplained presence of cosmic rays suggests that unsuspected processes may play a significant role in interstellar problems. It may be of interest, however, to follow out as far as possible the consequences of known physical processes and to see whether these consequences are in agreement with the known observational facts.

I. GENERAL FORMULAE FOR SUPERELASTIC COLLISIONS

The photoelectric effect is the primary source of kinetic energy in interstellar space. By this process light from the stars is converted into electron kinetic energy, and this energy is rapidly divided among the other particles in the medium. When an electron is captured and subsequently re-emitted on capture of a photon, the kinetic energy is usually increased. This difference between the kinetic energy after photoemission and the kinetic energy before capture may be called the "net energy gain." This quantity, multiplied by the probability that a free electron will be captured per second and averaged over all initial electron velocities and over all frequencies of the absorbed photons, is the average net energy gain per second per free electron and will be denoted by the symbol G_e . The following additional subscripts will be used to denote the type of particle with which the electron is colliding: p for protons; H for neutral hydrogen atoms; i for ions of atoms other than hydrogen and helium, especially calcium, sodium, etc.; m for

molecules; and g for grains. Thus G_{ep} will denote the average net energy gain per free electron per second in electron-proton encounters resulting in electron capture and subsequent photoemission. The total energy gain per second per free electron, resulting from all these processes, will then be the sum of all the G_e 's.

The number of each type of particle per cubic centimeter will be denoted throughout by n , with the subscripts e, p, H, i, m , and g referring, as before, to electrons, protons, neutral hydrogen atoms, ions of atoms other than hydrogen and helium, molecules, and grains, respectively. The velocity of an electron will be denoted by v , its kinetic energy before capture by E_1 , and after capture and re-emission by E_2 ; E_{2p} , for example, will be used to denote the kinetic energy of a photoelectron ejected after capture by a proton, while $\overline{E_{2p}}$ will denote the average value of this quantity. The quantity $\overline{E_1}$, the average kinetic energy of an interstellar particle, is assumed to be the same for all types of particles, in accordance with the results reached in a previous paper.³ It will be assumed throughout that the velocity of an electron relative to an atom, molecule, dust grain, etc., may be set equal to the electron velocity v and that all the kinetic energy of photoelectric emission is carried away by the electron. In view of the very small relative mass of the electron, this assumption is sufficiently accurate. The capture cross-section of each type of particle for electrons will be denoted by σ , with the appropriate subscripts; this choice of notation represents a change from previous work,³ where σ was taken as the radius of a grain.

First, we develop a general formula for G_e , which may be applied to all types of photoelectric emission. If the relative velocity of the two types of particles were the same in all encounters and if the kinetic energy before capture and after photoejection were also constant from one encounter to the next, G_e would be given by the simple formula

$$G_e = n \sigma v (E_2 - E_1), \quad (1)$$

where $n \sigma v$ is the number of electron captures per second per free electron by the type of particle in question, with a particle density n per cubic centimeter. For each specific process, all quantities in equation (1), except v , will carry a subscript indicating the type of particle which captures the electron. Since, in fact, v has a Maxwellian distribution and since σ and E_1 may both vary with v , we must average G_e over all velocities; in addition, E_2 must be averaged over all frequencies in the radiation field. If we denote averages by horizontal bars, we have

$$G_e = n (\overline{\sigma v} \times \overline{E_2} - \overline{\sigma v E_1}). \quad (2)$$

More specifically, the fraction of electrons whose velocities lie between v and $v + dv$ is given by $P(v)dv$, where

$$P(v) = \frac{4}{\pi^{1/2}} L^{3/2} v^2 e^{-Lv^2}. \quad (3)$$

The quantity L is related to the kinetic temperature, T , by the relationship

$$L = \frac{m_e}{2kT}, \quad (4)$$

where m_e is the mass of the electron. With this explicit function for $P(v)$, we may write down the two averages

$$\overline{\sigma v} = \frac{4L^{3/2}}{\pi^{1/2}} \int_0^\infty \sigma(v) v^3 e^{-Lv^2} dv, \quad (5)$$

and

$$\overline{\sigma v E_1} = \frac{2m_e L^{3/2}}{\pi^{1/2}} \int_0^\infty \sigma(v) v^5 e^{-Lv^2} dv,$$

where $\frac{1}{2}m_e v^2$ has been substituted for E_1 .

To find \bar{E}_2 we must know the absorption coefficient $\kappa(\nu)$ for photoelectric emission and $U(\nu)$, the density of radiant energy per cubic centimeter per frequency interval. Since $\kappa(\nu)$ is the ratio of the energy absorbed per particle per second to the energy flux per square centimeter per second, the total energy absorbed in a frequency interval $d\nu$ per second per particle will be $\kappa(\nu)cU(\nu)d\nu$. The corresponding number of photons absorbed is obtained on dividing this absorbed energy by the energy $h\nu$ of each individual photon. It should be noted that $\kappa(\nu)$ represents only that part of the absorption which leads to the emission of one photoelectron per absorbed quantum. In the general case a fraction $q(\nu)$ of this absorbed energy will appear as kinetic energy of the photoelectron. Some of the absorbed energy is required to increase the potential energy of the electrons—i.e., to eject them; in the case of solid grains some of the absorbed energy also goes into the internal thermal energy of the grain. The average energy of a photoelectron is obtained by dividing this total kinetic energy given to electrons by the number of photoelectrons emitted per second. Thus we have

$$\bar{E}_2 = \frac{\int_{\nu_0}^{\infty} q(\nu) \kappa(\nu) U(\nu) d\nu}{\int_{\nu_0}^{\infty} \frac{\kappa(\nu) U(\nu) d\nu}{h\nu}}; \quad (7)$$

the integration extends from the photoelectric threshold frequency, ν_0 , up to infinity. When the ionizing radiation is dilute black-body radiation, with a color temperature T_c , then \bar{E}_2 is usually about equal to kT_c . Thus for each process it will be convenient to introduce an effective color temperature, defined by the relationship

$$T_{cj} = \frac{\bar{E}_{2j}}{k}; \quad (8)$$

for each specific process, j is replaced by the appropriate subscript. Thus for the ionization of H atoms, the effective color temperature is denoted by T_{cp} . In the following sections the above equations will be used to compute G_e for a number of processes.

II. PROTONS

First, we consider encounters between electrons and protons and compute G_{ep} . This process has been considered in some detail by Menzel and others in a series of papers^{20, 21} dealing primarily with the electron temperatures in planetary nebulae. Electron captures have also been discussed by Cillié²² in connection with the Balmer decrement in gaseous nebulae. Since Cillié's work is not concerned with kinetic temperatures and since the viewpoint in the present paper is quite different from that of Menzel and his co-workers and may give added insight into the nature of the problem, this subject will be treated again here.

The cross-section for capture of an electron, whose velocity is v , in the n th quantum state of hydrogen may be written as $\sigma_{np}(v)$. This cross-section may be found from equation (23) of Menzel's basic paper.²⁰ The total number of emissions per second per frequency interval, given by Menzel's $E_{kn}/h\nu$, is equal to the total number of electron captures per corresponding velocity interval; hence we have

$$\frac{E_{kn}}{h\nu} d\nu = \sigma_{np} n_p n_e v P(v) dv. \quad (9)$$

²⁰ D. H. Menzel, *Ap. J.*, **85**, 330, 1937.

²¹ J. G. Baker, D. H. Menzel, and L. H. Aller, *Ap. J.*, **88**, 422, 1938.

²² G. Cillié, *M. N.*, **92**, 820, 1932.

The quantity ν may be eliminated by the equation

$$h\nu = \frac{1}{2} m v^2 + \frac{h\nu_0}{n^2}, \quad (10)$$

where ν_0 is the frequency of the Lyman series limit. Combining equations (3), (4), (9), and (10) with Menzel's equation (23) and substituting for Menzel's K from his equation (6), we have, finally,

$$\sigma_{np} = A \frac{\nu_0}{\nu} \frac{h\nu_0}{\frac{1}{2} m_e v^2} \frac{g}{n^3}, \quad (11)$$

where ν is given again by equation (10) and where

$$A = \frac{2^4}{3^{3/2}} \frac{h e^2}{m_e^2 c^3} = 2.11 \times 10^{-22} \text{ cm}^2. \quad (12)$$

Throughout the following we shall set the Gaunt factor, g , equal to unity. Menzel and his co-workers have investigated the error introduced by this assumption and find that it is small in general—usually less than about 20 per cent. In any hydrogenic atom, such as He^+ , or Li^{++} , where the nuclear charge is $+Ze$, equations (11) and (12) are still valid, provided that one takes into account the direct proportionality between ν_0 and Z^2 .

If now we introduce equation (11) into equations (5) and (6) and make the substitution

$$u = L v^2 = \frac{m_e v^2}{2kT}, \quad (13)$$

we find for the partial cross-section the following average:

$$\overline{\sigma_{np} v} = \frac{2A}{(\pi L)^{1/2}} \frac{1}{n^3} \frac{h\nu_0}{kT} \int_0^\infty \frac{e^{-u} du}{\frac{1}{n^2} + \frac{kT}{h\nu_0} u}. \quad (14)$$

If we introduce the quantities

$$\beta = \frac{h\nu_0}{kT} = \frac{158,000^\circ}{T}, \quad (15)$$

$$Ei(x) = \int_x^\infty e^{-w} \frac{dw}{w}, \quad (16)$$

and let

$$w = u + \frac{\beta}{n^2}, \quad (17)$$

we find, on summing over all quantum levels n ,

$$\overline{\sigma_p v} = \frac{2A}{(\pi L)^{1/2}} \beta \phi(\beta) \quad (18)$$

where

$$\phi(\beta) = \sum_{n=1}^\infty \frac{\beta}{n^3} e^{\beta/n^2} Ei\left(\frac{\beta}{n^2}\right). \quad (19)$$

Similarly, we find from equation (6),

$$\overline{\sigma_{np} v E_1} = \frac{m_e A}{\pi^{1/2} L^{3/2}} \frac{\beta^2}{n^3} \int_0^\infty \frac{u e^{-u}}{u + \frac{\beta}{n^2}}. \quad (20)$$

If we make the substitution (17) as before and sum over all n , equation (20) yields

$$\overline{\sigma_p v E_1} = \frac{m_e A}{\pi^2 L^{3/2}} \beta \chi(\beta), \quad (21)$$

where

$$\chi(\beta) = \sum_{n=1}^{\infty} \frac{\beta}{n^3} \left\{ 1 - \frac{\beta}{n^2} e^{\beta/n^2} \text{Ei}\left(-\frac{\beta}{n^2}\right) \right\}. \quad (22)$$

Values of the functions $\phi(\beta)$ and $\chi(\beta)$ are given in Table 1. These were found by direct summation up to $n = 10$, with the remaining terms approximated by an integral. These

TABLE 1
VALUES OF $\phi(\beta)$ AND $\chi(\beta)$ *

β	T	$\phi(\beta)$	$\chi(\beta)$	$2\chi(\beta)/3\phi(\beta)$
0.5	316,000°	0.70	0.35	0.33
1.0	158,000	0.96	0.55	.38
2.0	79,000	1.26	0.82	.43
5.0	31,600	1.69	1.24	.49
10.0	15,800	2.02	1.56	.52
20.0	7,900	2.36	1.89	.54
50.0	3,160	2.82	2.34	.55
100.0	1,580	3.16	2.67	.56
200.0	790	3.51	3.01	.57
500.0	316	3.98	3.47	.58
1,000.0	158	4.32	3.81	.59
2,000.0	79	4.67	4.16	.59
5,000.0	31.6	5.13	4.63	.60
10,000.0	15.8	5.47	4.97	.61
20,000.0	7.9	5.82	5.32	0.61

* As β increases, $\phi(\beta)$ approaches the ratio:

$$\frac{\text{Number of electrons captured in all levels of } H}{\text{Number of electrons captured in the ground level}},$$

while $\chi(\beta)$ approaches the ratio:

$$\frac{\text{Kinetic energy radiated by captures in all levels of } H}{\text{Kinetic energy radiated by captures in the ground level}}.$$

For all β , $\frac{2\chi(\beta)}{3\phi(\beta)}$ equals the ratio:

$$\frac{\text{Average kinetic energy of the electrons captured}}{\text{Average kinetic energy of the free electrons}}.$$

functions change so slowly with T that their values at any intermediate temperature may be found by simple interpolation. It may be noted that the function ϕ is equal to β times the function G_{T_e} used by Baker, Menzel, and Aller.²¹

The functions $\phi(\beta)$ and $\chi(\beta)$ have a simple physical significance when β is large. As β increases, $\phi(\beta)$ approaches the ratio between the number of electron captures in all states and the corresponding number of captures in the ground state. When β exceeds 20, for example, $\phi(\beta)$ is within 5 per cent of this ratio; but with decreasing β the agreement is less close. When β lies between 0.5 and 1.0, with $\phi(\beta)$ between 0.70 and 0.96, the total number of captures in all levels is between 1.5 and 1.6 times the number in the ground level. Similarly, for large β , $\chi(\beta)$ approaches the ratio of the kinetic energy radiated per second by electron captures in all levels to the corresponding energy radiated by captures in the ground level. When β lies between 0.5 and 2.0, $\chi(\beta)$ is less than unity, and this

ratio lies between 1.3 and 1.5. Evidently the relative importance of captures in excited levels changes extremely slowly with changing temperature.

The average kinetic energy of a captured electron is obtained on dividing equation (21) by equation (18), which yields $kT\chi(\beta)/\phi(\beta)$. Thus the ratio $\chi(\beta)/\phi(\beta)$ gives the average energy of the captured electrons, in units of kT . Since the mean kinetic energy of free electrons is $3kT/2$, the ratio of the electron energy lost per capture to the mean kinetic energy is $2\chi(\beta)/3\phi(\beta)$, and this quantity is listed in the last column of Table 1. The relatively low energy of the captured electrons results from the increase of capture cross-section with decreasing velocity. If no dissipation of energy occurred except through electron captures by protons, the kinetic temperature would adjust itself so that the average energy of a captured electron would equal kT_{cp} , the average energy of an electron emitted photoelectrically (see eq. [8]); hence in such a case the kinetic temperature would exceed the effective color temperature T_{cp} by a factor between 1.1 and 2.0. Actually, free-free transitions, which will be discussed subsequently, reduce the kinetic temperature more nearly to T_{cp} .

To evaluate numerically equation (2) for G_{ep} , it is necessary to determine \bar{E}_{2p} , the average kinetic energy of the ejected photoelectron. When an electron is ejected from a H atom in the ground state, the absorbed energy is $h\nu$, while the kinetic energy of the electron is $h(\nu-\nu_0)$, where ν_0 is again the frequency of the Lyman limit. Thus we may write for this case

$$q(\nu) = \frac{h(\nu - \nu_0)}{h\nu} = 1 - \frac{\nu_0}{\nu}. \quad (23)$$

The atomic absorption coefficient $\kappa(\nu)$ for a H atom in the ground state may, to a first approximation, be written as

$$\kappa(\nu) \propto \frac{1}{\nu^3}. \quad (24)$$

Examination of the exact formula²³ shows that equation (24) is a close approximation for electron energies of practical interest.

The energy density $U(\nu)$, which also appears in equation (7) for \bar{E}_2 , will depend on position in the Galaxy. In interstellar space as a whole the average values given by Dunham⁹ are probably the best available. The integral in equation (7) has been evaluated numerically for Dunham's values computed on the assumption of selective absorption. The effective color temperature T_{cp} , defined in equation (8), is then found directly from E_{2p} and is equal to 27,000°. The corresponding value found when no absorption is assumed is 32,000°, but this value is presumably less realistic than the previous one.

Near a single bright B star, this computed average value is no longer relevant. Close to a star the radiation will be approximately dilute black-body radiation at the color temperature T_c , where T_c is essentially the surface temperature of the star. In this case an explicit formula may be obtained for T_{cp} . If equations (23) and (24) are substituted in equation (7), and $U(\nu)$ is replaced by a constant times $B_\nu(T_c)$, the Planck function for the radiant intensity, we find

$$\bar{E}_{2p} = \frac{\int_{\nu_0}^{\infty} \left(1 - \frac{\nu_0}{\nu}\right) \frac{d\nu}{e^{h\nu/kT_c} - 1}}{\int_{\nu_0}^{\infty} \frac{1}{h\nu} \frac{d\nu}{e^{h\nu/kT_c} - 1}}. \quad (25)$$

If we introduce the quantity β_c , defined as

$$\beta_c = \frac{h\nu_0}{kT_c} = \frac{158,000^\circ}{T_c}, \quad (26)$$

²³ H. Bethe, *Handb. d. Phys.* (J. Springer, 1933), 24, Part I, 477.

equation (25) may be written in the form

$$\overline{E_{2p}} = kT_c \psi(\beta_c) = kT_{cp} \quad (27)$$

where use has been made of equation (8) and where

$$\psi(\beta) = \frac{\int_{\beta}^{\infty} \frac{dy}{e^y - 1}}{\int_{\beta}^{\infty} \frac{dy}{y(e^y - 1)}} - \beta. \quad (28)$$

Evidently $\psi(\beta_c)$ is the ratio of the effective color temperature, T_{cp} , to the actual color temperature, T_c . If the quantity $(e^y - 1)^{-1}$ in both integrands in equation (28) is expanded and the integrals are evaluated term by term, one finds

$$\psi(\beta) = \frac{\sum_{n=1}^{\infty} \frac{1}{n} e^{-n\beta}}{\sum_{n=1}^{\infty} Ei(n\beta)} - \beta. \quad (29)$$

Values of $\psi(\beta)$, computed from equation (29), are given in Table 2, together with the resultant values of the effective color temperature. It will be noted that $\psi(\beta_c)$ exceeds

TABLE 2
VALUES OF $\psi(\beta_c)$ AND T_{cp}

β_c	T_c^*	$\psi(\beta_c)^\dagger$	T_{cp}^\ddagger	β_c	T_c^*	$\psi(\beta_c)^\dagger$	T_{cp}^\ddagger
0.5.....	316,000°	0.449	142,000°	5.0.....	31,600°	0.868	27,400°
0.75.....	211,000	.537	113,000	10.0.....	15,800	.922	14,600
1.0.....	158,000	.599	94,600	20.0.....	7,900	.957	7,560
1.5.....	105,000	.686	72,000	50.0.....	3,160	.981	3,100
2.0.....	79,000	.739	58,400	100.0.....	1,580	.990	1,560
3.0.....	52,700	.808	42,600	200.0.....	790	0.995	786
4.0.....	39,500	0.844	33,300				

* T_c is the color temperature of radiation from a star.

† ψ is the ratio of T_{cp} to T_c .

‡ T_{cp} is the effective color temperature for photoionization of H.

0.80 as long as β_c exceeds 3; thus the effective color temperature is within 20 per cent of the actual color temperature of the ionizing radiation if this latter temperature is less than about 50,000°.

On the basis of a theory developed by B. Strömgren,¹⁰ the values given in Table 2 are always to be used whenever G_{ep} is appreciable. According to this picture, H atoms are ionized only in spherical regions surrounding each star, outside of which the hydrogen is almost completely neutral. The regions of ionized hydrogen are called H II regions, while the regions of neutral hydrogen are called H I regions. If the density of hydrogen in the galactic plane is about 1 atom per cubic centimeter, the H II regions are primarily confined to the immediate vicinity of the early-type stars. If this picture is correct, the only relevant values of T_{cp} are those near O and B stars and may be found from the top few lines of Table 2. In most other regions the hydrogen is neutral, and photoelectric

ionization of hydrogen will be negligible. However, there is some reason to suspect that interstellar atoms are predominantly concentrated in dust clouds,^{24, 25} between the clouds the density of hydrogen may be less than 1 atom per cubic centimeter and may be so small that most of the hydrogen outside the clouds is ionized,²⁶ i.e., that the entire interstellar gas, outside of dust clouds, is an *H II* region. In such a case T_{ep} may be set equal to 27,000°, except near O and B stars, where the values in Table 2 are applicable.

Now, if equations (18), (21), and (27) are substituted in equation (2), as applied to electron-proton encounters, and equations (4), (12), and (15) are used to eliminate L , A , and β , respectively, we have

$$G_{ep} = \frac{2.85 \times 10^{-27}}{T^{\frac{1}{2}}} n_p \{T_p \phi(\beta) - T_\chi(\beta)\} \text{ erg/sec.} \quad (30)$$

Equation (30) gives the average net gain of kinetic energy per free electron per second resulting from electron-proton encounters.

III. ATOMS OTHER THAN HYDROGEN

Next, the gain in kinetic energy resulting from electron captures by ions other than protons may be considered. In regions where the hydrogen is ionized (*H II* regions), the low abundance of most other atoms makes their contribution relatively negligible. Thus the value of G_e corresponding to electron capture by *O III* and other highly ionized atoms need not be considered. The only other type of atom which may add an important contribution to G_e in *H II* regions is helium. The density of helium relative to hydrogen is difficult to estimate; the available data for planetary nebulae, the sun, and τ Scorpii suggest²⁷ about 1 or 2 *He* atoms for each 10 atoms of hydrogen. In *H I* regions *He* atoms will not contribute an appreciable G_e , but in *H II* regions the photoelectric ionization of these atoms may increase the kinetic temperature somewhat. If this contribution from *He* atoms is comparable to that from hydrogen, the *He* atoms will be ionized only within a certain radius from the hot star, and this radius may be substantially less than the radius of the region of ionized hydrogen. The neglect of *He* atoms will give a lower limit for the temperature of *H II* regions. While no detailed analysis of the contribution from *He* atoms will be made here, the approximate equations derived in this section may be applied to *He* atoms as well as to others.

In *H I* regions, where hydrogen is neutral, the ionization of elements other than hydrogen and helium must be considered. The most important atoms are those which are cosmically abundant and which have a low ionization potential, such as *Na* and *Ca* atoms. As a first approximation, any atom may be treated by the equations developed above for hydrogen. The applicability of the hydrogenic formulae for other atoms has been investigated by Bates, Buckingham, Massey, and Unwin.²⁸ These authors point out that captures in highly excited states are predominantly captures in states of high angular momentum, which become hydrogen-like most rapidly with increasing n . Especially at low temperatures, at which captures in the highly excited states become increasingly important relative to captures in the ground state, the hydrogenic formulae should become valid.

This general expectation is supported by recent computations²⁹ of transition probabilities for the *Na* atom. From the oscillator strengths given for the transitions from

²⁴ L. Spitzer, Jr., *Pub. A.A.S.*, **10**, 235, 1941.

²⁵ J. H. Oort and H. C. van de Hulst, *B.A.N.*, Vol. **10**, No. 376, 1946.

²⁶ The importance of this possibility has been emphasized by B. Strömgren in correspondence.

²⁷ L. H. Aller and D. H. Menzel, *A.p. J.*, **102**, 263, 1945.

²⁸ *Proc. Roy. Soc. London, A*, **170**, 322, 1939.

²⁹ M. Rudkjöbing, *Pub. Copenhagen Obs.*, No. 124, 1940.

the various states of the Na atom up to the continuum, the probabilities of electron capture in these various states may be determined from Milne's formula,^{28, 30} based on the principle of detailed balancing in thermodynamic equilibrium. For captures in the ground $3s$ state and in the excited $4s$ state, the cross-sections so determined are less than 0.1 times the hydrogenic values. For capture of slow electrons in the excited $3p$ and $4p$ levels the cross-sections are equal to 1.17 and 1.06, respectively, times the hydrogenic values. Although similar computations of f -values for the Ca^{++} ion³¹ do not show such rapid convergence toward the hydrogenic values, one may tentatively adopt the hydrogenic-capture cross-sections as the best available general estimate, except for states of zero angular momentum. Since captures in such s states are relatively unimportant, we may safely use the hydrogenic formulae for all excited states. Certainly, for temperatures as low as 100° , which may be expected in $H\ I$ regions and for which electron captures in very highly excited states become dominant, use of the hydrogenic formulae should give accurate results for the rate of electron capture.

In summing the capture cross-section over all excited states, a problem arises concerning the ground state. If this ground state is an ns (or an ns^2) level, the captures to the excited np (or $nsnp$) levels may be important. Since the hydrogenic formulae derived in the previous section do not distinguish between states with different angular momentum but with the same total quantum number, it is necessary to include the captures in all the states with a particular value of n in order to take into account the captures in the p , d , or f levels. For atoms such as Na and Ca , the error thus introduced will not be serious, owing to the relative unimportance of the s levels. As a rough working rule, if half or less of the states with total quantum number n_1 are filled when the atom is ionized but unexcited, the capture cross-section may be determined by adding the values of σ_{np} for all n equal to or greater than n_1 ; but if more than half these states are filled, the sum begins with the capture cross-section for n equal to $n_1 + 1$. The symbol k will be used to denote the total quantum number n for which the hydrogenic cross-section should be used. On this basis, superelastic collisions between electrons and He^+ atoms are described by exactly the same formulae as are the corresponding collisions between electrons and protons; thus for He^+ as for H^+ , k equals 1. For capture of electrons by singly ionized atoms from lithium through nitrogen, however, k equals 2, while for atoms from oxygen through titanium, k equals 3, and for atoms from vanadium through silver, k equals 4. A more accurate method of interpolation between the values for adjacent k 's could, of course, be used, but the relatively crude scheme described here should provide an adequate first approximation.

On the basis of this approximation, we have, from equations (18) and (19),

$$\overline{\sigma_i v} = \frac{2A}{(\pi L)^{1/2}} \beta \phi_k(\beta) \quad (31)$$

where

$$\phi_k(\beta) = \sum_{n=k}^{\infty} \frac{\beta}{n^3} e^{\beta/n^2} Ei\left(\frac{\beta}{n^2}\right). \quad (32)$$

Similarly,

$$\overline{\sigma_i v E_1} = \frac{m_e A}{\pi^{1/2} L^{3/2}} \beta \chi_k(\beta), \quad (33)$$

where

$$\chi_k(\beta) = \sum_{n=k}^{\infty} \frac{\beta}{n^3} \left\{ 1 - \frac{\beta}{n^2} e^{\beta/n^2} Ei\left(\frac{\beta}{n^2}\right) \right\}. \quad (34)$$

Values of the functions $\phi_k(\beta)$ and $\chi_k(\beta)$ are given in Table 3.

³⁰ E. A. Milne, *Phil. Mag.*, **47**, 209, 1924.

³¹ L. Green, informal communication.

For capture of an electron by a singly ionized atom, β is given by equation (15) in the preceding section. For capture by an atom which has lost Z electrons, one must take into account the fact that ν_0 varies as Z^2 . Equations (31)–(34) are still valid in this case, provided that we use the following definition for β :

$$\beta = \frac{158,000Z^2}{T}. \quad (35)$$

It may be noted that, while these equations may be used to determine the rate of electron capture, given the kinetic temperature and the number of electrons and ions per cubic centimeter, they cannot be used to determine the rate of photoionization and the ionization equilibrium resulting. A captured electron will rapidly cascade to the ground state, from which the probability of photon capture may be very different from its hydrogenic value.

To evaluate G_{ei} it is also necessary to determine \bar{E}_{2i} , defined in equation (7), or the effective color temperature T_{ci} , defined by equation (8). The detailed value of these

TABLE 3
VALUES OF $\phi_k(\beta)$ AND $\chi_k(\beta)$

β	T	ϕ_2	ϕ_3	ϕ_4	ϕ_5	ϕ_6	χ_2	χ_3	χ_4	χ_5	χ_6
0.5.....	316,000°	0.24	0.12	0.075	0.052	0.038	0.082	0.034	0.018	0.011	0.008
1.0.....	158,000	0.36	0.20	0.125	0.087	0.065	0.15	0.063	0.034	0.021	0.014
2.....	79,000	0.54	0.31	0.20	0.14	0.11	0.27	0.13	0.082	0.058	0.044
5.....	31,600	0.84	0.52	0.36	0.25	0.21	0.49	0.27	0.17	0.12	0.09
10.....	15,800	1.11	0.73	0.52	0.39	0.31	0.71	0.41	0.27	0.19	0.14
20.....	7,900	1.41	0.98	0.74	0.58	0.47	0.97	0.61	0.41	0.29	0.21
50.....	3,160	1.84	1.37	1.09	0.89	0.75	1.37	0.94	0.68	0.51	0.38
100.....	1,580	2.17	1.69	1.38	1.16	1.00	1.69	1.23	0.96	0.75	0.61
200.....	790	2.51	2.02	1.70	1.47	1.28	2.02	1.54	1.25	1.02	0.86
500.....	316	2.98	2.49	2.16	1.92	1.72	2.44	1.98	1.65	1.42	1.22
1,000.....	158	3.32	2.82	2.50	2.25	2.05	2.81	2.32	1.99	1.75	1.55
2,000.....	79	3.67	3.17	2.84	2.59	2.39	3.16	2.66	2.33	2.09	1.89
5,000.....	31.6	4.13	3.63	3.30	3.05	2.85	3.63	3.13	2.80	2.55	2.35
10,000.....	15.8	4.47	3.97	3.64	3.39	3.19	3.97	3.47	3.14	2.89	2.69
20,000.....	7.9	4.82	4.32	3.98	3.73	3.53	4.32	3.82	3.48	3.23	3.03

quantities depends on the absorption coefficient $\kappa(\nu)$ for the transition in question. Recent studies^{32, 33} have cast some doubt on previous computations of this function, and an elaborate calculation of T_{ci} for different atoms is therefore not appropriate at the present time.

For an approximate evaluation of T_{ci} , we use the relationship that T_{ci} tends to be approximately equal to the color temperature T_c , provided that $h\nu_0/kT_c$ is large compared to unity. This relation, which was proved by Eddington,⁵ is based on the assumption that the absorption coefficient at the series limit is finite—a legitimate assumption for the photoelectric ionization of atoms and molecules. The color temperature of interstellar radiation may be found from the values of the energy density given by Dunham.⁹ The ratio of the energy densities at 1000 and 2000 Å, corresponding to photon energies between 6 and 12 electron-volts, corresponds to black-body radiation at 17,000°, if Dunham's values, corrected for the effect of selective absorption, are used. This result may be compared with the effective color temperatures of 13,000° and 24,000°, found for the photoionization by integrated starlight of H-like atoms whose ionization potentials are

³² S. Chandrasekhar, *Ap. J.*, **102**, 223, 1945.

³³ *Ibid.*, p. 395.

6 and 12 volts, respectively; in such atoms the absorption coefficient beyond the series limit varies as the inverse cube of the frequency, and the effective color temperature is found from equations (7) and (8) by a direct graphical integration based on Dunham's values. As a conservative estimate, designed to give an upper limit on the kinetic temperature in *H I* regions, we shall finally set T_{ei} equal to 20,000°. In *H II* regions near O and B stars, where a greater effective color temperature of the ionizing radiation might be expected, superelastic collisions between electrons and ionized atoms other than hydrogen or helium may be neglected.

Finally, then, we find for G_{ei} the following equation, applicable to any ions,

$$G_{ei} = \frac{2.85 \times 10^{-27} n_i}{T^{\frac{1}{2}}} \{ T_{ei} \phi_k(\beta) - T \chi_k(\beta) \} \text{ ergs/sec.} \quad (36)$$

The quantity k is the total quantum number n_1 for a captured electron in the ground state, provided that the number of electrons with this total quantum number in the ground state of the ion is no greater than n_1^2 ; otherwise k equals $n_1 + 1$.

IV. NEUTRAL HYDROGEN ATOMS

Next, the contribution of neutral hydrogen must be considered. There is an appreciable probability that a *H* atom will capture an electron, forming a H^- ion. It may be readily shown that such an ion will be neutralized rapidly by photon absorption, with the result that the relative number of H^- ions is relatively small. However, the number of electrons captured per second by *H* atoms is sufficiently great so that this process may actually be more important as a source of kinetic energy in *H I* regions than is the process of electron capture by atomic ions.

The capture cross-section σ_H may be computed from the atomic absorption coefficient for the H^- ion. From the condition that in thermodynamic equilibrium the number of electrons captured with a velocity v must equal the number of electrons ejected with the same velocity, one finds the equation

$$\frac{\sigma_H}{\kappa(\nu)} = \frac{h^2 \nu^2}{2 m^2 v^2 c^2}, \quad (37)$$

where $\kappa(\nu)$ is the atomic absorption coefficient for a H^- ion. Equation (37) is a special case of Milne's formula,³⁰ referred to above. From the values of $\kappa(\nu)$ (denoted by κ_λ) given by Chandrasekhar,³³ values of σ_H have been computed and are given in Table 4 for different values of v . For values of T less than 1000°, corresponding to wave lengths between 14,000 Å and 16,550 Å, an approximate formula,³⁴ based on a series expansion of the free-electron wave function, was used to compute κ_λ ; these approximate values may be in error by as much as 10 per cent. The table in the second column also lists values of the temperature at which the root-mean-square velocity equals the values in the first column. For comparison with electron captures by protons, the table also gives values of σ_{1p} , computed from equation (11) for n, g , and Z all equal to 1. The number of captures in the fourth-quantum level of hydrogen, corresponding to the captures in the lowest unoccupied levels of the Ca^+ ion would be less than a fourth of the values of σ_{1p} listed in the table. Since the number of *H* atoms in *H I* regions exceeds the number of metal ions by at least 10^3 , it is evident that electron captures of *H* atoms will be much more numerous than those by other ions, provided that the kinetic temperature is not less than 1000°. Hence, at temperatures greater than 1000°, G_{ei} may be neglected as compared to G_{eH} , but at lower temperatures G_{ei} may become more important. Electron captures by other neutral atoms, such as oxygen, are presumably negligible, owing to the relatively low abundance of such atoms compared with hydrogen.

³⁴ S. Chandrasekhar, informal communication.

Since the cross-section σ_H varies only slightly with the electron velocity v over the region of interest, a computation of the detailed averages given in equations (5) and (6) would scarcely be worth while. Instead, an approximate method will be used to determine G_{cH} . We may write

$$\overline{\sigma_H v} \approx \sigma_H(\bar{v}) \times \bar{v} \quad (38)$$

and

$$\overline{\sigma_H v E_1} \approx \sigma_H(\bar{v}) \times \overline{v E_1} \approx \sigma_H(\bar{v}) \times \frac{1}{2} m_e \bar{v}^3, \quad (39)$$

where \bar{v} denotes the root-mean-square electron velocity.

TABLE 4
CROSS-SECTIONS FOR ELECTRON CAPTURE

v	Velocity Temperature T	Protons σ_{1p}	H atoms σ_H
0.126×10^7 cm/sec.....	3.48°	$63,700 \times 10^{-22}$ cm ²	0.0231×10^{-22} cm ²
0.178.....	6.95	31,800	.0326
0.252.....	13.9	15,900	.0461
0.308.....	20.9	10,600	.0566
0.359.....	28.3	7,800	.0659
0.401.....	35.3	6,260	.0733
0.490.....	52.7	4,200	.0897
0.698.....	107	2,060	.124
0.952.....	199	1,110	.167
1.34.....	389	566	.230
1.65.....	599	368	.292
1.93.....	819	268	.347
2.17.....	1,040	212	.421
3.18.....	2,220	98.0	.554
4.10.....	3,700	58.0	.636
4.64.....	4,730	44.7	.657
5.01.....	5,520	38.3	.661
5.13.....	5,790	36.2	.663
5.80.....	7,390	27.8	.656
6.49.....	9,260	22.1	.632
6.92.....	10,500	19.4	.619
7.74.....	13,200	15.3	.585
8.47.....	15,800	12.2	.554
9.15.....	18,400	10.5	.527
9.67.....	20,600	9.00	.502
10.9.....	26,100	6.73	.456
12.9.....	36,600	4.45	.384
15.5.....	52,800	2.81	.303
19.6.....	84,500	1.46	.203
28.9.....	184,000	0.437	0.0814

The quantity $\overline{E_{2H}}$, as defined in equation (7), must also be known before G_{cH} can be computed. Since all the excess energy of the photon, above the photoelectric threshold energy, $h\nu_0$, appears as kinetic energy, $q(\nu)$ is given again by equation (23), where ν_0 is now the threshold for negative hydrogen absorption, corresponding to a threshold wave length of about 16,500 Å. The absorption coefficient $\kappa(\nu)$ may be taken from Chandrasekhar.³³ The energy density $U(\nu)$ may be taken from Dunham's values⁹ computed without regard to absorption. If, as before, we equate $\overline{E_{2H}}$ to kT_{cH} , the value of T_{cH} computed on these assumptions is about 11,000°, corresponding to a mean excess

energy of about 1 electron-volt for the absorbed photon. This is the value that would result if all the radiation in space had a wave length of about 7000 Å.

This value of T_{cH} is almost certainly too high; the presence of selective absorption will increase $U(\nu)$ in the infrared relative to the visible and thus reduce the average energy of an absorbed photon. Observations of interstellar absorption do not extend sufficiently far in the infrared to allow an evaluation of this effect; for example, Dunham's computed values of $U(\nu)$ extend only to 10,000 Å. For an accurate determination of T_{cH} , it would be necessary to recompute $U(\nu)$ on different assumptions concerning the selective absorption in space. Since G_{cH} does not usually play a significant role in interstellar space, an upper limit on T_{cH} will suffice for most purposes, and we shall accordingly set T_{cH} equal to 11,000°. With this assumption, equation (2) for G_{cH} becomes

$$G_{cH} = 1.40 \times 10^{-10} \sigma_H(\bar{\nu}) n_H T^{1/2} (7,300^\circ - T). \quad (40)$$

Values of $\sigma_H(\bar{\nu})$ may be read from Table 4.

V. MOLECULES

Photoionization and photodissociation of molecules must next be considered. Apparently little is known about the capture cross-section of ionized molecules for electrons. On the other hand, the abundance of the observed molecules is believed³⁵ to be low, with values of about 10^{-6} CH and CN molecules per cubic centimeter. This is considerably greater than the observed densities of Na and Ca^+ atoms. However, Na and Ca atoms are believed to be largely ionized, while the relative numbers of CH^+ and CH atoms, for example, seem to be about the same, since their absorption lines are apparently of comparable intensities. Thus the number of hydride molecules per cubic centimeter is apparently only a very small fraction of the corresponding number of interstellar atoms. As pointed out by P. W. Merrill,³⁶ it is even possible that the observed molecular lines are circumstellar and that the actual abundance of molecules between the stars is even lower than 10^{-6} per cubic centimeter. In any case, superelastic encounters between electrons and such molecules and between the component atoms making up a molecule may evidently be neglected.

Molecular hydrogen may possibly be much more abundant in HI regions of interstellar space than are the observed molecules CH and CN. However, the ionization energy of H_2 is 15.3 volts, 1.8 volts more than that of atomic hydrogen. Since ultraviolet radiation beyond the Lyman limit will be almost completely absorbed in HI regions, any H_2 molecules present will remain neutral and will therefore not contribute to the kinetic energy of the assembly. Photodissociation of H_2 molecules in HI regions is equally unlikely, since the energy required for this process is 14.5 volts when the molecule is in its ground state.

VI. SOLID GRAINS

Another source of kinetic energy in interstellar space is the photoelectric ionization of small solid particles, or grains. This effect may again be treated by the general equations developed at the beginning of this paper. Of all the electrons which strike a grain and stick to it, a fraction $1 - \alpha$ will be ejected by the photoelectric effect. Since the number of electrons captured by a grain must be very nearly equal to the number lost or neutralized, the remaining fraction α may be assumed to attach themselves to positive ions which strike the grain; electrons leaving in this way will soon be ejected when the atom absorbs a photon. Thus, as before, each encounter in which the electron sticks to the grain may be regarded as a superelastic collision, which may increase the kinetic energy of the assembly.

³⁵ T. H. Dunham, Jr., *Pub. A.A.S.*, **10**, 123, 1941.

³⁶ *Pub. A.S.P.*, **58**, 354, 1946.

This point of view neglects the positive ions which stick to the solid grains, neutralizing electrons captured by the grain. However, this virtual disappearance of ions and electrons from the interstellar gas will have a relatively minor effect on the kinetic temperature of the remaining particles, an effect which will be appreciable only during a time so great that at least half the atoms originally present become incorporated into the growing dust grains. Especially since the predominant H atoms adhere only rarely to the grains, this small effect is generally negligible and will not be considered here.

On this basis, the computation of G_{eg} for grains is a straightforward process but is somewhat involved, since the properties of photoelectric emission are not simple. One source of complexity is that the value of G_{eg} depends markedly on the charge of the grain, which, in turn, depends on the kinetic temperature. Thus it will be necessary to compute the potential of the grains for each assumed temperature and then, with the resultant value of G_{eg} and with the G_e 's found for other processes also, to solve for the kinetic temperature. This process must be repeated until the temperature found equals the assumed temperature. In this section, the formulae for the three average quantities occurring in equation (2) will be given first. Next, general formulae for the total number of photoelectrons emitted per second and for the resultant potential of the grain will be derived. Finally, the values of the various physical quantities occurring in these equations will be discussed.

The average product $\overline{\sigma_g v}$ which occurs in equation (2) is the number of electrons captured by a grain per second per unit electron density. A similar quantity, the total number of electrons captured by a grain per second, denoted by Γ , has been obtained in a previous paper.³ This formula for Γ must be multiplied by the sticking probability, ξ_e , for an electron, to take into account the fact that not all electrons may adhere to the grain; the appropriate values of ξ_e for metallic and nonmetallic grains are discussed in subsection *a* below. If also the previously derived value of Γ is divided by n_e to yield $\overline{\sigma_g v}$, and if $3kT/2$ is substituted for the kinetic energy E , we have

$$\overline{\sigma_g v} = 2 \xi_e \left(\frac{2\pi k}{m_e} \right)^{1/2} a^2 T^{1/2} \times \begin{cases} 1 - \gamma, & \gamma < 0, \\ e^{-\gamma}, & \gamma > 0, \end{cases} \quad (41)$$

where a is the radius of the solid grain (the symbol σ , previously used³ for this quantity is here used for the cross-section) and where

$$\gamma = - \frac{eV}{kT}; \quad (42)$$

the quantity V is the electrostatic potential of the grain, in e.s.u, while e is the electronic charge in the same units. Evidently γ is a measure of the potential energy of an electron at the surface of the grain; thus, if the grain is negatively charged, γ is positive, while for a positively charged grain γ is negative.

The total kinetic energy lost per second by collisions of electrons with a grain, per unit electron density, is readily found by methods similar to those formerly used³ and is given by the expression

$$\overline{\sigma_g v E_1} = 2 \left(\frac{2\pi}{m_e} \right)^{1/2} \xi_e k^{3/2} T^{3/2} a^2 (2 + |\gamma|) \times \begin{cases} 1, & \gamma < 0, \\ e^{-\gamma}, & \gamma > 0. \end{cases} \quad (43)$$

Equation (43) also has been multiplied by ξ_e to allow for the fact that not all the electrons will stick to the grain when they strike it.

The average value of E_{2g} for this process must also be evaluated. When the electrons leave the grain by attaching themselves to a positive ion, the average kinetic energy with which they are subsequently ejected from the atom will be the same as that already

computed for superelastic encounters between electrons and atoms. Thus for a fraction α of the electrons captured by a grain, \bar{E}_{2g} will be kT_{ci} , where T_{ci} is about $20,000^\circ$ in $H\ I$ regions; in $H\ II$ regions T_{cp} , lying between $20,000^\circ$ and $60,000^\circ$, replaces T_{ci} . It is fortunate that this process usually has a minor effect on the computed temperature, since, as shown below, its probability is most uncertain.

It is also conceivable that electrons might leave a grain by attaching themselves to a neutral H atom which strikes the grain. However, an electron attached to an otherwise neutral H atom has a total energy of only -0.75 electron-volts, as compared to the considerably lower energy of electrons in most solids. Hence this process seems improbable and will not be considered further.

It remains to compute \bar{E}_{2g} for the fraction $1 - \alpha$ of the captured electrons which are ejected from the grain by photoelectric absorption. Results will first be obtained for a grain with no electrical charge. Equation (7) is applicable in the present case, provided that we define $\kappa(\nu)$ as the energy absorbed photoelectrically by a grain per unit intensity of incident radiation. When radiation of energy density $U(\nu)$ per frequency interval is present in space, an amount $\pi a^2 c U(\nu)$ passes through the geometrical cross-section πa^2 of a grain per second. A fraction $Q(\nu)$ of this radiation is absorbed, but only a fraction $\chi(\nu)$ of the absorbed photons leads to the emission of a photoelectron. This quantity $\chi(\nu)$ is called the "photoelectric efficiency." The photoelectric absorption coefficient $\kappa(\nu)$ therefore becomes

$$\kappa(\nu) = \pi a^2 Q(\nu) \chi(\nu). \quad (44)$$

Equation (7) depends also on the quantity $q(\nu)$, the fraction of the photon energy which appears as kinetic energy of the emitted electron. Since an electron must be given a potential energy $h\nu_0$ to escape from a solid, where ν_0 is the threshold energy, the "available" energy for a free electron is, as before, $h(\nu - \nu_0)$. However, some of this available energy is lost by collisions as the electron leaves the solid, and additional energy is also required to eject electrons whose kinetic energy in the solid is less than the maximum zero-point energy. As a result of these two factors, the kinetic energy of the photoelectrons produced by photons of frequency ν will, on the average, be a fraction q_1 of the available energy. We may therefore write

$$q(\nu) = q_1 \left(1 - \frac{\nu_0}{\nu}\right). \quad (45)$$

The subsequent discussion of the factors determining q_1 indicates that this quantity does not change much with frequency; hence q_1 will be assumed constant.

If equations (44) and (45) are substituted in equation (7), we have, for an uncharged grain,

$$\bar{E}_{2g} = q_1 \frac{\int_{\nu_0}^{\infty} \left(1 - \frac{\nu_0}{\nu}\right) Q(\nu) \chi(\nu) U(\nu) d\nu}{\int_{\nu_0}^{\infty} Q(\nu) \chi(\nu) U(\nu) \frac{d\nu}{h\nu}}. \quad (46)$$

In accordance with equation (8), a color temperature T_{cg} may be defined so that kT_{cg} equals \bar{E}_{2g} . If we define I_1 and I_2 as follows:

$$I_1(\nu_0) = \int_{\nu_0}^{\infty} Q(\nu) \chi(\nu) U(\nu) \frac{d\nu}{h\nu}, \quad (47)$$

$$I_2(\nu_0) = \int_{\nu_0}^{\infty} Q(\nu) \chi(\nu) U(\nu) \frac{d\nu}{h\nu_0}, \quad (48)$$

then \overline{E}_{2g} and T_{cg} may conveniently be expressed in the form

$$\overline{E}_{2g} = kT_{cg} = q_1 h \nu_0 \left(\frac{I_2 - I_1}{I_1} \right). \quad (49)$$

The physical significance of the integral I_1 will become apparent below in the discussion following equation (54).

If the grain is charged, these results must be modified. A positive charge will attract some electrons back to the grain and prevent them from escaping. Thus the surface acts as though the effective photoelectric threshold were increased by an amount eV/h . The effective value of $\chi(\nu)$ will also be modified. Since $\chi(\nu)$ for an uncharged grain is not known very accurately, it will here be assumed that the effective value of $\chi(\nu)$ is equal to the appropriate value for an uncharged grain with a threshold equal to $\nu_0 + eV/h$. Thus equation (49) may be used in this case, provided that this effective photoelectric threshold is used.

If the charge on the grain is negative, two effects appear. In the first place, the kinetic energy of the photoelectron is increased by the electrostatic repulsion, the increase in \overline{E}_{2g} amounting to $|eV|$. In the second place, the threshold frequency will be diminished by the electrical field. For plane metallic surfaces of pure metal this reduction of threshold has been thoroughly studied. On the assumption that the threshold energy results from the presence of an image force, the reduction of the photoelectric threshold may be shown to be proportional to the square root of the accelerating electrical field; these results are in moderately good agreement with observation.³⁷ This theory, if applied to small grains, indicates that the photoelectric threshold energy is reduced by $|eV|/Z_g^{1/2}$, where Z_g is the number of electrons on the grain. For a potential of 1 volt, Z_g is in the neighborhood of 100, and the photoelectric threshold is reduced by only a tenth of a volt, which is quite negligible.³⁸ For surfaces contaminated with gas, the simple theory is no longer applicable; but, as long as the potential of the grain does not exceed 1 or 2 volts, yielding electrical fields of less than 200,000 volts per centimeter, the reduction of the photoelectric threshold produced by the electrical field is not likely to be large, and we shall therefore neglect it here.

Finally, then, if we take into account both photoemission and neutralization of positive ions, we have for a charged grain the following equation:

$$\overline{E}_{2g} = \alpha kT_{ci} + (1 - \alpha) kT_{cg}, \quad (50)$$

where

$$kT_{cg} = q_1 h \nu_{0e} \left[\frac{I_2(\nu_{0e}) - I_1(\nu_{0e})}{I_1(\nu_{0e})} \right] + \begin{cases} 0 & , \quad \gamma < 0 \\ \gamma kT & , \quad \gamma > 0 \end{cases}, \quad (51)$$

γ is given by equation (42), and ν_{0e} is related to ν_0 , the photoelectric threshold of an uncharged grain, by the equation

$$\nu_{0e} = \nu_0 + \begin{cases} \frac{-\gamma kT}{h} & , \quad \gamma < 0 \\ 0 & , \quad \gamma > 0 \end{cases}. \quad (52)$$

Next the total number of electrons emitted will be considered, together with the other factors determining the electrical charge on the grain. The denominator of equation (7), when applied to the present case, gives the total number of photoelectrons emitted by

³⁷ A. L. Hughes and L. A. DuBridge, *Photoelectric Phenomena* (New York: McGraw-Hill Book Co., 1932), sec. 6-15.

³⁸ A more exact analysis by H. C. van de Hulst (*Recherches astr. de l'Obs. d'Utrecht*, in preparation), which takes into account the curvature of the grain surface, gives essentially similar results.

the grain per second. As before,³ we may define K as the ratio of the photoelectrons emitted per second to the number of positive ions striking an uncharged grain per second; this latter quantity is obtained from equation (41), with γ and ξ_e set equal to 0 and 1, respectively, with m_e replaced by the ionic mass m_i , and with the ion density n_i inserted as a factor. Evidently, K will depend on the charge of the grain. The value for an uncharged grain will be derived first. We have

$$K = \frac{(6\pi)^{\frac{1}{2}} c}{4 n_i (\bar{v}_i^2)^{\frac{1}{2}}} \int_{\nu_0}^{\infty} \frac{Q(\nu) \chi(\nu) U(\nu) d\nu}{h\nu}, \quad (53)$$

where the mean square ionic velocity \bar{v}_i^2 has been substituted for $3kT/m_i$. Equation (53) is a more complete version of equation (7) in a previous paper.³

A positive charge on the grain will attract some electrons back to the grain and prevent them from escaping. As before, this effect may be taken into account by using a greater effective threshold ν_{0e} , given again by equation (52). The decrease in threshold produced by a negative charge on the grain will again be neglected. In terms of the integral I_1 , defined in equation (47), we have, finally, for a charged grain,

$$K = 2.06 \times 10^6 \frac{A_i^{\frac{1}{2}}}{n_i T^{\frac{1}{2}}} I_1(\nu_{0e}), \quad (54)$$

where A_i is the atomic weight of the positive ion. The quantity I_1 appearing in equations (49) and (54) may be regarded as the effective number of photons per cubic centimeter of interstellar space; i.e., the number of photoelectrons emitted from a grain per second equals I_1 multiplied by the velocity of light and by the geometrical cross-section of the grain.

From the value of K given in equation (54) it is possible to determine the charge on the solid grain. By an obvious generalization of equation (6) in a previous paper,³ we find

$$\begin{aligned} \xi_i (1 + \gamma) + K &= A_i^{\frac{1}{2}} \xi_e \left(\frac{m_0}{m_e} \right)^{\frac{1}{2}} e^{-\gamma}, \quad \gamma > 0; \\ \xi_i e^{\gamma} + K &= A_i^{\frac{1}{2}} \xi_e \left(\frac{m_0}{m_e} \right)^{\frac{1}{2}} (1 - \gamma), \quad \gamma < 0; \end{aligned} \quad (55)$$

where the quantity ξ_e is again the sticking probability for the electron, while ξ_i is the probability that an ion will leave with an electron captured from the grain (or stick to the grain); A_i is the atomic weight of the predominant positive ion present, while m_0 is the mass of unit atomic weight.

From the terms in equation (55) it is a simple matter to find α , the ratio of the number of positive ions neutralized per second to the number of electrons captured per second. We find

$$\alpha = \frac{\xi_i}{\xi_e A_i \left(\frac{m_0}{m_e} \right)^{\frac{1}{2}}} \times \left\{ \begin{aligned} &\frac{(1 + \gamma)}{e^{-\gamma}}, & \gamma > 0 \\ &\frac{e^{\gamma}}{(1 - \gamma)}, & \gamma < 0 \end{aligned} \right\}. \quad (56)$$

This completes the mathematical formalism required to determine G_{eg} . Equation (55), together with equations (54) and (52), determines γ , the ratio of the potential energy of an electron on a grain to kT , which is two-thirds of the average kinetic energy of a free particle; this quantity γ affects all the other processes. Equation (56) determines α , which must be substituted in equation (50) for \bar{E}_{2g} . Of the two temperatures in equation

(50), $T_{c\theta}$ is found from equation (51), while T_{ci} equals $20,000^\circ$ in H I regions; in H II regions T_{cp} , found from Section II above, replaces T_{ci} . Finally, equations (41) and (43) determine $\overline{\sigma_\theta v}$ and $\overline{\sigma_\theta v E_i}$, which, together with $\overline{E_{2\theta}}$, must be substituted in equation (2) for $G_{c\theta}$. If we substitute for the numerical values, this final equation becomes

$$G_{c\theta} = 2.70 \times 10^{-11} \xi_e n_\theta a^2 T^{1/2} \times \left\{ \begin{array}{ll} (1 - \gamma) \{ a T_{ci} + (1 - a) T_{c\theta} \} - (2 - \gamma) T, & \gamma < 0 \\ e^{-\gamma} \{ a T_{ci} + (1 - a) T_{c\theta} - (2 + \gamma) T \}, & \gamma > 0 \end{array} \right\}, \quad (57)$$

where $T_{c\theta}$, γ , and a are determined by equations (51), (55), and (56), respectively.

To apply these results it is necessary to specify the constants ξ_e , ξ_i , q_1 , and ν_0 , together with the functions $\chi(\nu)$ and $Q(\nu)$. The appropriate value to be used for each of these six quantities will now be discussed.

All these quantities depend on the composition of the grains, concerning which nothing very definite is known. If the grains form in interstellar space from initially small nuclei, different atoms sticking to the grain on impact, a rather conglomerate grain is to be expected, composed largely of the hydrides of carbon, nitrogen, and oxygen. A mixture of metallic atoms, such as sodium, magnesium, and some iron, should be present, however. Whether such impurities could impart some metallic properties to the grains is a matter of conjecture. In any case a surface layer of adsorbed H and He atoms should be present, so that, even if the grains were made of pure metal, their properties would be those of a contaminated surface rather than those of a pure metallic surface. In view of these many uncertainties, it is not possible to specify exact values for any of the above quantities. However, certain limits seem probable; these limits are discussed in each of the following six subsections.

a) STICKING PROBABILITY FOR ELECTRONS, ξ_e

First, we consider ξ_e , the sticking probability for free electrons. For low-energy electrons incident on pure metallic surfaces the fairly extensive literature^{39, 40} shows that electrons with energies of a few volts or less, incident on a pure metallic surface, mostly stick to the surface, a small fraction being reflected without loss of energy. The observed values of ξ_e for electrons whose energies lie between 0.05 and 2 electron-volts lie between about 0.8 and 0.96 for different metals. However, if the metallic surface is contaminated by gas, as by ordinary exposure to the atmosphere, the reflection coefficient is much greater, and the observed values of ξ_e for electron energies up to about 15 electron-volts lie mostly in the neighborhood of 0.50. The very low value of ξ_e noted by F. Cernuschi⁴¹ in Farnsworth's early work was not confirmed by subsequent more accurate investigations and may be attributed to the electrostatic repulsion of the electrons from the metallic surface in the experiment cited.

For dielectrics the evidence⁴⁰ is less extensive, but measurements have been made on the reflection of slow electrons from BaO and from $NaCl$ and similar chlorides and fluorides. These measurements refer to outgassed surfaces and, moreover, do not extend to electron energies below 1 or 2 electron-volts. The values of ξ_e show considerable variation with electron energy and tend to become negative for moderate electron energies, owing to the appearance of secondary electrons. For energies less than 15 electron-volts however, the reflection coefficient is less than 100 per cent in all cases, and ξ_e is therefore

³⁹ H. Farnsworth, *Phys. Rev.*, **20**, 258, 1922; **25**, 41, 1925; **27**, 413, 1926; **31**, 405 and 419, 1928; **34**, 679, 1929; also S. R. Rav. *Proc. Roy. Soc. London, A*, **128**, 41 and 57, 1930; also H. E. Krefft, *Phys. Rev.* **31**, 199, 1928; also J. B. Brinsmade, *Phys. Rev.*, **30**, 494, 1927.

⁴⁰ R. Hilsch, *Zs. f. Phys.*, **77**, 427, 1932; H. Bruining, *Physica*, **5**, 913, 1938.

⁴¹ *A. p. J.*, **105**, 241, 1947.

positive. For energies less than about 12 electron-volts the observed values of ξ_e range from 0.55 for 2-volt electrons incident on CaF_2 to 0.04 for 4-volt electrons on KI . A very rough average of all data for electron energies less than 12 volts yields a value of about 0.20 for ξ_e .

This result yields a value of 0.80 for the probability of reflection. So high a probability for electron reflection from ionic crystals has not been explained theoretically, and hence there is no theory to predict how the value of ξ_e may be expected to change as the electron energy is decreased further. An extrapolation of the observed data indicates that for very low-speed electrons ξ_e is greater than the average value of 0.20 indicated above, since, when a small value of ξ_e was found, the values were observed to be rising with decreasing electron energy at the lowest energies observed. A value of about 0.40 for the sticking probability of low-speed electrons (0.5 electron-volts or less) would be consistent with the data for all the nonmetallic substances investigated.

These measurements do not distinguish between electrons captured by the crystal and those which penetrate through the crystal and are captured by the metal electrode beyond. Cernuschi⁴¹ has argued that, since all the bound electron states in an ionic crystal are occupied, an electron may be expected to pass through the crystal without being captured. However, measurements of the electron affinity of such crystals⁴² show that there exist in these crystals allowed energy levels lying about $\frac{1}{2}$ electron-volt below the free state. Since these levels are normally unoccupied, electrons may be captured in them. When account is taken of the probable heterogeneity of the grains, it is evident that there should be many unoccupied bound levels into which a free electron may be captured.

The measurements also do not indicate what effect adsorbed gases may have on the sticking probability for electrons incident on dielectric crystals. However, it seems unlikely that the resultant values of ξ_e could be reduced much below 0.10 by the presence of surface gases.

While the foregoing evidence does not provide any conclusive determination of ξ_e , certain results seem probable. We shall here assume that for metallic grains ξ_e equals 0.5, while for dielectric grains ξ_e lies between 0.1 and 0.5. Since the electron energies of interest are usually less than about 1 or 2 electron-volts, corresponding to kinetic temperatures of 10,000°–20,000°, no variation of ξ_e with electron energy will be considered.

b) NEUTRALIZATION PROBABILITY FOR IONS, ξ_i

Next we must consider ξ_i , the probability that an ion will be neutralized on impact with a solid grain. While some data on ion neutralization at solid surfaces have been obtained for energies of several kilovolts, very little information seems available for ions with energies of only a few volts. Some measurements have been made⁴³ on the probability that low-speed ions, incident on a metallic surface, capture 2 electrons and leave the surface as negative ions. The probability of this process tends to be rather low, with measured values of about 10^{-5} – 10^{-6} for 60-volt ions of various types. With decreasing ion energy, the probability apparently decreases steadily, and an extrapolation of the data down to energies of a few electron-volts gives probabilities less than 10^{-6} . Thus this process may be neglected for collisions of ions with solid grains.

The neutralization of protons on impact with metal surfaces has been considered theoretically by Massey,⁴⁴ who showed that the protons must penetrate within about 1 atomic radius of a metallic surface, under typical conditions, before they are neutralized.

⁴² N. F. Mott and R. W. Gurney, *Electronic Processes in Ionic Crystals* (New York: Clarendon Press, 1944), see Table 20, p. 97.

⁴³ F. L. Arnot and J. C. Milligan, *Proc. Roy. Soc. London, A*, **156**, 538, 1936; F. L. Arnot, *Proc. Roy. Soc. London, A*, **158**, 137 and 157, 1937.

⁴⁴ H. S. W. Massey, *Proc. Cambridge Phil. Soc.*, **26**, 386, 1930.

Since the theory breaks down when the ion is this close to the metal, it is not possible to use the theory for a specific computation of ξ_i . Measurements⁴⁵ on the neutralization of H_2^+ and Ar^+ ions, with energies of 100–600 volts, indicate that the number of ions which become neutralized at grazing incidence is less than 10^{-4} of the number which are reflected without change of charge. However, these experiments cast no light on the probability of neutralization to be expected at much lower energies and at normal incidence.

In view of this almost complete lack of accurate information, we must consider that ξ_i lies between wide limits. We shall assume only that ξ_i lies between 1 and 10^{-4} . Theoretical considerations suggest that for protons a high value is more probable, since the ionization energy of a proton exceeds the binding energy of an electron in most metallic or dielectric solids. For atoms of low ionization potential, the neutralization probability may be near the lower limit, since the binding energy of an electron in a pure dielectric crystal such as *NaCl* much exceeds the ionization energy of a sodium atom, for example, and the neutralization of an ion in this case, if it occurs at all, must be dependent on the presence of impurities, adsorbed gases, or excess electrons. Fortunately, this very large uncertainty in ξ_i has usually a small effect on the computed temperature.

c) FRACTION OF AVAILABLE ENERGY CONVERTED TO PHOTOELECTRON KINETIC ENERGY, q_1

The quantity q_1 is defined as the average kinetic energy of the photoelectrons emitted from an uncharged grain, on absorption of radiation of frequency ν , divided by the available energy $h(\nu - \nu_0)$, where ν_0 is the threshold frequency. This ratio q_1 may be found from the distribution of photoelectron energies, which are observed to range from zero up to the maximum available energy $h(\nu - \nu_0)$.

Observations of the kinetic energies of photoelectrons show that this distribution depends on the thickness of the photoelectric surface, on the state of the surface, and on other factors which are imperfectly understood. Under many conditions, however, the distribution follows a certain standard form⁴⁶ for a wide variety of wave lengths and surfaces. The average kinetic energy of the photoelectrons, found by a graphical integration over the distribution shown in Hughes and DuBridge's Figure 4-10,⁴⁶ is 45 per cent of the available energy. For thin films, with a thickness of less than 5×10^{-6} cm., this percentage increases and presumably reaches its theoretical value⁴⁷ of $\frac{2}{3}$ for very thin films at absolute zero. Since the grains which are observed to extinguish starlight have diameters about four times this critical value, the results for thick films are probably more relevant here. However, there is some experimental evidence⁴⁸ that, even for thick films, this theoretical distribution may be nearly attained at low temperatures. Evidently, there is still considerable uncertainty on the factors determining the distribution of photoelectron velocities. It will be assumed here that q_1 equals 0.55. This is a rough average between the empirical value of 0.45 and the theoretical value of 0.67 for films at absolute zero. This assumed value should therefore not be in error by more than 20 per cent.

d) THRESHOLD FREQUENCY, ν_0 ; PHOTOELECTRIC EFFICIENCY, $\chi(\nu)$

The two quantities, threshold frequency and photoelectric efficiency, may conveniently be discussed together, since each of them depends on the detailed condition of the photoelectric surface. Most studies of the photoelectric effect have apparently been carried out with metals, and attempts are usually made to obtain pure surfaces. Effects produced by impurities and adsorbed gases are so complicated that little is known con-

⁴⁵ A. Rostagni, *Zs. f. Phys.*, **88**, 55, 1934.

⁴⁶ Hughes and DuBridge, *op. cit.*, sec. 4 2.

⁴⁷ L. A. DuBridge, *Phys. Rev.*, **43**, 727, 1933.

⁴⁸ W. W. Rochr, *Phys. Rev.*, **44**, 866, 1933.

cerning them. The following summary of information therefore applies primarily to clean metal surfaces. Instead of the photoelectric threshold frequency, ν_0 , the more customary threshold wave length, λ_0 , measured in angstroms, will be used.

In the usually observed photoelectric effect⁴⁹ characteristic of most pure metals, λ_0 is in the neighborhood of 2500–3500 Å. The photoelectric efficiency $\chi(\nu)$ rises beyond the threshold as about $(\nu - \nu_0)^n$, where n is generally between 2 and 3, and reaches a maximum value, χ_{\max} , at ν equal to about $3\nu_0/2$; this maximum value is about 10^{-4} electrons per absorbed photon. The photoelectric efficiency then falls off with increasing frequency. At very high frequencies it may rise again, when electrons begin to be released throughout the volume of the solid as well as at the surface. The volume photoelectric effect should also be present in nonmetallic crystals, where no surface effect is to be expected. However, this volume effect usually lies so far in the ultraviolet that it may be neg-

TABLE 5
PHOTOELECTRIC EFFICIENCY AND THRESHOLD

Substance	Threshold Wave Length	Electrons/Photon χ_{\max}	Wave Length of Maximum Efficiency
K*	5,500 Å	1×10^{-4}	3200 Å
K sensitized*	5,500	2×10^{-2}	3200
Pt†	2,800	3×10^{-5}	
Al†	3,500?	2.3×10^{-4}	
Ag-Cs ₂ -Cs‡	12,000	1.2×10^{-3} §	7500
		5×10^{-3}	4000
Ag-Na ₂ O-Na‡	6,800	8×10^{-3}	4100

* F. Klauser, *Ann. d. Phys.*, **5**, 20, 909–18, 1934.

† *International Critical Tables*.

‡ W. Kluge, *Phys. Zs.*, **34**, 115, 1933.

§ Shows two maxima of $\chi(\nu)$.

lected in interstellar space. The resultant “typical” distribution-curve may be represented quite approximately by the equation

$$\chi(\nu) = \frac{b}{\nu^4} \left(1 - \frac{\nu_0}{\nu} \right)^2. \quad (58)$$

where b is a constant which depends, of course, on the nature of the surface. This expression has a maximum value when ν is $3\nu_0/2$ and fits many of the observed data in a general way. Specific observational curves sometimes show large deviations from this wholly empirical relationship, which is introduced here simply for an approximate evaluation of what may be expected.

A selective photoelectric effect of higher photoelectric efficiency is also observed, which depends markedly on the state of the surface and which shows a much sharper maximum than does equation (58). The values of χ_{\max} reached for surfaces specially sensitized in a hydrogen-glow discharge, for example, are in the neighborhood of 10^{-2} electrons per absorbed photon.

The distinction between these two types of photoelectric effects is not always clear cut. In addition, there is the so-called “normal” photoelectric effect, in which no maximum of $\chi(\nu)$ is observed. Despite its name, this particular effect is apparently of rare occurrence⁴⁹ and will not be considered. Values of λ_0 , χ_{\max} , and the frequency at which $\chi(\nu)$ reaches χ_{\max} are listed in Table 5 for a number of surfaces, together with the sources

⁴⁹ K. Mitchell, *Proc. Roy. Soc., London, A*, **153**, 513, 1936.

of the information. This table is not presented as definitive but merely as illustrative of the range of values observed. The measured values of $\chi(\nu)$ refer to the number of electrons emitted per photon incident on the photoelectric surface; but, since the reflection coefficients of most metals are generally much less than 50 per cent in the ultraviolet region, the correction for reflected light is unimportant.

In view of the many uncertainties both in the nature of interstellar grains and in the photoelectric emission to be expected from complex surfaces, it is obviously not possible to specify the values of λ_0 and $\chi(\nu)$ to be expected for these grains, and a wide range of possibilities must be considered. To indicate the nature of the possible effects to be expected, three different surfaces will be considered, as follows: surface A is a highly photoemissive surface, with a threshold at 5000 Å and a maximum photoelectric efficiency χ_{\max} of 10^{-2} ; surface B is a moderately photoemissive surface, with a threshold at 2500 Å and a χ_{\max} of 10^{-4} ; surface C is a dielectric surface for which χ_{\max} is so small that it may be set equal to zero. Equation (58) will be assumed for surfaces A and B; the broad maximum assumed for $\chi(\nu)$ will result in an overestimate of the photoelectric emission for surface A, since so high a value of χ_{\max} usually corresponds to a highly selective photoelectric effect. The actual grains in space probably correspond more to surface C than to either A or B, but the possibility of photoemissive grains cannot be excluded at the present time.

e) RELATIVE ABSORPTION CROSS-SECTION, $Q(\nu)$

Since measurements of the photoelectric efficiency are made with surfaces large compared to the wave length, a correction must be made for grains whose dimensions are comparable with, or smaller than, the wave length. The quantity $Q(\nu)$ has been defined as the absorption cross-section of the grain for radiation of frequency ν , divided by the geometrical cross-section. It is well known that for a spherical grain the ratio of the extinction cross-section (the sum of the scattering and absorption cross-sections) to the geometrical cross-section is small for long wave lengths, increases to a maximum value of about 3 for wave lengths equal to the circumference of the grain, and then decreases to a value of unity. The observational evidence on the sizes of the grains actually present is not conclusive, but it is frequently assumed that the grains have about the size required for maximum extinguishing power. Since the albedo of interstellar dust grains is apparently in the neighborhood of about $\frac{1}{2}$,⁵⁰ it is evident that a value of 1 for $Q(\nu)$ will be in accord with present conceptions. The assumption of a constant value for $Q(\nu)$ is presumably not valid in the visible and the infrared but should not be far from the truth in the ultraviolet, where the wave length presumably becomes less than the circumference of the grains. We shall accordingly set $Q(\nu)$ equal to 1. The uncertainty in this estimate is obviously very much less than the uncertainty in χ_{\max} .

With this constant value for $Q(\nu)$ and with $\chi(\nu)$ found from equation (58), the integrals I_1 and I_2 , defined in equations (47) and (48), may readily be computed; if also q_1 is set equal to 0.55, then, from equation (49), the effective color temperature T_{eff} for photoemission from uncharged grains may be computed for any threshold frequency ν_0 . For integrated starlight, these computations may be carried out with the use of Dunham's values⁹ again for $U(\nu)$, computed for selective absorption. Such computations have been carried out for several threshold wave lengths, and the results are given in Table 6. By the use of this table, together with equations (52) and (54), the effective color temperature T_{eff} for photoemission from a charged grain with surface A or B and the total photoelectric emission, measured by K , may readily be found. For comparison with former results³ it may be noted that the upper limit of 10 found previously for K corresponds to a value of 5×10^{-7} for I_1 , about three times the corresponding value for moderately emissive surface B.

⁵⁰ J. Greenstein, informal communication.

The computations may also be carried out on the assumption that the light from one star is dominant. This assumption is required near an early-type star, whose radiation outshines that of other stars, and may be required in all $H\ II$ regions if the picture pre-

TABLE 6
PHOTOEMISSION WITH DIFFERENT THRESHOLDS

Threshold Wave Length λ_t in Å	I_1/χ_{\max}^* (Per Cubic Centimeter)	I_2/χ_{\max} (Per Cubic Centimeter)	$\frac{I_2 - I_1}{I_1}$	Effective Color Tem- perature T_{cd}
2000.....	0.85×10^{-3}	1.24×10^{-3}	0.467	18,500°
2500.....	1.72	2.59	.507	16,000
3000.....	2.95	4.52	.532	14,000
4000.....	6.68	10.2	.525	10,500
5000.....	12.8	19.5	.528	8,500
6000.....	22.5	37.4	0.502	6,500

* The number of photoelectrons emitted from a grain per second per unit geometrical cross-section is I_1 times the velocity of light; thus I_1 is the effective density of photoelectron-producing photons.

sented by Strömgen¹⁰ is correct. If we introduce the usual dilution factor W , given in terms of the stellar radius R , and the distance h of the star by the expression

$$W = \frac{R^2}{4h^2} \quad (59)$$

and assume that the radiation from the star is that from a black body with a color temperature T_c , then the integrals I_1 and I_2 are given by

$$I_1 = A \chi_{\max} W T_c^3 \frac{e^{-\beta}}{\beta^3} \psi_1(\beta), \quad (60)$$

$$I_2 = A \chi_{\max} W T_c^3 \frac{e^{-\beta}}{\beta^3} \psi_2(\beta), \quad (61)$$

where

$$A = \frac{3^6 \pi}{2} \left(\frac{k}{hc} \right)^3 = 3.84 \times 10^2 \text{ cm}^{-3} \text{ deg}^{-3}, \quad (62)$$

and where, now,

$$\beta = \frac{h\nu_{0e}}{kT_c} = \frac{1.44}{\lambda_{0e} T_c}. \quad (63)$$

For threshold wave lengths between 1000 and 5000 Å and temperatures between 5000° and 50,000°, β ranges from about 0.5 to about 30. The functions ψ_1 and ψ_2 are integrals which may be evaluated in the same way as the integral in equation (28). Approximate values of these two functions are given in Table 7 for a few values of β . For large values of β both these functions approach unity. From equation (51) it is evident that the value of T_{cg} is given by

$$T_{cg} = \frac{q_1 T_c \beta (I_2 - I_1)}{I_1} = \psi_3(\beta) T_c, \quad (64)$$

where q_1 may be set equal to 0.55 as before. Values of $\psi_3(\beta)$, defined by this equation, are also given in Table 7. It will be noted that, with increasing β , T_{cg} tends to exceed T_c

by a considerable margin, a result of the fact that $\chi(\nu)$ is assumed to vanish as ν approaches the threshold frequency. From Table 7 the values of I_1 and T_{eg} needed in equations (50) and (54) may readily be determined for any values of ν_{0e} and T_c .

The assumptions made in these five subsections are summarized in Table 8, where the constants adopted for each of the three types of surfaces are listed. Values of constants in the first four rows must be used, together with Tables 6 and 7, to solve for the charge on the grain and G_{eg} . Those in the last two rows are required for the computation of values in Tables 6 and 7, but are not needed further.

TABLE 7
VALUES OF $\psi_1(\beta)$, $\psi_2(\beta)$, AND $\psi_3(\beta)$

β	$\psi_1(\beta)$	$\psi_2(\beta)$	$\psi_3(\beta) = T_{eg}/T_c$	β	$\psi_1(\beta)$	$\psi_2(\beta)$	$\psi_3(\beta) = T_{eg}/T_c$
0.5	0.0076	0.018	0.42	10	0.41	0.50	1.2
1.0	.025	.050	0.55	20	.59	.66	1.3
2.0	.073	.12	0.72	50	0.81	0.85	1.4
5.0	0.22	0.31	1.1				

TABLE 8
SUMMARY OF ADOPTED CONSTANTS FOR INTERSTELLAR GRAINS

Constant	Surface	A Metal Specially Sensitized	B Metal Unsen- sitized	C Nonmetallic Crystal
ξ_e	Sticking probability for electrons	0.5	0.5	0.1-0.5
ξ_i	Neutralization probability for ions	1	to	10^{-4}
λ_0	Photoelectric threshold for uncharged grain	5000 Å	2500 Å
χ_{max}	Maximum photoelectric efficiency, in electrons per photon	10^{-2}	10^{-4}	0
q_1	Fraction of available photoelectric energy appearing as kinetic energy	0.55	0.55
$Q(\nu)$	Ratio of absorption cross-section of grain to geometrical cross-section	1.0	1.0

VII. COSMIC RAYS

Encounters of cosmic rays with interstellar atoms will ionize these atoms and provide the emitted electrons with appreciable kinetic energy. Of course, kinetic energy gained by the electrons in this way is more than counterbalanced by the kinetic energy lost by the cosmic rays, which are believed to be rapidly moving protons. But the cosmic rays, or cosmic particles, as they will be called here, are moving so rapidly that they do not interact very strongly either with one another or with the more slowly moving electrons and atoms in interstellar space and obviously do not enter into the kinetic equilibrium established among the more numerous slowly moving electrons, atoms, and solid grains. It follows that any transfer of kinetic energy from the cosmic particles to the less energetic particles of the interstellar gas will increase the kinetic temperature of this gas.

The gain in kinetic energy resulting from such interactions between known cosmic particles and neutral H atoms may be computed quite simply. Specifically, one must find

the average net kinetic energy gained per encounter between an atom and a cosmic particle and then multiply this by the number of such encounters per particle per second; this product will equal the gain of kinetic energy per neutral H atom per second, denoted by G_{He} .

The kinetic energy carried off by the free electron will be denoted by E_{2c} , in conformity with previous notation. The energy lost when an electron is captured will be, as before, E_1 . Since the distribution of cosmic-ray energies is not accurately known, we shall assume here that all cosmic particles have an energy of 10^{10} electron-volts, which is the order of magnitude of the average energy⁵¹ of all the particles reaching the earth. A proton of this energy has a velocity within about $\frac{1}{2}$ per cent of the velocity of light, c . We may write

$$G_{He} = n_c v_c \sigma_{He} (\overline{E_{2c}} - \overline{E_1}), \quad (65)$$

where n_c is the number of cosmic particles per cubic centimeter and σ_{He} is the ionization cross-section of hydrogen for protons of 10^{10} volts. According to Bethe,⁵² the value of σ_{He} is 1.06×10^{-19} cm² for 10^6 -volt electrons, corresponding to protons of about 10^9 volts, and 1.33×10^{-19} cm² for electrons of 10^8 volts, corresponding to 10^{11} -volt protons. Since σ_{He} changes very slowly with the energy of the primary particle in this range, we may set σ_{He} equal to 1.2×10^{-19} cm²; the error of this estimate will scarcely exceed 10 per cent. The quantity $n_c v_c$ is four times the number of primary cosmic particles per square centimeter per second reaching the earth, which is known⁵³ to be 0.09. Hence $n_c v_c$ may be set equal to 0.36 per second per cm².

It remains to determine E_{2c} and $\overline{E_1}$. From Bethe⁵² one finds that the energy loss per ionization is about 68 electron-volts for the primary-particle energies of interest here. Since some 14 volts are required to ionize the atom, this leaves 54 electron-volts for the electron to carry away as kinetic energy. Hence $\overline{E_{2c}}$ equals 8.6×10^{-11} ergs. If, as in equation (8), we define a color temperature T_{ce} as $\overline{E_{2c}}/k$, T_{ce} is equal to $630,000^\circ$. The average energy $\overline{E_1}$ lost per electron capture, on the other hand, is approximately equal to the mean kinetic energy of the electrons, which is so small compared to $\overline{E_{2c}}$ that we may neglect it in equation (60).

Combining these various results we have, for G_{He} , the equation

$$G_{He} = 4.1 \times 10^{-30} \text{ erg/sec.} \quad (66)$$

Ionization of other atoms by cosmic particles will also occur. However, hydrogen is believed to be much the most abundant element in interstellar space, and equation (66) should certainly give the dominant contribution of known cosmic particles to the kinetic temperature of the slowly moving interstellar atoms in H I regions.

In H II regions the hydrogen is mostly ionized, and the interaction of cosmic particles with free electrons must be considered. It may be shown that the energy gain, G_{ec} , per free electron per second resulting from interactions with cosmic particles is about equal to the value of G_{He} found above. This equality results from the high velocities of these cosmic particles; the interaction between such a rapidly moving particle and an electron is much the same whether the electron is bound or free.

A detailed analysis indicates that for a free electron the lower limit for the energy gained per encounter is, of course, less than for a bound electron, and thus a free electron will gain energy from cosmic particles which pass too far away to affect a bound electron. The exact computation of the energy gained by free electrons is rather complicated,

⁵¹ J. A. Wheeler, informal communication.

⁵² *Op. cit.*, p. 519.

⁵³ I. S. Bowen, R. A. Millikan, and H. V. Neher, *Phys. Rev.*, **53**, 217, 1938.

since the elementary formulae for two-body encounters under inverse-square forces give divergent results when summed over infinitely distant encounters.⁵⁴ Approximate results can be obtained by considering only those encounters within a certain critical distance. Fortunately, the energy gain depends only logarithmically on this critical distance. As a result of this very weak dependence on the critical distance, the energy gain for a free electron per second will not much exceed that for a hydrogen atom, on the average, and we may set, approximately,

$$G_{ec} = 10^{-29} \text{ erg/sec.} \quad (67)$$

The greatest uncertainty in equations (66) and (67) results from the possible presence in interstellar space of cosmic particles whose energies are less than about 3×10^9 electron-volts. Such low-energy particles are not observed to reach the earth, presumably because of the cutoff resulting from the sun's magnetic field.⁵⁵ If, for example, the flux of particles per unit energy continues to increase with the inverse cube of the energy—the observed variation at high energies—down to proton energies as low as 10^6 volts, the total flux of particles would be greater than assumed by a factor of 10^7 . Since the cross-section for interaction between cosmic particles and either H atoms or electrons increases with decreasing energy, G_{He} and G_{ec} would be increased to at least 10^{-21} erg/sec per neutral atom or electron. Such a large rate of energy gain would constitute much the largest source of kinetic energy in both H I and H II regions. These low-energy particles would require strong replenishment in times of the order of 10^9 years, but at the present time their possible presence in interstellar space cannot be ruled out.

If the assumed flux of cosmic particles is accepted, then equations (66) and (67) are essentially correct. In such a case the contribution of cosmic rays to interstellar kinetic temperatures is generally negligible in regions where the density is as great as 10^{-24} gm per cubic centimeter, the value usually assumed for interstellar space. However, G_{ec} is independent of the density of the interstellar medium, while the other processes for energy gain and loss tend to vary proportionally with the density. Thus in a sufficiently rarefied gas the contribution of cosmic rays would be significant, and the kinetic temperature would be unexpectedly high. The densities at which such effects would occur are several orders of magnitude less than the accepted densities for interstellar gas close to the galactic plane, but it is not impossible that far from the galactic plane or even in some regions close to the plane cosmic rays may have an important effect. This subject will be discussed in more detail in a subsequent paper.

⁵⁴ S. Chandrasekhar, *Ap. J.*, **93**, 285, 1941.

⁵⁵ M. S. Vallarta and Godart, *Rev. Mod. Phys.*, **11**, 180, 1939.

A THEORETICAL DISCUSSION OF THE ULTIMATE LIMITS OF ASTRONOMICAL PHOTOELECTRIC PHOTOMETERS*

HAROLD L. JOHNSON

Lick Observatory

Received August 21, 1947

ABSTRACT

The various instrumental sources of error in astronomical photoelectric photometry are discussed from a theoretical standpoint. Methods of constructing photoelectric photometers for maximum performance are suggested, and the ultimate performance limits attainable with presently available components are discussed.

The largest available resistors (10^{13} ohms) should be used for the photoelectric-cell load-resistor in order to obtain the most favorable signal-to-noise ratio. With a 10^{13} -ohm resistor, a gas multiplication in the photoelectric cell of 3.5 is sufficient to extend the limiting magnitude to the point at which the cell begins to limit the precision of measure. The photoelectric-cell limit for a cell having the antimony-caesium surface (such as the 1P21 electron-multiplier phototube) is about magnitude 11.3 with a 12-inch refracting telescope while, if sufficient multiplication is used in the cell, it should be possible, although with less precision, to reach magnitude 16.3 with a 12-inch telescope.

I. INTRODUCTION

It has been known for some time that the "constant-deflection" method of measuring the small current from the photoelectric cell is inferior to the "rate-of-deflection" meth-

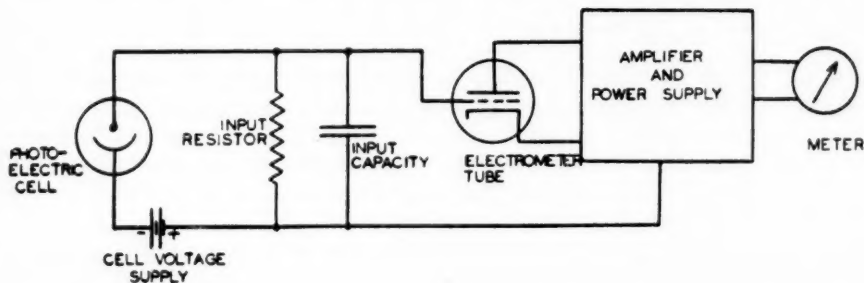


FIG. 1.—Simplified schematic diagram of a typical photoelectric photometer

od.¹ However, the former's greater convenience has caused it to be widely used. In the constant-deflection method the current from the photoelectric cell produces a voltage drop across a resistor, and this voltage is then measured by a sensitive vacuum-tube voltmeter. Both the resistor² and the tubes³ in a circuit of the type shown in Figure 1 produce random electrical disturbances, which are commonly called "noise." This noise will limit the use of the photometer to objects brighter than a certain limiting magnitude, which depends upon (1) the amplifier signal-to-noise ratio, (2) the characteristics of the photoelectric cell, and (3) the precision desired from the observations and the amount of time devoted to making the observations.

* Contributions from the Lick Observatory, Ser. II, No. 21.

¹ Sinclair Smith, *Ap. J.*, **76**, 1, 1932.

² J. B. Johnson, *Phys. Rev.*, **32**, 97, 1928.

³ W. Schottky, *Ann. d. Phys.*, **57**, 541, 1918.

II. THE AMPLIFIER SIGNAL-TO-NOISE RATIO⁴

The two sources of noise in the amplifier are the input resistor and the vacuum tubes (in practical astronomical photometer amplifiers the noise from only the first tube is important).

The mean-square noise-voltage produced by a resistor is:⁵

$$\overline{E_R^2} = 4kTR \int_0^\infty \Psi(f) df, \quad (1)$$

where

k = Boltzman's constant = 1.374×10^{-23} joule/° K ;

T = The absolute temperature of the resistor ;

R = The resistance of the resistor in ohms ;

$\Psi(f)$ = The relative power gain as a function of the frequency, f , of the device used to detect the noise .

In the case of astronomical photoelectric photometers, in which a single RC circuit limits the band-width of the entire photometer,

$$\Psi(f) = \frac{1}{1 + 4\pi^2 R^2 C^2 f^2}. \quad (2)$$

Note that when $f = 0$ (direct current), $\Psi(f) = 1$. There will be a frequency for which $\Psi(f) = \frac{1}{2}$, called the "half-power point" and designated by f_0 . From equation (2) we obtain

$$f_0 = \frac{1}{2\pi RC}. \quad (3)$$

Substituting equation (2) in equation (1) and noting equation (3), we have

$$\overline{E_R^2} = 2\pi kTR f_0. \quad (4)$$

There are two sources of noise from a vacuum tube: externally from the shot-effect of the grid current and internally from the tube itself, even when the grid is connected to the cathode. Only the shot-noise of the grid current is important in astronomical photoelectric photometers. The mean-square noise-voltage produced across the input resistor by the grid current is

$$\overline{E_g^2} = 2qI_g R^2 \int_0^\infty \Psi(f) df, \quad (5)$$

⁴ In the following sections these references may be of use: Johnson, *op. cit.*; H. Nyquist, *Phys. Rev.*, **32**, 110, 1928; F. B. Llewellyn, *Proc. I.R.E.*, **18**, 243, 1930; J. B. Johnson and F. B. Llewellyn, *Bell System Tech. J.*, **14**, 85, 1935; G. L. Pearson, *Bell System Tech. J.*, **13**, 634, 1934, or *Physics*, **5**, 233, 1934; E. A. and A. G. Johnson, *Phys. Rev.*, **50**, 170, 1936; E. A. Johnson and C. Neitzert, *Rev. Sci. Inst.*, **5**, 196, 1934; and F. E. Terman, *Radio Engineers' Handbook* (New York: McGraw-Hill Book Co., 1943).

⁵ These formulae are deduced on the assumption of a gaussian distribution of the instantaneous noise current, which assumption is valid so long as a large number of electrons are counted within the time-constant of the photometer. In the event that cases should arise in which the distribution law cannot be assumed to be normal, further information is given by S. O. Rice, *Bell System Tech. J.* **23**, 282, 1944, and **24**, 46, 1945.

where

q = The charge on the electron = 1.603×10^{-19} coulomb ;

I_g = The D.C. grid current in amperes ;⁶

R = The input resistor as in equation (1) ;

$\Psi(f)$ = The relative power gain as in equation (1) .

Substituting equation (2) in equation (5) and noting equation (3), we have

$$\overline{E_g^2} = \pi q I_g R^2 f_0 . \quad (6)$$

The total noise-voltage produced by the input resistor and the first tube's grid current is

$$(\overline{E^2})_{\text{amplifier}}^{1/2} = (\overline{E_R^2} + \overline{E_g^2})^{1/2} = [(2\pi kTR + \pi q I_g R^2) f_0]^{1/2} . \quad (7)$$

Designating the signal current from the photoelectric cell by S , we find that the signal-to-noise ratio for the amplifier is

$$\begin{aligned} \left(\frac{S}{N}\right)_{\text{amplifier}} &= \frac{SR}{[(2\pi kTR + \pi q I_g R^2) f_0]^{1/2}} , \\ \text{or} \quad \left(\frac{S}{N}\right)_{\text{amplifier}} &= \frac{S}{\left[\left(\frac{2\pi kT}{R} + \pi q I_g\right) f_0\right]^{1/2}} . \end{aligned} \quad (8)$$

This equation shows that, in order to obtain the largest possible signal-to-noise ratio, the grid current, I_g , of the electrometer tube must be as small as possible and the input resistor, R , must be as large as possible. If we set

$$\begin{aligned} \frac{2\pi kT}{R} &= \pi q I_g , \\ \text{or} \quad R &= \frac{2kT}{q I_g} , \end{aligned} \quad (9)$$

we obtain nearly the maximum possible signal-to-noise ratio. It will increase the signal-to-noise ratio only 40 per cent to increase R to infinity from the value given by equation (9).

In practice, I_g is fixed by the electrometer tubes which are available and is about 10^{-15} ampere. For this value of I_g , a 10^{-15} -ampere signal current, and for $f_0 = 0.010$ cycle per second, Table 1 gives, for several values of R , the amplifier noise-voltage at the grid of the tube, the signal-to-noise ratio, the improvement (in magnitudes) to be expected over the results with a 10^{11} -ohm resistor, and, finally, the time-constant to be expected with the several resistors, for a typical photometer having an input capacity of 1.6×10^{-11} farad. T is taken as 300°K .

The "optimum"-size resistor, i.e., that resistor for which the resistor noise is equal to the shot-noise from grid current, is, according to equation (9), 5×10^{13} ohms, for a tube whose total grid current is 10^{-15} ampere. Resistors of this size are not available at

⁶ The grid current of a vacuum tube consists of two currents flowing in opposite directions. The symbol I_g denotes the sum of these two currents without regard to sign.

the present time, the highest value obtainable being 10^{13} ohms. Nevertheless, a 10^{13} -ohm resistor is worth using, for Table 1 shows that a 10^{13} -ohm resistor gives a 2.4-mag. improvement over a 10^{11} -ohm resistor. The plate resistance of the photoelectric cell is in parallel with the input resistor, and the size of the effective input resistance will always be limited to the plate resistance of the cell. The plate resistance of a cell is the slope of the curve, anode current versus anode voltage, at the operating point, and Steinke⁷ has given such a curve for a gas cell operated on potentials up to 75 volts. The slope of this curve is of the order of 10^{17} ohms at 75 volts, but at this voltage it is dropping rapidly. Plate resistances of this size, or even down to 2 or 3×10^{14} ohms, will not be troublesome so long as the electrometer-tube grid current is 10^{-15} ampere. Such resistances, however, will limit the improvement obtainable from reduction of the tube grid current below 10^{-15} ampere.

When a 10^{13} -ohm resistor is installed in a photometer, the time-constant of 160 seconds becomes inconveniently long; and, with a 10^{14} -ohm resistor, the time-constant of

TABLE 1
AMPLIFIER CHARACTERISTICS

Input Resistor R (Ohms)	Amplifier Noise (Volts)	$(S/N)_{\text{amplifier}}$	Improvement in Magnitudes	Time-Constant (Seconds)
10^{10}	1.6×10^{-6}	6.3	-1.25	0.16
10^{11}	5.1×10^{-6}	20	0.0	1.6
10^{12}	1.6×10^{-5}	63	+1.25	16
10^{13}	5.5×10^{-5}	182	+2.4	160
10^{14}	2.8×10^{-4}	357	+3.1	1600
10^{15}	2.3×10^{-3}	434	+3.3	16,000

1600 seconds would be much too long. Accordingly, if an input resistance of this size is to be used, the time-constant of the photometer must be reduced. One might think, at first, of reducing the input capacity of the photometer, but 1.6×10^{-11} farad is nearly as small as can be obtained. It is necessary, then, to find some other method of reducing the effect of this capacity, and two methods of accomplishing this result will be considered later in this paper. Let it be assumed, for the present, that, in some unspecified way, the time-constant of the photometer has been made compatible with the desired observation time.

III. THE CHARACTERISTICS OF THE PHOTOELECTRIC CELL AND THE APPLICATION TO ACTUAL PHOTOMETRY

The signal current from the photoelectric cell consists of a definite number of electrons per second and, as a result, it produces noise in exactly the same manner as does the grid current of the electrometer tube. In this case, however, before the current is fed through the input resistor, it is multiplied⁸ M times in the photoelectric cell. Therefore, the mean-square noise-voltage produced across this input resistor by the shot-noise of the photoelectric current is, from considerations similar to those leading to equation (6),

$$\overline{E_{pc}^2} = \pi q I_1 M^2 R^2 f_0, \quad (10)$$

⁷ Eduard Steinke, *Zs. f. Phys.*, **38**, 378, Fig. 3, 1926. Such curves may also be found in the R.C.A. *Tube Handbook*, but they are given there for much too large anode currents.

⁸ The term "multiplication" will be used to denote amplification taking place entirely within the photoelectric cell, whether it be gas amplification or secondary-emission amplification.

where

I_1 = The initial photocurrent from the photosensitive surface.

Even if a photometer which produced no noise of its own could be constructed, it would be found that the accuracy of measurement of the brightness of a star would still be limited by the signal-to-noise ratio of starlight itself. This finite signal-to-noise ratio of starlight is due to two effects: (1) seeing fluctuations in the earth's atmosphere and (2) random arrival of light quanta at the photosensitive surface. Only the first effect will be considered here, since the second will not become important until photosensitive surfaces whose quantum efficiency is more than 30 per cent become available.

The mean-square noise-voltage produced across the input resistor by the seeing fluctuations is

$$\overline{E_s^2} = AM^2 I_1^2 R^2 f_0, \quad (11)$$

where

A = The seeing constant.

Since at Mount Hamilton the relative root-mean-square fluctuation due to seeing is 1.4 per cent for a band-width of 0.1 c.p.s.,⁹ $A = 2 \times 10^{-3}$ second. There will be a value of I_1 for which the shot-noise from the photoelectric cell will be equal to the seeing noise. This value of I_1 , which will be termed I_L , is found, by equating equations (10) and (11), to be

$$I_L = \frac{\pi q}{A} = 2.5 \times 10^{-16} \text{ ampere}. \quad (12)$$

For smaller initial photocurrents the photoelectric cell limits the precision of measure; for larger currents the seeing limits the precision. Accordingly, this current, defined by equation (12), will be called the "photoelectric-cell limit."

By the same reasoning, the point at which the amplifier noise and the noise from the photoelectric cell are equal should be called the "amplifier limit." Setting the sum of equations (4) and (6) equal to the sum of equations (10) and (11), we have

$$2\pi kTRf_0 + \pi q I_g R^2 f_0 = \pi q I_1 R^2 M^2 f_0 + AM^2 I_1^2 R^2 f_0,$$

or

$$M^2 = \frac{2\pi kT}{R(\pi q I_1 + A^2 I_1^2)} + \frac{\pi q I_g}{(\pi q I_1 + A I_1^2)}, \quad (13)$$

from which the multiplication necessary in the photoelectric cell to make the amplifier and photoelectric-cell noises equal can be computed. Table 2 and Figure 2 contain this information for several values of R and for two values of I_1 : 2.5×10^{-16} and 2.5×10^{-18} amperes. In Case I the amplifier and photoelectric-cell limits coincide, while in Case II the amplifier limit occurs at $\frac{1}{10}$ the current for which the photoelectric-cell limit occurs. As before, it is assumed that $I_g = 10^{-15}$ ampere, and that $T = 300^\circ \text{K}$.

The values in Table 2 for 10^2 and 10^4 ohms are given to show the minimum resistance which can be used with an electron-multiplier phototube such as the 1P21. Of course, a resistor of only 100 ohms would never be used in any practicable amplifier following a 1P21, but this figure may be of interest to those who are planning to operate a 1P21 directly into a low-impedance galvanometer.

⁹ G. E. Kron, *Pub. A.S.P.*, **52**, 250, 1940. Kron gives the signal-to-noise ratio of starlight at Mount Hamilton as 100 to 1 for an instrument with a period of 10 seconds. He has stated to the writer that this means that the probable error of a single deflection taken in 10 seconds is 1 per cent and that, for this instrument, $2\pi RC = 10$ seconds.

TABLE 2
MULTIPLICATION WITHIN PHOTOELECTRIC CELL, M

Input Resistor, R (Ohms)	Case I ($I_1 = I_L$)	Case II ($I_1 = 0.01 I_L$)
10^2	1.02×10^6	1.44×10^7
10^4	1.02×10^6	1.44×10^6
10^{10}	102	1440
10^{11}	32	455
10^{12}	10.3	145
10^{13}	3.5	50
10^{14}	1.8	25
10^{15}	1.4	21

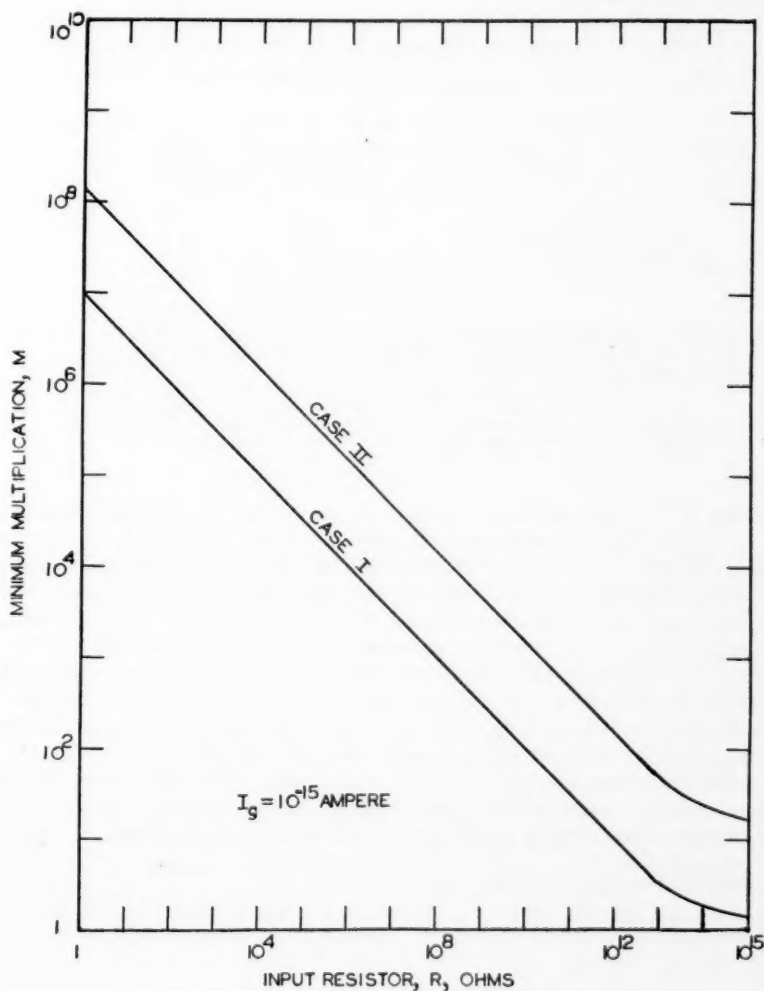


FIG. 2.—Minimum multiplication in the photoelectric cell as a function of the input resistance

With the foregoing results, it is possible to compute the limiting magnitudes for particular photoelectric cells. Table 3 contains such information for three cells and for a 1P21 tube whose performances have been evaluated by Kron.¹⁰ The standard light-source was the image of an A0 star at the focus of the 12-inch Lick refractor.

In order to reach the limits of Case I it is necessary to reduce the dark current from the photosensitive surface to less than 2.5×10^{-16} ampere. All these cells (except the Kunz) will require refrigeration in order to reach so small a current. In order to reach the limits of Case II the dark current from the photosensitive surface must be reduced to less than 2.5×10^{-18} ampere. That this can be done for the antimony-caesium surface has been shown by Engstrom,¹¹ who has obtained a dark current of about 2×10^{-21} ampere at the temperature of liquid air (-190°C). With regard to the caesium oxide surface Z. Bay¹² has observed a dark current of only $\frac{1}{60}$ electron per second (3×10^{-21} ampere) from a secondary-emission multiplier tube having this initial surface and cooled to the temperature of liquid air.

TABLE 3
LIMITING MAGNITUDE*

Type of Cell	Case I ($I_1 = I_L$)	Case II ($I_1 = 0.01 I_L$)
Kunz (K-H).....	7.8	12.8
K97087 (CsO-Ag).....	8.5	13.5
(929)† (Sb-Cs).....	11.3	16.3
1P21 (Sb-Cs).....	11.3	16.3

* The magnitude at which the amplifier begins to limit the precision seriously. In all cases the proper multiplication, M , given in Table 2, must be used to obtain the tabulated results.

† Since the 929 is a vacuum cell, these magnitudes do not apply to it. R.C.A. phototubes 5581, 5582, and 5583, recently announced, are gas cells having the same photosensitive surface as the 929, and presumably they will give the performance indicated in the table, within the limits of multiplication assigned by the manufacturer.

From Table 2, it is found that a multiplication of 3.5 for the 10^{13} -ohm resistor is necessary to attain the photoelectric-cell limit. This multiplication can be obtained from commercial gas-filled cells currently available. Accordingly, it should be possible to build, at the present time, a photoelectric-cell photometer which reaches the point at which the cell begins to limit the precision of measurement. In order to extend this point to fainter magnitudes, it will be necessary to obtain photosensitive surfaces with a higher quantum efficiency than those now available. The quantum efficiency of the antimony-caesium surface is about 10 per cent.¹³ If a photosensitive surface with a quantum efficiency of 100 per cent were available, the limiting magnitudes would be about 2.5 mag. fainter than for the antimony-caesium surface.

It is possible, of course, to go to fainter magnitudes (with less precision) with the present photosensitive surfaces by pushing the amplifier limit to fainter magnitudes. This procedure, however, would require a multiplication of 50 or more. A multiplication

¹⁰ *Ap. J.*, **103**, 326, 1946; *Lick Obs. Contr.*, Ser. II, No. 13.

¹¹ *J. Opt. Soc. Amer.*, **37**, 420, 1947. G. E. Kron (*Ap. J.*, **103**, 326, 1946; *Lick Obs. Contr.*, Ser. II, No. 13) has obtained a dark current of about 10^{-18} ampere at the temperature of dry ice (-78°C).

¹² *Rev. Sci. Inst.*, **12**, 127, 1941.

¹³ G. E. Kron, "The Adaptation of Photo-electric Devices to the Properties of the Electron," to be published soon in the "Harvard Symposium on Eclipsing Binaries." This figure may also be deduced from data given in the *R.C.A. Tube Handbook*.

of this order is obtainable in the Kunz cell, and it should be possible to attain this value with the other photosensitive surfaces, although not in the presently available cells. Stable gas multiplications as high as 615 have been obtained,⁷ and it may be possible in the future to obtain photoelectric cells which can be operated stably with a gas multiplication of 100.

In this connection it should be pointed out that, when a photoelectric cell has a gas multiplication of 5, this does not mean that every electron which leaves the cathode produces, on its way to the anode, exactly 4 electrons from the gas. What it does mean is that, *on the average*, 5 electrons reach the anode for every one which leaves the cathode. The dispersion about this mean produces additional noise, and the precision of measure will be poorer than that considered here. Steinke¹⁴ has found that for gas multiplications up to about 50 this effect is quite small but that for larger multiplications the additional noise can be several times that predicted by the shot-effect alone. B. A. Kingsbury¹⁵ has obtained similar data, but his results show that the critical value of gas multiplication for which the additional noise becomes serious is considerably smaller than that found by Steinke. It may be that this additional source of noise in the photoelectric cell will preclude the use of larger gas multiplications than can be obtained in commercially available cells.

These remarks also apply, in part, to the electron-multiplier phototube. In this case the random variations in secondary emission cause a slight increase in the noise output, probably of the order of 15 per cent.¹⁶ This increase will have only a small effect upon the results given above.

IV. THE PRECISION OBTAINED FROM THE OBSERVATIONS AND THE TIME SPENT MAKING THEM

The over-all signal-to-noise ratio of the photometer plus seeing, from considerations similar to those leading to equation (8), is

$$\left(\frac{S}{N}\right)_{\text{over all}} = \frac{I_1 M}{\left[\left\{ \frac{2\pi kT}{R} + \pi q I_g + (\pi q I_1 + A I_1^2) M^2 \right\} f_0 \right]^{1/2}}. \quad (14)$$

Since the signal-to-noise ratio is the reciprocal of the relative root-mean-square error of measurement, the probable error of measurement is therefore given by

$$\epsilon = \frac{0.6745}{\left(\frac{S}{N}\right)_{\text{over all}}}; \quad (15)$$

and Figure 3 shows the variation of ϵ as a function of I_1 , for the two cases previously considered, together with the limiting case for $M = \infty$.

It is possible now to compute the probable errors at the limiting magnitudes for the two cases in Tables 2 and 3. For Case I, $\epsilon = 0.059(f_0)^{1/2}$; for Case II, $\epsilon = 0.42(f_0)^{1/2}$. Remembering that $f_0 = 1/2\pi RC$, we find that, for a 16-second time-constant, the probable error at the limiting magnitude of Case I is ± 0.006 mag., and for Case II, ± 0.04 mag.

¹⁴ *Op. cit.* Apparently, Steinke has taken his data from only one cell.

¹⁵ *Phys. Rev.*, **38**, 1458, 1931.

¹⁶ Engstrom, *op. cit.*

The question of the most efficient time of reading the meter now arises. The probable errors obtained in these calculations are based upon a given band-width for the photometer and upon a single completed deflection of the meter; they do not, therefore, depend upon the time at which the meter is read. It has been the practice at the Lick Observatory to take the meter reading $2\pi RC$ seconds after the deflection is begun. After this time the deflection is 99.8 per cent complete, and the probable errors obtained here apply. Since the deflection of the meter is an exponential function of time ($1 - e^{-t/RC}$), the time of reading the meter can be reduced considerably from $2\pi RC$ seconds, with no

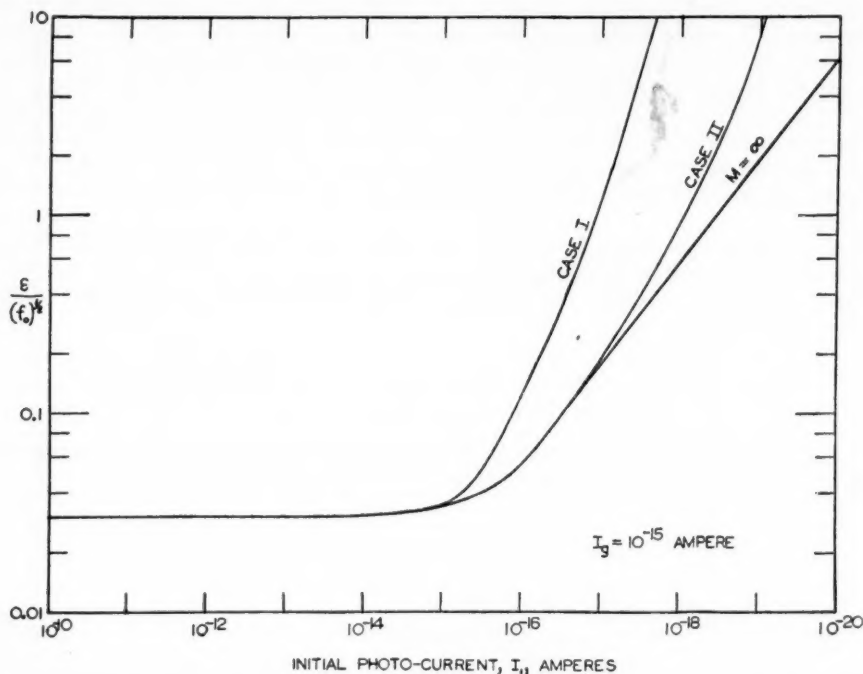


FIG. 3.—The probable error as a function of the initial photocurrent

great reduction in the deflection. As a result, it should be possible thereby to obtain an appreciable increase in the precision in a given interval of time.

V. METHODS OF REDUCING THE OVER-ALL TIME-CONSTANT OF THE PHOTOMETER

We now consider two methods of reducing the effect of the input capacity of the photometer: (1) partial neutralization of the input capacity by positive feedback¹⁷ and (2) the use of a differentiating amplifier following the electrometer tube.¹⁸

¹⁷ Kron, *Pub. A.S.P.*, **59**, 190, 1947.

¹⁸ In a private communication to R. W. Engstrom, (n. 16) D. O. North of R.C.A. Laboratories Division, Princeton, N.J., has stated that the optimum detection circuit should have a very large input impedance, with compensating networks in the amplifier to give net band-width much greater than that of the input circuit. The statement was made with regard to the electron multiplier (such as the 1P21), but it applies equally well to all types of photoelectric cells.

1. *Partial neutralization of the input capacity by positive feedback.*—For convenience in the initial computations, we shall use the simplified circuit in Figure 4, where

R = The total resistance in the circuit (plate resistance of the photoelectric cell, grid resistor, input resistance of the electrometer tube—all in parallel) ;

C = The total circuit capacity (not including the feedback capacity) ;

KC = The feedback capacity ($K = \frac{\text{Feedback capacity}}{\text{Circuit capacity}}$) ;

μ = An ideal amplifier having a gain of μ , infinite input impedance, and zero output impedance ;

E = The voltage to be measured ;

I = Current from an infinite-impedance source into the circuit.

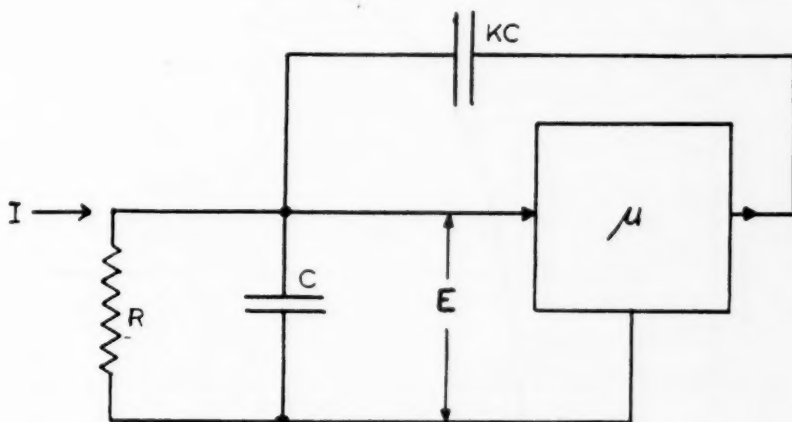


FIG. 4.—Simplified feedback circuit

It may readily be shown¹⁹ that

$$|E| = \frac{IR}{\{1 + 4\pi^2 f^2 R^2 C^2 [K(1 - \mu) + 1]^2\}^{1/2}} \quad (16)$$

To impose the condition of constant band-width, we have

$$\mu = \frac{1}{K} \left(1 - \frac{1}{2\pi f_0 R C} \right) + 1, \quad (17)$$

or

$$R = \frac{1}{2\pi f_0 C [K(1 - \mu) + 1]}.$$

¹⁹ For methods of obtaining the formulae in this section consult: Hendrick W. Bode, *Network Analysis and Feedback Amplifier Design* (New York: D. Van Nostrand Co., 1945); and Terman, *op. cit.*

Substituting this value of R in equation (16), we obtain

$$|E| = \frac{IR}{\left[1 + \left(\frac{f}{f_0}\right)^2\right]^{1/2}} = \frac{I}{\left[1 + \left(\frac{f}{f_0}\right)^2\right]^{1/2} \{2\pi f_0 C [K(1 - \mu) + 1]\}}. \quad (18)$$

It may be noted that the band-width (and therefore the time-constant) is independent of R , provided that the value of μ given by equation (17) is used. The required value of μ is given in Figure 5, where it has been assumed, as an example, that

$$f_0 = 0.010 \text{ c.p.s. (effective } RC = 16 \text{ seconds) ,}$$

$$K = 0.25 ,$$

$$C = 1.6 \times 10^{-11} \text{ farad.}$$

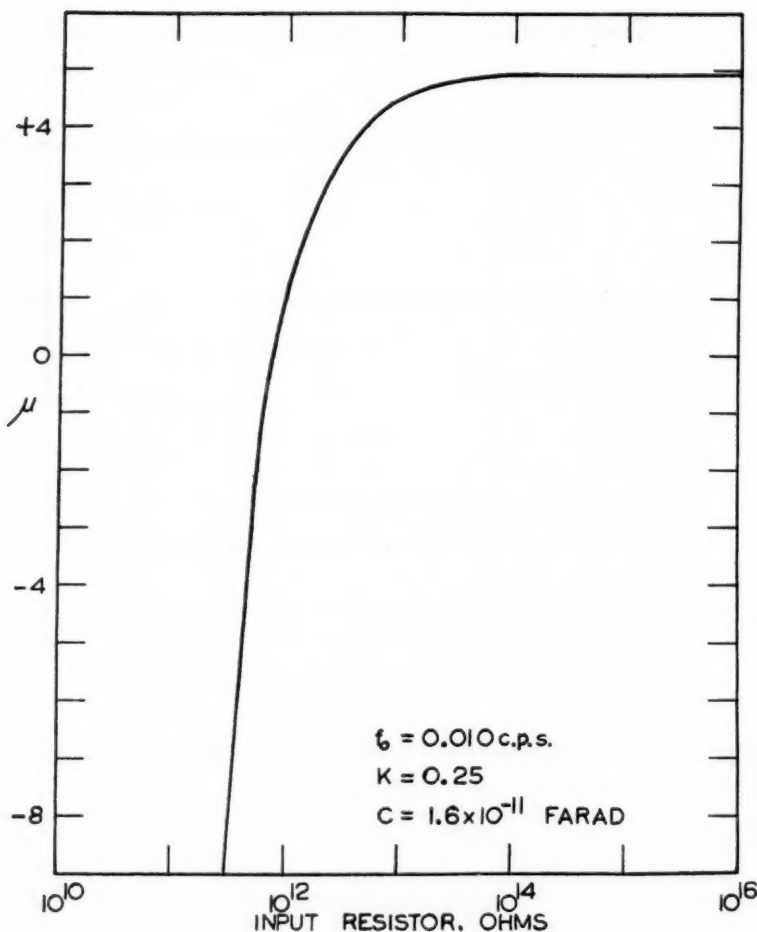


FIG. 5.—Feedback amplifier gain, μ , as a function of the input resistance. Negative μ indicates 180° phase shift in the feedback amplifier.

It should be pointed out that, while the gain of the feedback amplifier need not be large, it must be *extremely* stable. Reference to Figure 5 will show this point very well. For example, the effective capacity of the circuit changes by a factor of 10 as the resistor changes from 10^{13} to 10^{14} ohms, but the gain of the amplifier changes only from 4.60 to 4.96. The second method of reducing the effect of the input capacity does not have this disadvantage, as will become evident in the following discussion.

2. *The use of a differentiating amplifier following the electrometer tube.*—Let us consider the simplified schematic diagram shown in Figure 6, where

R_1 = The photoelectric cell load-resistor (the same as R in Part I of this section) ;

C_1 = The input capacity of the photometer ;

R_2, C_2 , and R_3 are the component parts of the differentiating circuit.

Furthermore, each amplifier is assumed to be an ideal one, with an infinite input impedance and zero output impedance. For convenience the amplifier gains are as-

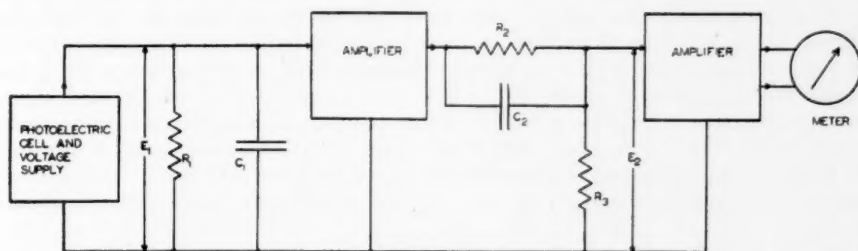


FIG. 6.—Simplified schematic diagram of a photoelectric photometer using a differentiating amplifier following the electrometer tube.

sumed to be unity (the gains of the amplifiers do not enter into the calculations). Also the photoelectric-cell current will be assumed to be 1 ampere.

On the basis of the foregoing assumptions we have

$$E_1 = \frac{R_1}{1 + j2\pi f R_1 C_1}, \quad (j = \sqrt{-1}) \quad (19)$$

$$E_2 = \frac{R_1}{1 + j2\pi f R_1 C_1} \cdot \frac{1 + j2\pi f R_2 C_2}{1 + \frac{R_2}{R_3} + j2\pi f R_2 C_2}. \quad (20)$$

If $R_2 C_2 = R_1 C_1$, we have an equation of the same form as equation (19):

$$E_2 = \frac{\frac{R_1 R_3}{R_2 + R_3}}{1 + j2\pi f R_1 C_1 \left[\frac{R_3}{R_2 + R_3} \right]}. \quad (21)$$

The final result is, then, that we have the effect of a simple RC circuit exactly like $R_1 C_1$, except that the band-width is now greater—or that the time-constant is shorter.

Since only relative voltages are involved, the resistances may be taken to the left member of the equation. Since the phase response is of no interest, we may take the absolute value:

$$|E_{\text{relative}}|^2 = \frac{1}{1 + 4\pi^2 f^2 R_1^2 C_1^2 \left[\frac{R_3}{R_2 + R_3} \right]^2}. \quad (22)$$

If f_0 is the half-power point, we have

$$R_3 = \frac{R_2}{2\pi f_0 R_1 C_1 - 1}, \quad (23)$$

$$R_2 C_2 = R_1 C_1.$$

These last two equations completely describe a simple circuit which may be inserted in an appropriate place in the D.C. amplifier and which will result in exactly the same performance from the completed photometer as the neutralization previously discussed. This circuit operates by amplifying the higher frequencies very much more than the lower frequencies, in order to make up the high-frequency deficiency appearing in the long time-constant photoelectric-cell load-circuit. Therefore, one is justified in inquiring whether additional tube noises, such as the shot-noise at the anode or thermal noise in the plate resistance of the first tube (previously neglected in the discussion), could not limit the usefulness of the circuit. If this additional tube noise-voltage is $\frac{1}{3}$, or less, of the noise-voltages already considered, it will have a negligible effect upon the signal-to-noise ratio. In astronomical photoelectric photometers, such additional tube noise should not exceed 10^{-6} volt r.m.s. after reduction for the gain of the first tube. It can be seen from Table 1 that, for input resistors of 10^{11} ohms or higher, the noise-voltage from the input resistor and from the grid current is at least three times larger than this additional tube noise.

A disadvantage of this circuit is that it is a very high-impedance device, at least for the time-constants which appear in astronomical photoelectric photometers, and care will have to be taken when including the circuit in a D.C. amplifier. If the network is installed in a push-pull amplifier, one such network should be inserted in each side of the push-pull circuit.

It should be emphasized here that, when properly used, these circuits (or any other method of accomplishing the same result) do not affect the signal-to-noise ratio in any way; they merely make it possible to take readings more rapidly or more often.

VI. SUMMARY

Since the signal-to-noise ratio of a photoelectric photometer increases as the photoelectric cell load-resistor increases, a considerable improvement can be obtained by the use of the largest available resistors. The shot-noise of the electrometer-tube grid current limits the signal-to-noise ratio for large resistors; but, for resistors which at present can be obtained (up to 10^{13} ohms), the resistor noise still predominates.

The impracticably long time-constants which result from the use of such large input resistors can be effectively reduced in at least two ways. Therefore, it should be possible to build a photometer which has a convenient time-constant and which employs resistors of 10^{13} ohms or higher.

The resistor noise and grid-current noise can be overcome for any size photoelectric cell load-resistor by employing enough multiplication in the photoelectric cell itself. If sufficient multiplication (3.5 with a 10^{13} ohm resistor) is employed in a cell having the antimony-caesium surface, magnitude 11.3 can be reached with a 12-inch refracting telescope before the photometer begins to interfere seriously with the precision of the meas-

ures. Further, if it is sufficient to have a probable error of 4 per cent with a time-constant of 16 seconds, the foregoing limit can be extended by another 5 mag.—to magnitude 16.3—provided, of course, that sufficient multiplication is employed in the photoelectric cell. A commercial gas-filled cell can be operated with sufficient multiplication to reach the first, or photoelectric-cell, limit; but, at the present time a secondary-emission multiplier is necessary if objects so faint as magnitude 16.3 are to be observed with a 12-inch telescope.

It may be of some interest to extrapolate these results to a 100-inch telescope. For the antimony-caesium surface the photoelectric-cell limit is magnitude 15.9; and it should be possible, with a 1P21 electron-multiplier phototube, to attain magnitude 20.9 with a probable error of ± 0.04 mag.²⁰

In many cases a photometer sensitive to red light is wanted, and the caesium oxide-silver surface is the best one available. The photoelectric-cell limit for this surface is magnitude 8.5 with a 12-inch refracting telescope; and this limit can be reached with commercially available components. The corresponding limit with a 100-inch telescope is magnitude 13.1. If a cell which has this surface and a stable multiplication of 50 or more becomes available,²¹ it should be possible to attain magnitude 18.1 in red light with a 100-inch telescope.

It should be pointed out that the faintest limiting magnitudes computed above are those to be expected on the basis of the ultimate sensitivity of the photoelectric photometer alone. Unfortunately, in actual astronomical photometry there are other factors which may prevent the attainment of such faint limiting magnitudes. Chief among these factors is sky illumination, the effect of which is normally reduced by use of the smallest possible diaphragm in front of the photoelectric cell. This device, however, may not be sufficient to permit the observation of celestial objects so faint as the twenty-first magnitude.

²⁰ G. E. Kron (*Ap. J.*, **103**, 326, 1946) gives a magnitude of 21.4 ± 0.03 with a 100-inch telescope, in substantial agreement with the result obtained here.

²¹ A secondary-emission electron multiplier with the caesium oxide surface has been announced by R.C.A. as "Developmental Tube Type C-7050."

ON THE RADIATIVE EQUILIBRIUM OF A STELLAR ATMOSPHERE. XXII

S. CHANDRASEKHAR

Yerkes Observatory

Received November 3, 1947

ABSTRACT

In the present paper exact solutions are found for the problems of diffuse reflection and transmission considered in Paper XXI in a general finite approximation. The method consists in starting with the functional equations of Paper XVII governing the laws of diffuse reflection and transmission; reducing them to pairs of functional equations of the standard form,

$$X(\mu) = 1 + \mu \int_0^1 \frac{\Psi(\mu')}{\mu + \mu'} [X(\mu)X(\mu') - Y(\mu)Y(\mu')] d\mu' \quad (i)$$

and

$$Y(\mu) = e^{-\tau_1/\mu} + \mu \int_0^1 \frac{\Psi(\mu')}{\mu - \mu'} [Y(\mu)X(\mu') - X(\mu)Y(\mu')] d\mu', \quad (ii)$$

where $\Psi(\mu)$ is an even polynomial in μ satisfying the condition

$$\int_0^1 \Psi(\mu) d\mu \leq \frac{1}{2},$$

and τ_1 is the optical thickness of the atmosphere; and, finally, relating in a unique manner the various constants occurring in the solutions with the moments of the X - and Y -functions appropriate for the problem.

There is, however, one important difference between the present theory and the corresponding theory of transfer in semi-infinite atmospheres as developed in Paper XIV. It is that, in all conservative cases of perfect scattering, the solutions of the functional equations incorporating the invariances of the problem are not unique but form a one-parametric family. For the removal of the resulting arbitrariness in the solutions, appeal must be made to the flux and the K -integrals, which conservative problems of perfect scattering always admit.

The paper is divided into five main sections. Section I is devoted to a general study of functional equations of the form (i) and (ii) and to deriving various integral properties of these functions useful in the subsequent analysis. The one-parametric nature of the solution of these equations for the case

$$\int_0^1 \Psi(\mu) d\mu = \frac{1}{2}$$

is proved in this section; also the basic correspondence between the solutions of equations (i) and (ii) and the *rational functions* X and Y introduced in Paper XXI is established. The following sections deal with the problem of diffuse reflection and transmission under conditions of (i) isotropic scattering with an albedo $\omega_0 \leq 1$; (ii) scattering in accordance with Rayleigh's phase function; (iii) scattering in accordance with the phase function $\lambda(1 + x \cos \Theta)$; and (iv) Rayleigh scattering with proper allowance for the polarization of the radiation field.

1. Introduction.—This paper is a continuation of Paper XXI¹ and completes the theory of diffuse reflection and transmission by plane-parallel atmospheres of finite optical thicknesses. By considering the functional equations for the laws of diffuse reflection and transmission derived in Paper XVII² we shall show how the exact solutions for the various problems can be found. Now these functional equations governing the angular distributions of the reflected and the transmitted radiations are simultaneous

¹ *Ap. J.*, **106**, 152, 1947.

² *Ibid.*, **105**, 441, 1947.

nonlinear nonhomogeneous systems of such high order³ that they might be considered impossible for practical solution if it were not for the guidance provided by the analysis of Paper XXI regarding the forms of the solutions to be sought. Indeed, it will appear that the solutions of the reflected and the transmitted radiations in the various cases have exactly the same forms as those found in Paper XXI, with, however, the X - and Y -functions occurring in them redefined as solutions of a simultaneous pair of functional equations of the form.

$$X(\mu) = 1 + \mu \int_0^1 \frac{\Psi(\mu')}{\mu + \mu'} [X(\mu) X(\mu') - Y(\mu) Y(\mu')] d\mu' \quad (1)$$

and

$$Y(\mu) = e^{-\tau_1/\mu} + \mu \int_0^1 \frac{\Psi(\mu')}{\mu - \mu'} [Y(\mu) X(\mu') - X(\mu) Y(\mu')] d\mu', \quad (2)$$

where τ_1 denotes the optical thickness of the atmosphere and $\Psi(\mu)$ is an even polynomial in μ , satisfying the condition

$$\int_0^1 \Psi(\mu) d\mu \leq \frac{1}{2}. \quad (3)$$

Equations (1) and (2) therefore play the same basic role in the theory of radiative transfer in atmospheres of finite optical thicknesses as the equation

$$H(\mu) = 1 + \mu H(\mu) \int_0^1 \frac{\Psi(\mu')}{\mu + \mu'} H(\mu') d\mu' \quad (4)$$

played in the theory of semi-infinite atmospheres.⁴ It is, in fact, clear that

$$X(\mu) \rightarrow H(\mu) \quad \text{and} \quad Y(\mu) \rightarrow 0 \quad \text{as} \quad \tau_1 \rightarrow \infty. \quad (5)$$

There is, however, one important respect in which the present theory differs from the theory of radiative transfer in semi-infinite atmospheres, namely, that, in all conservative cases of perfect scattering, the functional equations governing the angular distributions of the emergent radiations derived from the invariances discussed in Paper XVII do not suffice to characterize the physical solutions uniquely; for, as we shall see, the general solutions of the relevant equations have a single arbitrary parameter in them. Thus, for the case

$$\int_0^1 \Psi(\mu) d\mu = \frac{1}{2}, \quad (6)$$

we shall show that if $X(\mu)$ and $Y(\mu)$ are solutions of equations (1) and (2), then so are

$$X(\mu) + Q\mu [X(\mu) + Y(\mu)] \quad (7)$$

and

$$Y(\mu) - Q\mu [X(\mu) + Y(\mu)], \quad (8)$$

where Q is an arbitrary constant. Similar ambiguities arise in the solutions of the more complicated systems representing general cases of perfect scattering. The physical origin of this nonuniqueness in the solution is not clear; but we shall see that in all cases the ambiguity can be removed by appealing to the "K-integral,"

$$K = \frac{1}{2} \int_{-1}^{+1} I(\tau, \mu) \mu^2 d\mu = \frac{1}{4} \mu_0 F(-\mu_0 e^{-\tau/\mu_0} + \gamma_1 \tau + \gamma_2), \quad (9)$$

³ For example, in the case of Rayleigh scattering, the order of the system is eight.

⁴ See Paper XIV (*A. p. J.*, **105**, 164, 1947); also the author's Josiah Willard Gibbs Lecture in the *Bull. Amer. Math. Soc.*, **53**, 641-711, 1947.

which all conservative problems admit.⁵ (In eq. [9], μ_0 is the direction cosine of the angle of incidence of a parallel beam of radiation of net flux πF per unit area normal to itself, and γ_1 and γ_2 are two constants.)

The plan of this paper is as follows:

Section I is devoted to a general study of the functional equations (1) and (2) and to deriving certain relations useful in our subsequent analysis. The ambiguity in the solutions of equations (1) and (2) for the case (6) is proved in this section. The basic correspondence between the solutions of equations (1) and (2) and the *rational functions*, X and Y , introduced in Paper XXI (eqs. [125] and [126]) is also established in this section. Sections II, III, IV, and V deal with the problem of diffuse reflection and transmission under conditions, respectively, of (i) isotropic scattering with an albedo $\omega_0 \leq 1$; (ii) scattering in accordance with Rayleigh's phase function; (iii) scattering in accordance with the phase function $\lambda(1 + x \cos \Theta)$; and, finally, (iv) Rayleigh scattering with proper allowance for the polarization of the radiation field.

I. ON THE FUNCTIONAL EQUATIONS SATISFIED BY X AND Y

2. *Definitions and alternative forms of the basic equations.*—In dealing with the solutions of equations (1) and (2) it is convenient to introduce the following abbreviations:

$$x_n = \int_0^1 X(\mu) \Psi(\mu) \mu^n d\mu, \quad y_n = \int_0^1 Y(\mu) \Psi(\mu) \mu^n d\mu, \quad (10)$$

$$a_n = \int_0^1 X(\mu) \mu^n d\mu, \quad \text{and} \quad \beta_n = \int_0^1 Y(\mu) \mu^n d\mu; \quad (11)$$

i.e., x_n and y_n are the moments of order n and $X(\mu)$ and $Y(\mu)$, weighted by the *characteristic function* $\Psi(\mu)$, while a_n and β_n are the simple moments themselves.

Certain alternative forms of the basic equations which we shall find useful may also be noted here. Writing

$$\frac{\mu}{\mu + \mu'} = 1 - \frac{\mu'}{\mu + \mu'}, \quad \text{respectively,} \quad \frac{\mu}{\mu - \mu'} = 1 + \frac{\mu'}{\mu - \mu'}, \quad (12)$$

in equations (1) and (2), we readily find that

$$\int_0^1 \frac{\mu' \Psi(\mu')}{\mu + \mu'} [X(\mu) X(\mu') - Y(\mu) Y(\mu')] d\mu' = 1 - [(1 - x_0) X(\mu) + y_0 Y(\mu)] \quad (13)$$

and

$$\int_0^1 \frac{\mu' \Psi(\mu')}{\mu - \mu'} [Y(\mu) X(\mu') - X(\mu) Y(\mu')] d\mu' = -e^{-\tau_1/\mu} + [y_0 X(\mu) + (1 - x_0) Y(\mu)]. \quad (14)$$

We also have

$$\int_0^1 \frac{\mu'^2 \Psi(\mu')}{\mu + \mu'} [X(\mu) X(\mu') - Y(\mu) Y(\mu')] d\mu' = x_1 X(\mu) - y_1 Y(\mu) - \mu + \mu [(1 - x_0) X(\mu) + y_0 Y(\mu)] \quad (15)$$

and

$$\int_0^1 \frac{\mu'^2 \Psi(\mu')}{\mu - \mu'} [Y(\mu) X(\mu') - X(\mu) Y(\mu')] d\mu' = y_1 X(\mu) - x_1 Y(\mu) - \mu e^{-\tau_1/\mu} + \mu [y_0 X(\mu) + (1 - x_0) Y(\mu)]. \quad (16)$$

⁵ In the case of Rayleigh scattering there are two such integrals to be considered (cf. Sec. V).

The foregoing equations can be verified by writing

$$\frac{\mu'^2}{\mu + \mu'} = \mu' - \frac{\mu\mu'}{\mu + \mu'}, \quad \text{respectively,} \quad \frac{\mu'^2}{\mu - \mu'} = -\mu' + \frac{\mu\mu'}{\mu - \mu'}, \quad (17)$$

and using equations (13) and (14).

3. Integrodifferential equations for $X(\mu, \tau_1)$ and $Y(\mu, \tau_1)$.—In equations (1) and (2), $0 < \tau_1 < \infty$ is, of course, to be regarded as some assigned constant. Nevertheless, it is sometimes convenient to emphasize explicitly the dependence of the solutions X and Y on τ_1 . We shall then write $X(\mu, \tau_1)$ and $Y(\mu, \tau_1)$ instead of simply as $X(\mu)$ and $Y(\mu)$. And, considered as functions of τ_1 also, X and Y satisfy certain integrodifferential equations which are of importance. We shall state them in the form of the following theorem:

Theorem 1.—If $X(\mu, \tau_1)$ and $Y(\mu, \tau_1)$ are solutions of equations (1) and (2) for a particular value of τ_1 , then solutions for other values of τ_1 can be obtained from the integrodifferential equations

$$\begin{aligned} \frac{\partial X(\mu, \tau_1)}{\partial \tau_1} &= Y(\mu, \tau_1) \int_0^1 \frac{d\mu'}{\mu'} \Psi(\mu') Y(\mu', \tau_1) \\ &= y_{-1}(\tau_1) Y(\mu, \tau_1) \end{aligned} \quad (18)$$

and

$$\begin{aligned} \frac{\partial Y(\mu, \tau_1)}{\partial \tau_1} + \frac{Y(\mu, \tau_1)}{\mu} &= X(\mu, \tau_1) \int_0^1 \frac{d\mu'}{\mu'} \Psi(\mu') Y(\mu', \tau_1) \\ &= y_{-1}(\tau_1) X(\mu, \tau_1). \end{aligned} \quad (19)$$

Proof.—According to equations (18) and (19),

$$\begin{aligned} \mu \frac{\partial}{\partial \tau_1} \int_0^1 \frac{\Psi(\mu')}{\mu + \mu'} [X(\mu) X(\mu') - Y(\mu) Y(\mu')] d\mu' \\ = \mu \int_0^1 \frac{\Psi(\mu')}{\mu + \mu'} \left\{ y_{-1} X(\mu) Y(\mu') + y_{-1} X(\mu') Y(\mu) \right. \\ \left. - Y(\mu) \left[-\frac{Y(\mu')}{\mu'} + y_{-1} X(\mu') \right] - Y(\mu') \left[-\frac{Y(\mu)}{\mu} + y_{-1} X(\mu) \right] \right\} d\mu'. \end{aligned} \quad (20)$$

Hence

$$\mu \frac{\partial}{\partial \tau_1} \int_0^1 \frac{\Psi(\mu')}{\mu + \mu'} [X(\mu) X(\mu') - Y(\mu) Y(\mu')] d\mu' = y_{-1} Y(\mu). \quad (21)$$

Similarly,

$$\begin{aligned} \mu \frac{\partial}{\partial \tau_1} \int_0^1 \frac{\Psi(\mu')}{\mu - \mu'} [Y(\mu) X(\mu') - X(\mu) Y(\mu')] d\mu' \\ = \int_0^1 \frac{\Psi(\mu')}{\mu - \mu'} \left[-Y(\mu) X(\mu') + \frac{\mu}{\mu'} X(\mu) Y(\mu') \right] d\mu'. \end{aligned} \quad (22)$$

We therefore have

$$\begin{aligned} \int_0^1 \frac{\Psi(\mu')}{\mu - \mu'} [Y(\mu) X(\mu') - X(\mu) Y(\mu')] d\mu' \\ + \mu \frac{\partial}{\partial \tau_1} \int_0^1 \frac{\Psi(\mu')}{\mu - \mu'} [Y(\mu) X(\mu') - X(\mu) Y(\mu')] d\mu' = y_{-1} X(\mu). \end{aligned} \quad (23)$$

On the other hand, if X and Y are solutions of equations (1) and (2), we must have

$$\frac{\partial X}{\partial \tau_1} = \mu \frac{\partial}{\partial \tau_1} \int_0^1 \frac{\Psi(\mu')}{\mu + \mu'} [X(\mu) X(\mu') - Y(\mu) Y(\mu')] d\mu' \quad (24)$$

and

$$\begin{aligned} \frac{\partial Y}{\partial \tau_1} + \frac{Y}{\mu} &= \int_0^1 \frac{\Psi(\mu')}{\mu - \mu'} [Y(\mu) X(\mu') - X(\mu) Y(\mu')] d\mu' \\ &+ \mu \frac{\partial}{\partial \tau_1} \int_0^1 \frac{\Psi(\mu')}{\mu - \mu'} [Y(\mu) X(\mu') - X(\mu) Y(\mu')] d\mu'. \end{aligned} \quad (25)$$

From equations (21), (23), (24), and (25) we now conclude that, if $X(\mu, \tau_1)$ and $Y(\mu, \tau_1)$ are solutions of equations (1) and (2) for a particular value of τ_1 , then

$$X(\mu, \tau_1) + y_{-1} Y(\mu, \tau_1) d\tau_1 \quad (26)$$

and

$$Y(\mu, \tau_1) + \left[-\frac{Y(\mu, \tau_1)}{\mu} + y_{-1} X(\mu, \tau_1) \right] d\tau_1 \quad (27)$$

are solutions of the same equations for an infinitesimally larger value of τ_1 , namely, $\tau_1 + d\tau_1$. This proves the theorem.

Corollary.—

$$X^2(\mu, \tau_1) - Y^2(\mu, \tau_1) = H^2(\mu) - \frac{2}{\mu} \int_{\tau_1}^{\infty} Y^2(\mu, t) dt. \quad (28)$$

Proof.—Eliminating y_{-1} between equations (18) and (19), we have

$$X \frac{\partial X}{\partial \tau_1} = Y \frac{\partial Y}{\partial \tau_1} + \frac{Y^2}{\mu} \quad (29)$$

or

$$\frac{\partial}{\partial \tau_1} (X^2 - Y^2) = \frac{2}{\mu} Y^2. \quad (30)$$

Integrating equation (30) and remembering that

$$X(\mu, \tau_1) \rightarrow H(\mu) \quad \text{and} \quad Y(\mu, \tau_1) \rightarrow 0 \quad \text{as} \quad \tau_1 \rightarrow \infty \quad (31)$$

we obtain the result stated.

4. Some integral properties of the functions X and Y .—As in the case of the H -functions, there are a number of integral theorems (of an essentially elementary kind) which can be proved for functions satisfying equations of the form (1) and (2). The theorems which follow are the analogues for the X - and Y -functions, of the theorems proved for the H -functions in Paper XIV, § 12.

Theorem 2.—

$$\int_0^1 X(\mu) \Psi(\mu) d\mu = 1 - \left[1 - 2 \int_0^1 \Psi(\mu) d\mu + \left\{ \int_0^1 Y(\mu) \Psi(\mu) d\mu \right\}^2 \right]^{1/2}. \quad (32)$$

Proof.—Multiplying the equation satisfied by $X(\mu)$ by $\Psi(\mu)$ and integrating over the range of μ , we have (cf. eq. [10])

$$\begin{aligned} x_0 &= \int_0^1 \Psi(\mu) d\mu \\ &+ \int_0^1 \int_0^1 \frac{\mu}{\mu + \mu'} \Psi(\mu) \Psi(\mu') [X(\mu) X(\mu') - Y(\mu) Y(\mu')] d\mu d\mu'. \end{aligned} \quad (33)$$

Interchanging μ and μ' in the double integral on the right-hand side and taking the average of the two equations, we have

$$\begin{aligned} x_0 &= \int_0^1 \Psi(\mu) d\mu + \frac{1}{2} \int_0^1 \int_0^1 \Psi(\mu) \Psi(\mu') [X(\mu) X(\mu') - Y(\mu) Y(\mu')] d\mu d\mu' \\ &= \int_0^1 \Psi(\mu) d\mu + \frac{1}{2} (x_0^2 - y_0^2). \end{aligned} \quad (34)$$

Solving this equation for x_0 , we have

$$x_0 = 1 \pm \left[1 - 2 \int_0^1 \Psi(\mu) d\mu + y_0^2 \right]^{1/2}. \quad (35)$$

The ambiguity in the sign in equation (35) can be removed by the consideration that the quantity on the right-hand side must uniformly converge to zero when $\Psi(\mu) \rightarrow 0$ uniformly in the interval $(0, 1)$. This requires us to choose the negative sign in equation (35), and the result stated follows.

Corollary.—In the conservative case

$$\int_0^1 \Psi(\mu) d\mu = \frac{1}{2}, \quad (36)$$

we have

$$\int_0^1 [X(\mu) + Y(\mu)] \Psi(\mu) d\mu = 1. \quad (37)$$

Theorem 3.—

$$(1 - x_0) x_2 + y_0 y_2 + \frac{1}{2} (x_1^2 - y_1^2) = \int_0^1 \Psi(\mu) \mu^2 d\mu. \quad (38)$$

Proof.—Multiplying equation (1) by $\Psi(\mu)\mu^2$ and integrating over the range of μ , we have

$$\begin{aligned} x_2 &= \int_0^1 \Psi(\mu) \mu^2 d\mu \\ &\quad + \int_0^1 \int_0^1 \frac{\mu^3}{\mu + \mu'} \Psi(\mu) \Psi(\mu') [X(\mu) X(\mu') - Y(\mu) Y(\mu')] d\mu d\mu' \\ &= \int_0^1 \Psi(\mu) \mu^2 d\mu \\ &\quad + \frac{1}{2} \int_0^1 \int_0^1 (\mu^2 - \mu\mu' + \mu'^2) \Psi(\mu) \Psi(\mu') [X(\mu) X(\mu') - Y(\mu) Y(\mu')] d\mu d\mu'. \end{aligned} \quad (39)$$

Hence

$$x_2 = \int_0^1 \Psi(\mu) \mu^2 d\mu + x_2 x_0 - y_2 y_0 - \frac{1}{2} (x_1^2 - y_1^2), \quad (40)$$

which is equivalent to equation (38).

Corollary.—In the conservative case,

$$y_0 (x_2 + y_2) + \frac{1}{2} (x_1^2 - y_1^2) = \int_0^1 \Psi(\mu) \mu^2 d\mu. \quad (41)$$

This follows from equation (38) and the corollary of theorem 2 (eq. [37]), according to which

$$x_0 + y_0 = 1. \quad (42)$$

Theorem 4.—When the characteristic function $\Psi(\mu)$ has the form

$$\Psi(\mu) = a + b\mu^2, \quad (43)$$

where a and b are two constants,⁶ we have the relations

$$\alpha_0 = 1 + \frac{1}{2} [a(\alpha_0^2 - \beta_0^2) + b(\alpha_1^2 - \beta_1^2)], \quad (44)$$

$$\begin{aligned} (a + b\mu^2) \int_0^1 \frac{d\mu'}{\mu + \mu'} [X(\mu) X(\mu') - Y(\mu) Y(\mu')] \\ = \frac{1}{\mu} [X(\mu) - 1] - b [(\alpha_1 - \mu\alpha_0) X(\mu) - (\beta_1 - \mu\beta_0) Y(\mu)], \end{aligned} \quad (45)$$

and

$$\begin{aligned} (a + b\mu^2) \int_0^1 \frac{d\mu'}{\mu - \mu'} [Y(\mu) X(\mu') - X(\mu) Y(\mu')] \\ = \frac{1}{\mu} [Y(\mu) - e^{-\tau_1/\mu}] - b [(\beta_1 + \mu\beta_0) X(\mu) - (\alpha_1 + \mu\alpha_0) Y(\mu)], \end{aligned} \quad (46)$$

where α_0, β_0 and α_1, β_1 are moments of order zero and one of $X(\mu)$ and $Y(\mu)$, respectively.

To prove equation (44), we simply integrate the equation satisfied by $X(\mu)$. We find

$$\begin{aligned} \alpha_0 &= 1 + \int_0^1 \int_0^1 \frac{(a + b\mu'^2) \mu}{\mu + \mu'} [X(\mu) X(\mu') - Y(\mu) Y(\mu')] d\mu d\mu' \\ &= 1 + \frac{1}{2} \int_0^1 \int_0^1 (a + b\mu\mu') [X(\mu) X(\mu') - Y(\mu) Y(\mu')] d\mu d\mu' \\ &= 1 + \frac{1}{2} [a(\alpha_0^2 - \beta_0^2) + b(\alpha_1^2 - \beta_1^2)]. \end{aligned} \quad (47)$$

The relation (46) can be proved in the following manner:

$$\begin{aligned} a \int_0^1 \frac{d\mu'}{\mu - \mu'} [Y(\mu) X(\mu') - X(\mu) Y(\mu')] \\ = \int_0^1 \frac{a + b\mu'^2}{\mu - \mu'} [Y(\mu) X(\mu') - X(\mu) Y(\mu')] d\mu' \\ + b \int_0^1 \left(\mu + \mu' - \frac{\mu^2}{\mu - \mu'} \right) [Y(\mu) X(\mu') - X(\mu) Y(\mu')] d\mu' \quad (48) \\ = \frac{1}{\mu} [Y(\mu) - e^{-\tau_1/\mu}] + b [(\alpha_1 + \mu\alpha_0) Y(\mu) - (\beta_1 + \mu\beta_0) X(\mu)] \\ - b\mu^2 \int_0^1 \frac{d\mu'}{\mu - \mu'} [Y(\mu) X(\mu') - X(\mu) Y(\mu')]. \end{aligned}$$

Hence the result. Equation (45) follows quite similarly.

5. The nonuniqueness of the solution in the conservative case. The standard solution.—We shall now prove the following theorem:

Theorem 5.—In the conservative case,

$$\int_0^1 \Psi(\mu) d\mu = \frac{1}{2}, \quad (49)$$

⁶ The condition $\int_0^1 \Psi(\mu) d\mu \leq \frac{1}{2}$ requires that $a + \frac{1}{3}b \leq \frac{1}{2}$.

the solutions of equations (1) and (2) are not unique; more particularly, if $X(\mu)$ and $Y(\mu)$ are solutions, then so are

$$X(\mu) + Q\mu [X(\mu) + Y(\mu)] \quad (50)$$

and

$$Y(\mu) - Q\mu [X(\mu) + Y(\mu)], \quad (51)$$

where Q is an arbitrary constant.

Proof.—Writing

$$F(\mu) = X(\mu) + Q\mu [X(\mu) + Y(\mu)] \quad (52)$$

and

$$G(\mu) = Y(\mu) - Q\mu [X(\mu) + Y(\mu)], \quad (53)$$

we verify that

$$\begin{aligned} F(\mu)F(\mu') - G(\mu)G(\mu') &= X(\mu)X(\mu') - Y(\mu)Y(\mu') \\ &\quad + Q(\mu + \mu')[X(\mu) + Y(\mu)][X(\mu') + Y(\mu')] \end{aligned} \quad (54)$$

and

$$\begin{aligned} G(\mu)F(\mu') - F(\mu)G(\mu') &= Y(\mu)X(\mu') - X(\mu)Y(\mu') \\ &\quad - Q(\mu - \mu')[X(\mu) + Y(\mu)][X(\mu') + Y(\mu')]. \end{aligned} \quad (55)$$

Hence

$$\begin{aligned} \mu \int_0^1 \frac{\Psi(\mu')}{\mu + \mu'} [F(\mu)F(\mu') - G(\mu)G(\mu')] d\mu' \\ = \mu \int_0^1 \frac{\Psi(\mu')}{\mu + \mu'} [X(\mu)X(\mu') - Y(\mu)Y(\mu')] d\mu' \\ + Q\mu [X(\mu) + Y(\mu)] \int_0^1 [X(\mu') + Y(\mu')] \Psi(\mu') d\mu'. \end{aligned} \quad (56)$$

Using equation (1) and the corollary of theorem 2 (eq. [37]), we have

$$\begin{aligned} \mu \int_0^1 \frac{\Psi(\mu')}{\mu + \mu'} [F(\mu)F(\mu') - G(\mu)G(\mu')] d\mu' \\ = X(\mu) - 1 + Q\mu [X(\mu) + Y(\mu)] \\ = F(\mu) - 1. \end{aligned} \quad (57)$$

Similarly,

$$\begin{aligned} \mu \int_0^1 \frac{\Psi(\mu')}{\mu - \mu'} [G(\mu)F(\mu') - F(\mu)G(\mu')] d\mu' \\ = Y(\mu) - e^{-\tau_1/\mu} - Q\mu [X(\mu) + Y(\mu)] \\ = G(\mu) - e^{-\tau_1/\mu}. \end{aligned} \quad (58)$$

Hence $F(\mu)$ and $G(\mu)$ satisfy the same equations as $X(\mu)$ and $Y(\mu)$, and the theorem follows.

Corollary.—The solutions derivable from a given one according to equations (52) and (53) form a one-parametric family which can be generated by any of its members.

Proof.—Let

$$F_1(\mu) = F(\mu) + Q_1\mu [F(\mu) + G(\mu)] \quad (59)$$

and

$$G_1(\mu) = G(\mu) - Q_1\mu [F(\mu) + G(\mu)], \quad (60)$$

where Q_1 is an arbitrary constant. According to theorem 5, F_1 and G_1 are also solutions of equations (1) and (2). On the other hand, since (cf. eqs. [52] and [53])

$$F(\mu) + G(\mu) = X(\mu) + Y(\mu), \quad (61)$$

we can express F_1 and G_1 alternatively in the forms

$$F_1(\mu) = X(\mu) + (Q + Q_1)\mu [X(\mu) + Y(\mu)] \quad (62)$$

and

$$G_1(\mu) = Y(\mu) - (Q + Q_1)\mu [X(\mu) + Y(\mu)]. \quad (63)$$

In other words, $F_1(\mu)$ and $G_1(\mu)$ can also be derived directly from $X(\mu)$ and $Y(\mu)$.

It would appear that, in a given conservative case, all the solutions are included in one and only one family. In nonconservative cases, on the other hand, it would seem that the solutions are unique.

In view of the ambiguity in the solutions of equations (1) and (2) in conservative cases, it would be convenient to select, in each case, a particular member of the one-parametric family of solutions as a *standard solution*.

Definition.—In a conservative case we shall define the solutions which have the property

$$x_0 = \int_0^1 X(\mu) \Psi(\mu) d\mu = 1 \quad (64)$$

and

$$y_0 = \int_0^1 Y(\mu) \Psi(\mu) d\mu = 0 \quad (65)^7$$

as the standard solutions of equations (1) and (2).

Such solutions can always be found; for, if a particular X and Y do not satisfy equations (64) and (65), we can always find a Q such that the solutions derived from X and Y in the manner of equations (52) and (53) have the required property. Standard solutions defined in this manner have several interesting properties. We shall state them in the form of the following theorems:

Theorem 6.—The standard solutions are invariant to increments of τ_1 according to the integrodifferential equations of theorem 1.

Multiplying equations (18) and (19) by $\Psi(\mu)$ and integrating over the range of μ , we have

$$\frac{dx_0}{d\tau_1} = y_0 y_{-1} = 0 \quad (66)$$

and

$$\frac{dy_0}{d\tau_1} = -(1 - x_0) y_{-1} = 0. \quad (67)$$

Theorem 7.—Let $X(\mu, \tau_1)$ and $Y(\mu, \tau_1)$ denote the standard solutions of equations (1) and (2) in a conservative case for a particular value of τ_1 . Consider the solutions

$$F(\mu, \tau_1) = X(\mu, \tau_1) + Q\mu [X(\mu, \tau_1) + Y(\mu, \tau_1)] \quad (68)$$

and

$$G(\mu, \tau_1) = Y(\mu, \tau_1) - Q\mu [X(\mu, \tau_1) + Y(\mu, \tau_1)] \quad (69)$$

of equations (1) and (2) derived from X and Y and continue them for other values of τ_1 according to the equations of theorem 1. These solutions for other values of τ_1 can, in turn, be derived from the standard solutions appropriate for these values of τ_1 with vary-

⁷ Since $x_0 + y_0 = 1$, eq. (64) implies eq. (65) and vice versa.

ing values of Q . The quantity Q , considered as a function of τ_1 in this manner, satisfies the differential equation

$$\frac{d}{d\tau_1} \left(\frac{1}{Q} \right) - \frac{2y_{-1}}{Q} = -1. \quad (70)$$

Proof.—According to equations (18) and (19),

$$\frac{\partial F}{\partial \tau_1} = G \int_0^1 \frac{d\mu'}{\mu'} \Psi(\mu') G(\mu'), \quad (71)$$

and

$$\frac{\partial G}{\partial \tau_1} + \frac{G}{\mu} = F \int_0^1 \frac{d\mu'}{\mu'} \Psi(\mu') G(\mu'). \quad (72)$$

Now (cf. eq. [69])

$$\begin{aligned} \int_0^1 \frac{d\mu'}{\mu'} \Psi(\mu') G(\mu') &= \int_0^1 \frac{d\mu'}{\mu'} \Psi(\mu') Y(\mu') - Q \int_0^1 [X(\mu') + Y(\mu')] \Psi(\mu') d\mu' \\ &= y_{-1} - Q. \end{aligned} \quad (73)$$

Hence

$$\frac{\partial F}{\partial \tau_1} = (y_{-1} - Q) G, \quad (74)$$

and

$$\frac{\partial G}{\partial \tau_1} + \frac{G}{\mu} = (y_{-1} - Q) F. \quad (75)$$

On the other hand, since X and Y remain standard solutions when continued for other values of τ_1 , we must have

$$\begin{aligned} \frac{\partial F}{\partial \tau_1} &= \frac{\partial X}{\partial \tau_1} + Q\mu \left(\frac{\partial X}{\partial \tau_1} + \frac{\partial Y}{\partial \tau_1} \right) + \mu (X + Y) \frac{dQ}{d\tau_1} \\ &= y_{-1} Y + Q\mu \left(y_{-1} Y - \frac{Y}{\mu} + y_{-1} X \right) + \mu (X + Y) \frac{dQ}{d\tau_1} \\ &= (y_{-1} - Q) Y + \mu (X + Y) \left(y_{-1} Q + \frac{dQ}{d\tau_1} \right). \end{aligned} \quad (76)$$

We can re-write the foregoing equation in the form

$$\frac{\partial F}{\partial \tau_1} = (y_{-1} - Q) [Y - Q\mu (X + Y)] + \mu (X + Y) \left[Q(y_{-1} - Q) + y_{-1} Q + \frac{dQ}{d\tau_1} \right], \quad (77)$$

or

$$\frac{\partial F}{\partial \tau_1} = (y_{-1} - Q) G + \mu (X + Y) \left(2y_{-1} Q - Q^2 + \frac{dQ}{d\tau_1} \right). \quad (78)$$

Comparing equations (74) and (78), we must have

$$\frac{dQ}{d\tau_1} + 2y_{-1} Q - Q^2 = 0. \quad (79)$$

A similar consideration of the equation for $\partial G / \partial \tau_1$ leads to the same equation for Q .

Equation (79) can be re-written in the form

$$\frac{1}{Q^2} \frac{dQ}{d\tau_1} + \frac{2y_{-1}}{Q} = 1, \quad (80)$$

which is equivalent to equation (70).

The various relations (eqs. [13]–[16] and [41]) derived in the preceding sections for solutions of equations (1) and (2) in general take particularly simple forms for standard solutions of conservative cases. We shall collect these relations in the form of the following theorem:

Theorem 8.—For the standard solutions in a conservative case we have the relations

$$x_0 = 1, \quad y_0 = 0, \quad (81)$$

$$x_1^2 - y_1^2 = 2 \int_0^1 \Psi(\mu) \mu^2 d\mu, \quad (82)$$

$$\int_0^1 \frac{\mu' \Psi(\mu')}{\mu + \mu'} [X(\mu) X(\mu') - Y(\mu) Y(\mu')] d\mu' = 1, \quad (83)$$

$$\int_0^1 \frac{\mu' \Psi(\mu')}{\mu - \mu'} [Y(\mu) X(\mu') - X(\mu) Y(\mu')] d\mu' = -e^{-\tau_1/\mu}, \quad (84)$$

$$\int_0^1 \frac{\mu' \Psi(\mu')}{\mu + \mu'} [X(\mu) X(\mu') - Y(\mu) Y(\mu')] d\mu' = x_1 X(\mu) - y_1 Y(\mu) - \mu, \quad (85)$$

and

$$\int_0^1 \frac{\mu' \Psi(\mu')}{\mu - \mu'} [Y(\mu) X(\mu') - X(\mu) Y(\mu')] d\mu' = y_1 X(\mu) - x_1 Y(\mu) - \mu e^{-\tau_1/\mu}. \quad (86)$$

6. *The correspondence between the solutions of equations (1) and (2) and the functions X and Y introduced into the solution of the equations of transfer in a finite approximation.*—In solving the equations of transfer appropriately for the problem of diffuse reflection and transmission in Paper XXI, we found that we had to introduce certain functions, X and Y, involving the nonvanishing roots of a characteristic equation of the form

$$1 = 2 \sum_{j=1}^n \frac{a_j \Psi(\mu_j)}{1 - k^2 \mu_j^2}, \quad (87)$$

where, as usual, the μ_j 's are the zeros of $P_{2n}(\mu)$ and the a_j 's are the corresponding Gaussian weights. In terms of these functions X and Y it was possible to express the solutions of the emergent radiations in closed forms in all cases considered. In analogy with the theory of the H-functions (Paper XIV, § 11), we may therefore expect that the functions X and Y appearing in the solutions in a finite approximation are rational approximations to the solutions of equations (1) and (2) when they are replaced by their "finite forms," namely,

$$X(\mu) = 1 + \mu \sum_{j=1}^n \frac{a_j \Psi(\mu_j)}{\mu + \mu_j} [X(\mu) X(\mu_j) - Y(\mu) Y(\mu_j)] \quad (88)$$

and

$$Y(\mu) = e^{-\tau_1/\mu} + \mu \sum_{j=1}^n \frac{a_j \Psi(\mu_j)}{\mu - \mu_j} [Y(\mu) X(\mu_j) - X(\mu) Y(\mu_j)]. \quad (89)$$

We shall now examine in what sense the functions X and Y introduced in Paper XXI, equations (125) and (126), are related to equations (88) and (89).

The definitions of the functions X and Y in Paper XXI (eqs. [125] and [126]) suggest that, in seeking solutions of the equations (88) and (89), we try the forms

$$X(\mu) = F(\mu) - e^{-\tau_1/\mu} G(-\mu) \quad (90)$$

and

$$Y(\mu) = e^{-\tau_1/\mu} F(-\mu) - G(\mu), \quad (91)$$

where $F(\mu)$ and $G(\mu)$ are certain rational functions in μ , satisfying the conditions

$$F(-\mu_j) = G(-\mu_j) = 0 \quad (j = 1, \dots, n). \quad (92)$$

For the forms (90) and (91)

$$X(\mu) = e^{-\tau_1/\mu} Y(-\mu) \quad \text{and} \quad Y(\mu) = e^{-\tau_1/\mu} X(-\mu). \quad (93)$$

For X and Y related in this manner, it may be directly verified that equations (88) and (89) are equivalent to each other and that therefore it would suffice to consider only one of them.⁸

Now substituting for X and Y according to equations (90) and (91) in equations (88) and (89) and remembering the further conditions (eq. [92]) imposed on F and G , we find, after some minor reductions, that

$$F(\mu) - e^{-\tau_1/\mu} G(-\mu) = 1 + \mu \sum_{j=1}^n \frac{a_j \Psi(\mu_j)}{\mu + \mu_j} [F(\mu) F(\mu_j) - G(\mu) G(\mu_j)] \quad (94)$$

$$- \mu e^{-\tau_1/\mu} \sum_{j=1}^n \frac{a_j \Psi(\mu_j)}{\mu + \mu_j} [G(-\mu) F(\mu_j) - F(-\mu) G(\mu_j)].$$

Equating the terms with and without the exponential factor in this equation, we obtain

$$F(\mu) = 1 + \mu \sum_{j=1}^n \frac{a_j \Psi(\mu_j)}{\mu + \mu_j} [F(\mu) F(\mu_j) - G(\mu) G(\mu_j)] \quad (95)$$

and

$$G(-\mu) = \mu \sum_{j=1}^n \frac{a_j \Psi(\mu_j)}{\mu + \mu_j} [G(-\mu) F(\mu_j) - F(-\mu) G(\mu_j)]. \quad (96)$$

We can re-write these equations alternatively in the forms

$$F(\mu) \left[1 - \mu \sum_{j=1}^n \frac{a_j \Psi(\mu_j)}{\mu + \mu_j} F(\mu_j) \right] + G(\mu) \left[\mu \sum_{j=1}^n \frac{a_j \Psi(\mu_j)}{\mu + \mu_j} G(\mu_j) \right] = 1 \quad (97)$$

and

$$G(-\mu) \left[1 - \mu \sum_{j=1}^n \frac{a_j \Psi(\mu_j)}{\mu + \mu_j} F(\mu_j) \right] + F(-\mu) \left[\mu \sum_{j=1}^n \frac{a_j \Psi(\mu_j)}{\mu + \mu_j} G(\mu_j) \right] = 0. \quad (98)$$

Solving for the quantities in brackets in equations (97) and (98), we find

$$F(-\mu) = [F(\mu) F(-\mu) - G(\mu) G(-\mu)] \left[1 - \mu \sum_{j=1}^n \frac{a_j \Psi(\mu_j)}{\mu + \mu_j} F(\mu_j) \right] \quad (99)$$

⁸ It is of interest to note in this connection that the substitution (93) makes the functional equations (1) and (2) also equivalent to each other.

and

$$G(-\mu) = [F(\mu)F(-\mu) - G(\mu)G(-\mu)] \left[-\mu \sum_{j=1}^n \frac{a_j \Psi(\mu_j)}{\mu + \mu_j} G(\mu_j) \right]. \quad (100)$$

So far we have pursued only the consequences of assumptions (90), (91), and (92) regarding the form of the solutions of equations (88) and (89) adopted. We shall now write down explicitly the formulae for $F(\mu)$ and $G(\mu)$ suggested by the expressions for $X(\mu)$ and $Y(\mu)$ given in Paper XXI (eqs. [125] and [126]) and see how well they satisfy equations (99) and (100).

From a comparison of equations (90) and (91) and the equations (125) and (126) of Paper XXI, we conclude that

$$\begin{aligned} F(\mu) &= \frac{(-1)^n P(-\mu)}{\mu_1 \dots \mu_n W(\mu)} \frac{C_0(-\mu)}{[C_0^2(0) - C_1^2(0)]^{1/2}} \\ &= \frac{1}{\mu_1 \dots \mu_n} \frac{\prod_{i=1}^n (\mu + \mu_i)}{\prod_a (1 + k_a \mu)} \frac{C_0(-\mu)}{[C_0^2(0) - C_1^2(0)]^{1/2}} \end{aligned} \quad (101)$$

and

$$\begin{aligned} G(\mu) &= \frac{(-1)^n P(-\mu)}{\mu_1 \dots \mu_n W(\mu)} \frac{C_1(-\mu)}{[C_0^2(0) - C_1^2(0)]^{1/2}} \\ &= \frac{1}{\mu_1 \dots \mu_n} \frac{\prod_{i=1}^n (\mu + \mu_i)}{\prod_a (1 + k_a \mu)} \frac{C_1(-\mu)}{[C_0^2(0) - C_1^2(0)]^{1/2}}, \end{aligned} \quad (102)$$

where $C_0(\mu)$ and $C_1(\mu)$ are certain polynomials in μ , of degree n in nonconservative cases and $n-1$ in conservative cases, satisfying the conditions (cf. Paper XXI, eqs. [50], [108], and [109])

$$C_0(1/k_a) = \lambda_a C_1(-1/k_a) \quad (103)$$

and

$$\lambda_a = e^{k_a \tau_1} \frac{P(-1/k_a)}{P(+1/k_a)}. \quad (104)^9$$

According to the theorems proved in Paper XXI, § 4, the relations (103) and (104) are sufficient to determine $C_0(\mu)$ and $C_1(\mu)$ uniquely, apart from two arbitrary constants of proportionality in $C_0(\mu) + C_1(\mu)$ and $C_0(\mu) - C_1(\mu)$. For the particular "normalization" adopted in Paper XXI (eqs. [100] and [101])

$$C_0(\mu) \rightarrow \prod_{a>0} (1 + k_a \mu) = R(-\mu) \quad \text{as} \quad \tau_1 \rightarrow \infty, \quad (105)$$

and

$$C_1(\mu) \rightarrow 0 \quad \text{as} \quad \tau_1 \rightarrow \infty. \quad (106)$$

⁹ In equations (103) and (104) (as in eqs. [101] and [102]), a runs through positive and negative indices corresponding to all the nonvanishing roots k_a ($a = \pm 1, \dots, \pm n$ or $\pm n \mp 1$ and $k_a = -k_{-a}$) of the characteristic equation.

These further conditions, which we shall now also require, suffice to characterize the functions $C_0(\mu)$ and $C_1(\mu)$ without any arbitrariness.

Remembering that, in the approximation in which we are at present working,

$$H(\mu) = \frac{1}{\mu_1 \dots \mu_n} \frac{\prod_{i=1}^n (\mu + \mu_i)}{\prod_{a>0} (1 + k_a \mu)}, \quad (107)$$

we can re-write equations (101) and (102) in the forms

$$F(\mu) = \frac{H(\mu)}{R(\mu)} \frac{C_0(-\mu)}{[C_0^2(0) - C_1^2(0)]^{1/2}} \quad \text{and} \quad G(\mu) = \frac{H(\mu)}{R(\mu)} \frac{C_1(-\mu)}{[C_0^2(0) - C_1^2(0)]^{1/2}}. \quad (108)$$

For $F(\mu)$ and $G(\mu)$, defined, in this manner (cf. Paper XXI, eq. [105]),

$$\begin{aligned} & F(\mu) F(-\mu) - G(\mu) G(-\mu) \\ &= \frac{H(\mu) H(-\mu)}{[C_0^2(0) - C_1^2(0)] W(\mu)} [C_0(\mu) C_0(-\mu) - C_1(\mu) C_1(-\mu)] = H(\mu) H(-\mu). \end{aligned} \quad (109)$$

Using this result and also equations (108) in equations (99) and (100), we find that our problem is reduced to examining the validity of the equations

$$\frac{C_0(\mu)}{[C_0^2(0) - C_1^2(0)]^{1/2}} = H(\mu) R(-\mu) \left[1 - \mu \sum_{j=1}^n \frac{a_j \Psi(\mu_j)}{\mu + \mu_j} F(\mu_j) \right] \quad (110)$$

and

$$\frac{C_1(\mu)}{[C_0^2(0) - C_1^2(0)]^{1/2}} = H(\mu) R(-\mu) \left[-\mu \sum_{j=1}^n \frac{a_j \Psi(\mu_j)}{\mu + \mu_j} G(\mu_j) \right], \quad (111)$$

or, equivalently,

$$C_0(\mu) = \frac{(-1)^n}{\mu_1 \dots \mu_n} [C_0^2(0) - C_1^2(0)]^{1/2} P(-\mu) \left[1 - \mu \sum_{j=1}^n \frac{a_j \Psi(\mu_j)}{\mu + \mu_j} F(\mu_j) \right] \quad (112)$$

and

$$C_1(\mu) = \frac{(-1)^n}{\mu_1 \dots \mu_n} [C_0^2(0) - C_1^2(0)]^{1/2} P(-\mu) \left[-\mu \sum_{j=1}^n \frac{a_j \Psi(\mu_j)}{\mu + \mu_j} G(\mu_j) \right]. \quad (113)$$

The validity (or otherwise) of equations (112) and (113) will depend essentially on whether the quantities on the right-hand sides of these equations are related in the manner required by equations (103). To examine this we have to evaluate the summations which occur in equations (112) and (113).

To carry out the summations in equations (112) and (113), we have first to break $F(\mu)$ and $G(\mu)$ into partial fractions. This requires us to treat the conservative and the non-conservative cases separately.

Considering, first, the nonconservative case, we have $2n$ distinct roots for the char-

acteristic equation (87), which occur in pairs ($k_a = -k_{-a}$, $a = 1, \dots, n$), and $F(\mu)$ and $G(\mu)$ can be expressed in the forms

$$F(\mu) = \sum_{a=-n}^{+n} \frac{L_a}{1 + k_a \mu} + \frac{1}{k_1^2 \dots k_n^2 \mu_1 \dots \mu_n} \frac{c_0^{(n)}}{[C_0^2(0) - C_1^2(0)]^{1/2}} \quad (114)$$

and

$$G(\mu) = \sum_{a=-n}^{+n} \frac{L_a e^{-k_a \tau_1}}{1 - k_a \mu} + \frac{1}{k_1^2 \dots k_n^2 \mu_1 \dots \mu_n} \frac{c_1^{(n)}}{[C_0^2(0) - C_1^2(0)]^{1/2}}, \quad (115)^{10}$$

where the $2n$ constants L_a ($a = \pm 1, \dots, \pm n$) are to be determined from the conditions (cf. eq. [92])

$$F(-\mu_j) = G(-\mu_j) = 0 \quad (j = 1, \dots, n), \quad (116)$$

and $c_0^{(n)}$ and $c_1^{(n)}$ are the coefficients of the highest power, μ^n , in $C_0(\mu)$ and $C_1(\mu)$.

To verify that $F(\mu)$ and $G(\mu)$, defined in the manner of the foregoing equations, agree with our earlier definitions (eqs. [108]), we first observe that conditions (116) enable us to express $F(\mu)$ and $G(\mu)$ in the forms

$$F(\mu) = \frac{(-1)^n P(-\mu)}{\mu_1 \dots \mu_n W(\mu)} f(-\mu) \quad (117)$$

and

$$G(\mu) = \frac{(-1)^n P(-\mu)}{\mu_1 \dots \mu_n W(\mu)} g(-\mu), \quad (118)$$

where $f(\mu)$ and $g(\mu)$ are polynomials of degree n in μ ; and that, further,

$$f(1/k_a) = \lambda_a g(-1/k_a) \quad (a = \pm 1, \dots, \pm n), \quad (119)$$

where λ_a has the same meaning as in equation (104).¹¹ These latter conditions arise from a comparison of the values

$$L_a = \frac{(-1)^n P(+1/k_a)}{\mu_1 \dots \mu_n W_a(1/k_a)} f(1/k_a) \quad (a = \pm 1, \dots, \pm n) \quad (120)$$

and

$$L_a e^{-k_a \tau_1} = \frac{(-1)^n P(-1/k_a)}{\mu_1 \dots \mu_n W_a(1/k_a)} g(-1/k_a) \quad (a = \pm 1, \dots, \pm n), \quad (121)$$

which follow from equations (114), (115), (117), and (118). In accordance with the theorems of Paper XXI, § 4, we therefore conclude that $f(\mu)$ and $g(\mu)$ must be expressible in the forms

$$f(\mu) = q_0 C_0(\mu) + q_1 C_1(\mu) \quad \text{and} \quad g(\mu) = q_0 C_1(\mu) + q_1 C_0(\mu), \quad (122)$$

where q_0 and q_1 are constants. And, finally, from a comparison of the coefficients of the highest power of μ in f and g as deducible from equations (114) and (115) and equations (117) and (118), respectively, we readily verify that

$$q_0 = \frac{1}{[C_0^2(0) - C_1^2(0)]^{1/2}} \quad \text{and} \quad q_1 = 0, \quad (123)$$

as required.

¹⁰ As in Paper XXI (cf. p. 153, n. 6), in all summations and products over a there is no term with $a = 0$.

¹¹ Negative values of a are permitted (cf. n. 9).

For convenience we shall re-write equations (114) and (115) in the forms

$$F(\mu) = \sum_{a=-n}^{+n} \frac{L_a}{1 + k_a \mu} + a \quad (124)$$

and

$$G(\mu) = \sum_{a=-n}^{+n} \frac{L_a e^{-k_a \tau_1}}{1 - k_a \mu} + b, \quad (125)$$

where

$$a = \frac{1}{k_1^2 \dots k_n^2 \mu_1 \dots \mu_n} \frac{c_0^{(n)}}{[C_0^2(0) - C_1^2(0)]^{1/2}} \quad (126)$$

and

$$b = \frac{1}{k_1^2 \dots k_n^2 \mu_1 \dots \mu_n} \frac{c_1^{(n)}}{[C_0^2(0) - C_1^2(0)]^{1/2}}.$$

Moreover (cf. eqs. [120] and [121]),

$$L_a = \frac{(-1)^n P(+1/k_a)}{\mu_1 \dots \mu_n W_a(1/k_a)} \frac{C_0(1/k_a)}{[C_0^2(0) - C_1^2(0)]^{1/2}}, \quad (127)$$

and

$$L_a e^{-k_a \tau_1} = \frac{(-1)^n P(-1/k_a)}{\mu_1 \dots \mu_n W_a(1/k_a)} \frac{C_1(-1/k_a)}{[C_0^2(0) - C_1^2(0)]^{1/2}}. \quad (128)$$

Returning, now, to the evaluation of the summations on the right-hand sides of equations (112) and (113), we consider, first,

$$\Sigma_1(\mu) = 1 - \mu \sum_{j=1}^n \frac{a_j \Psi(\mu_j)}{\mu + \mu_j} F(\mu_j). \quad (129)$$

Since $F(-\mu_j) = 0$ ($j = 1, \dots, n$) we can, without altering anything, extend the summation also over negative values of j . We thus have

$$\Sigma_1(\mu) = 1 - \mu \sum_{j=-n}^{+n} \frac{a_j \Psi(\mu_j)}{\mu + \mu_j} \left(\sum_{\beta=-n}^{+n} \frac{L_\beta}{1 + k_\beta \mu_j} + a \right), \quad (130)$$

where we have further substituted for $F(\mu_j)$ according to equation (124). Remembering that, according to the characteristic equation defining the roots k_a and k_β (cf. eq. [87]),

$$1 = \sum_{j=-n}^{+n} \frac{a_j \Psi(\mu_j)}{1 + k_a \mu_j} = \sum_{j=-n}^{+n} \frac{a_j \Psi(\mu_j)}{1 + k_\beta \mu_j} \quad (131)$$

for all a 's and β 's ($= \pm 1, \dots, \pm n$), we have for $\mu = 1/k_a$

$$\begin{aligned} \Sigma_1(1/k_a) &= 1 - \sum_{j=-n}^{+n} \frac{a_j \Psi(\mu_j)}{1 + k_a \mu_j} \left(\sum_{\beta=-n}^{+n} \frac{L_\beta}{1 + k_\beta \mu_j} + a \right) \\ &= 1 - a - \sum_{j=-n}^{+n} \sum_{\beta=-n}^{+n} L_\beta \frac{a_j \Psi(\mu_j)}{(1 + k_a \mu_j)(1 + k_\beta \mu_j)}. \end{aligned} \quad (132)$$

Alternatively, inverting the order of the summation, we can also write

$$\Sigma_1(1/k_a) = 1 - a - \sum_{\substack{\beta=-n \\ \beta \neq a}}^{+n} \frac{L_\beta}{k_a - k_\beta} \sum_{j=-n}^{+n} a_j \Psi(\mu_j) \left(\frac{k_a}{1 + k_a \mu_j} - \frac{k_\beta}{1 + k_\beta \mu_j} \right) - L_a \sum_{j=-n}^{+n} \frac{a_j \Psi(\mu_j)}{(1 + k_a \mu_j)^2}. \quad (133)$$

Hence

$$\Sigma_1(1/k_a) = 1 - a - \sum_{\beta=-n}^{+n} L_\beta + L_a \left[1 - \sum_{j=-n}^{+n} \frac{a_j \Psi(\mu_j)}{(1 + k_a \mu_j)^2} \right]. \quad (134)$$

But

$$1 - \sum_{j=-n}^{+n} \frac{a_j \Psi(\mu_j)}{(1 + k_a \mu_j)^2} = \sum_{j=-n}^{+n} \frac{a_j \Psi(\mu_j)}{1 + k_a \mu_j} \left(1 - \frac{1}{1 + k_a \mu_j} \right) = k_a \sum_{j=-n}^{+n} \frac{a_j \mu_j \Psi(\mu_j)}{(1 + k_a \mu_j)^2}. \quad (135)$$

We therefore have (cf. eq. [124])

$$\Sigma_1(1/k_a) = 1 - F(0) + L_a k_a \sum_{j=-n}^{+n} \frac{a_j \mu_j \Psi(\mu_j)}{(1 + k_a \mu_j)^2} \quad (\alpha = \pm 1, \dots, \pm n). \quad (136)$$

The summation

$$\begin{aligned} \Sigma_2(\mu) &= -\mu \sum_{j=1}^n \frac{a_j \Psi(\mu_j)}{\mu + \mu_j} G(\mu_j) \\ &= -\mu \sum_{j=-n}^{+n} \frac{a_j \Psi(\mu_j)}{\mu + \mu_j} G(\mu_j) \end{aligned} \quad (137)$$

can be similarly reduced. For $\mu = -1/k_a$ we find

$$\Sigma_2(-1/k_a) = -G(0) + L_a k_a e^{-k_a \tau_1} \sum_{j=-n}^{+n} \frac{a_j \mu_j \Psi(\mu_j)}{(1 + k_a \mu_j)^2} \quad (\alpha = \pm 1, \dots, \pm n). \quad (138)$$

An expression for the quantity

$$\sum_{j=-n}^{+n} \frac{a_j \mu_j \Psi(\mu_j)}{(1 + k_a \mu_j)^2}, \quad (139)$$

which occurs in both equations (136) and (138), can be found by differentiating the identity¹²

$$\begin{aligned} 1 - \sum_{j=-n}^{+n} \frac{a_j \Psi(\mu_j)}{1 + \mu_j/z} &= \frac{1}{H(z) H(-z)} \\ &= \frac{\mu_1^2 \dots \mu_n^2}{P(z) P(-z)} \prod_{\alpha=-n}^{+n} (1 + k_\alpha z), \end{aligned} \quad (140)$$

¹² Cf. eq. (285) in the author's Gibbs Lecture (reference given in n. 4).

with respect to z and setting $z = 1/k_a$. In this manner we find

$$k_a \sum_{j=-n}^{+n} \frac{a_j \mu_j \Psi(\mu_j)}{(1 + k_a \mu_j)^2} = \mu_1^2 \dots \mu_n^2 \frac{W_a(1/k_a)}{P(1/k_a)P(-1/k_a)}. \quad (141)$$

Using this result in equations (136) and (138) and substituting also for L_a and $L_a e^{-k_a \tau_1}$ according to equations (127) and (128), we have

$$\Sigma_1(1/k_a) = 1 - F(0) + (-1)^n \mu_1 \dots \mu_n \frac{C_0(1/k_a)}{[C_0^2(0) - C_1^2(0)]^{1/2} P(-1/k_a)} \quad (142)$$

($\alpha = \pm 1, \dots, \pm n$)

and

$$\Sigma_2(-1/k_a) = -G(0) + (-1)^n \mu_1 \dots \mu_n \frac{C_1(-1/k_a)}{[C_0^2(0) - C_1^2(0)]^{1/2} P(+1/k_a)} \quad (143)$$

($\alpha = \pm 1, \dots, \pm n$).

The right-hand sides of equations (112) and (113) for $\mu = +1/k_a$, respectively $-1/k_a$, therefore become

$$\frac{(-1)^n}{\mu_1 \dots \mu_n} [C_0^2(0) - C_1^2(0)]^{1/2} P(-1/k_a) [1 - F(0)] + C_0(1/k_a) \quad (144)$$

and

$$\frac{(-1)^{n+1}}{\mu_1 \dots \mu_n} [C_0^2(0) - C_1^2(0)]^{1/2} P(+1/k_a) G(0) + C_1(-1/k_a). \quad (145)$$

Now the validity of equations (112) and (113) requires that expressions (144) and (145) be *exactly* $C_0(1/k_a)$ and $C_1(-1/k_a)$. This will be the case only if $F(0) = 1$ and $G(0) = 0$. But, according to equations (108),

$$F(0) = \frac{C_0(0)}{[C_0^2(0) - C_1^2(0)]^{1/2}} \quad \text{and} \quad G(0) = \frac{C_1(0)}{[C_0^2(0) - C_1^2(0)]^{1/2}}; \quad (146)$$

and it is *not* true that $C_1(0) = 0$ identically, in all approximations, and for all values of τ_1 . However, according to equations (105) and (106), the conditions $F(0) = 1$ and $G(0) = 0$ will be met with increasing accuracy as $\tau_1 \rightarrow \infty$. Also, actual numerical calculations have shown that the errors with which the conditions $F(0) = 1$ and $G(0) = 0$ are met in the third or the fourth approximations (in our method of solution) are not large even for values of τ_1 of the order of 0.25 or less.

Turning, next, to the consideration of conservative cases, we have only $2n - 2$ non-vanishing roots for the characteristic equation. The expressions corresponding to (114) and (115) for $F(\mu)$ and $G(\mu)$ in partial fractions are, in consequence,

$$F(\mu) = \sum_{\alpha=-n+1}^{n-1} \frac{L_\alpha}{1 + k_\alpha \mu} + L_0 - \frac{1}{k_1^2 \dots k_{n-1}^2 \mu_1 \dots \mu_n} \frac{c_0^{(n-1)}}{[C_0^2(0) - C_1^2(0)]^{1/2}} \mu \quad (147)$$

and

$$G(\mu) = \sum_{\alpha=-n+1}^{n-1} \frac{L_\alpha e^{-k_\alpha \tau_1}}{1 - k_\alpha \mu} + \mathfrak{L}_0 - \frac{1}{k_1^2 \dots k_{n-1}^2 \mu_1 \dots \mu_n} \frac{c_1^{(n-1)}}{[C_0^2(0) - C_1^2(0)]^{1/2}} \mu, \quad (148)$$

where the $2n$ constants, $L_\pm \alpha (\alpha = 1, \dots, n-1)$, L_0 , and \mathfrak{L}_0 are again to be determined by conditions of the form (116) and $c_0^{(n-1)}$ and $c_1^{(n-1)}$ are, respectively, the coefficients

of the highest power, μ^{n-1} , in $C_0(\mu)$ and $C_1(\mu)$, defined in terms of the reduced number of characteristic roots appropriate for the conservative case.¹³ With expressions (147) and (148) for $F(\mu)$ and $G(\mu)$, the rest of the analysis proceeds exactly as in the nonconservative case. The only difference is that use must also be made of the equation

$$\sum_{j=-n}^{+n} \frac{a_j \mu_j \Psi(\mu_j)}{1 + k_a \mu_j} = 0 \quad (a = \pm 1, \dots, \pm n \mp 1), \quad (149)$$

which is valid only in conservative cases (cf. Paper XIV, eq. [159]).

One special characteristic of the solution (148) should be noted. We have

$$\begin{aligned} - \sum_{j=1}^n a_j \Psi(\mu_j) Y(\mu_j) &= \sum_{j=1}^{+n} a_j \Psi(\mu_j) G(\mu_j) = \sum_{j=-n}^{+n} a_j \Psi(\mu_j) G(\mu_j) \\ &= \sum_{a=-n+1}^{n-1} L_a e^{-k_a \tau_1} \left(\sum_{j=-n}^{+n} \frac{a_j \Psi(\mu_j)}{1 + k_a \mu_j} \right) + \mathfrak{Q}_0 \sum_{j=-n}^{+n} a_j \Psi(\mu_j). \end{aligned} \quad (150)$$

Since (conservative case!)

$$\sum_{j=-n}^{+n} a_j \Psi(\mu_j) = 1, \quad (151)$$

we have

$$- \sum_{j=1}^n a_j \Psi(\mu_j) Y(\mu_j) = \sum_{a=-n+1}^{n-1} L_a e^{-k_a \tau_1} + \mathfrak{Q}_0 = G(0). \quad (152)$$

We have already seen that the nonvanishing of $G(0)$ is a measure of the inaccuracy of our scheme of approximation. We therefore conclude that, for the exact solutions in the limit of infinite approximation,

$$\int_0^1 Y(\mu) \Psi(\mu) d\mu = 0, \quad (153)$$

and that the functions X and Y , defined in terms of the reduced number of the characteristic roots in conservative cases, must be associated with the *standard solutions* of the functional equations (1) and (2) as defined in § 5 (eqs. [64] and [65]).

We now summarize the conclusions that we have reached in the form of the following theorem:

Theorem 9.—The functions $X(\mu)$ and $Y(\mu)$ defined in terms of the nonvanishing roots of the characteristic equation

$$1 = 2 \sum_{j=1}^n \frac{a_j \Psi(\mu_j)}{1 - k^2 \mu_j^2} \quad (154)$$

in the manner

$$\begin{aligned} X(\mu) &= \frac{(-1)^n}{\mu_1 \dots \mu_n} \frac{1}{[C_0^2(0) - C_1^2(0)]^{1/2}} \frac{1}{W(\mu)} \\ &\quad [P(-\mu) C_0(-\mu) - e^{-\tau_1/\mu} P(\mu) C_1(\mu)] \end{aligned} \quad (155)$$

¹³ See particularly the remarks in Paper XXI, n. 12.

and

$$Y(\mu) = \frac{(-1)^n}{\mu_1 \dots \mu_n} \frac{1}{[C_0^2(0) - C_1^2(0)]^{1/2}} \frac{1}{W(\mu)} \quad (156)$$

$$[e^{-\tau_1/\mu} P(\mu) C_0(\mu) - P(-\mu) C_1(-\mu)],$$

where

$$C_0(\mu) = \sum_{\substack{l=n, n-2, \dots \\ 2^{n-1} \text{ terms}}} \epsilon_l^{(0)} \frac{\prod_{i=1}^l \prod_{m=1}^{n-l} (k_{r_i} + k_{s_m})}{\prod_{i=1}^l \prod_{m=1}^{n-l} (k_{r_i} - k_{s_m})} \prod_{i=1}^l (1 + k_{r_i} \mu) \prod_{m=1}^{n-l} \frac{1}{\lambda_{s_m}} (1 - k_{s_m} \mu) \quad (157)$$

and

$$C_1(\mu) = (-1)^{n-1} \sum_{\substack{l=n-1, n-3, \dots \\ 2^{n-1} \text{ terms}}} \epsilon_l^{(1)} \frac{\prod_{i=1}^l \prod_{m=1}^{n-l} (k_{r_i} + k_{s_m})}{\prod_{i=1}^l \prod_{m=1}^{n-l} (k_{r_i} - k_{s_m})} \times \prod_{i=1}^l (1 + k_{r_i} \mu) \prod_{m=1}^{n-l} \frac{1}{\lambda_{s_m}} (1 - k_{s_m} \mu), \quad (158)$$

where

$$\begin{aligned} \epsilon_l^{(0)} &= +1 \text{ for integers of the form } n-4l \\ &= -1 \text{ for integers of the form } n-4l-2 \\ &= 0 \text{ otherwise,} \end{aligned} \quad (159)$$

and

$$\begin{aligned} \epsilon_l^{(1)} &= +1 \text{ for integers of the form } n-4l-1 \\ &= -1 \text{ for integers of the form } n-4l-3 \\ &= 0 \text{ otherwise,} \end{aligned} \quad (160)$$

and

$$\lambda_a = e^{k_a \tau_1} \frac{P(-1/k_a)}{P(+1/k_a)}, \quad (161)$$

are, in the limit of infinite approximation, to be associated with the solutions of the functional equations

$$X(\mu) = 1 + \mu \int_0^1 \frac{\Psi(\mu')}{\mu + \mu'} [X(\mu) X(\mu') - Y(\mu) Y(\mu')] d\mu' \quad (162)$$

and

$$Y(\mu) = e^{-\tau_1/\mu} + \mu \int_0^1 \frac{\Psi(\mu')}{\mu - \mu'} [Y(\mu) X(\mu') - X(\mu) Y(\mu')] d\mu'. \quad (163)$$

In conservative cases, $X(\mu)$ and $Y(\mu)$ (defined in terms of the reduced number of nonvanishing characteristic roots) are in the limit of infinite approximation to be associated with the standard solutions of equations (162) and (163), having the property

$$\int_0^1 X(\mu) \Psi(\mu) d\mu = 1 \quad \text{and} \quad \int_0^1 Y(\mu) \Psi(\mu) d\mu = 0. \quad (164)$$

II. ISOTROPIC SCATTERING WITH AN ALBEDO $\varpi_0 \leq 1$

7. *Equations of the problem.*—For the problem of diffuse reflection and transmission by an atmosphere scattering radiation isotropically with an albedo $\varpi_0 \leq 1$, the basic equations are (cf. Paper XVII, eqs. [115]–[120])

$$I(0, \mu) = \frac{\varpi_0}{4\mu} FS(\mu, \mu_0); \quad I(\tau_1, -\mu) = \frac{\varpi_0}{4\mu} FT(\mu, \mu_0), \quad (165)$$

$$\left(\frac{1}{\mu_0} + \frac{1}{\mu}\right) S(\mu, \mu_0) = X(\mu) X(\mu_0) - Y(\mu) Y(\mu_0), \quad (166)$$

$$\left(\frac{1}{\mu_0} - \frac{1}{\mu}\right) T(\mu, \mu_0) = Y(\mu) X(\mu_0) - X(\mu) Y(\mu_0), \quad (167)$$

$$\frac{\partial S}{\partial \tau_1} = Y(\mu) Y(\mu_0), \quad (168)$$

and

$$\left(\frac{1}{\mu_0} - \frac{1}{\mu}\right) \frac{\partial T}{\partial \tau_1} = \frac{1}{\mu_0} X(\mu) Y(\mu_0) - \frac{1}{\mu} Y(\mu) X(\mu_0). \quad (169)$$

Further, the definitions of $X(\mu)$ and $Y(\mu)$ in terms of $S(\mu, \mu_0)$ and $T(\mu, \mu_0)$ are

$$X(\mu) = 1 + \frac{1}{2}\varpi_0 \int_0^1 S(\mu, \mu') \frac{d\mu'}{\mu'}, \quad (170)$$

and

$$Y(\mu) = e^{-\tau_1/\mu} + \frac{1}{2}\varpi_0 \int_0^1 T(\mu, \mu') \frac{d\mu'}{\mu'}. \quad (171)$$

In virtue of equations (166), (167), (170), and (171), we have the equations

$$X(\mu) = 1 + \frac{1}{2}\varpi_0 \mu \int_0^1 \frac{d\mu'}{\mu + \mu'} [X(\mu) X(\mu') - Y(\mu) Y(\mu')] \quad (172)$$

and

$$Y(\mu) = e^{-\tau_1/\mu} + \frac{1}{2}\varpi_0 \mu \int_0^1 \frac{d\mu'}{\mu - \mu'} [Y(\mu) X(\mu') - X(\mu) Y(\mu')]. \quad (173)$$

Thus X and Y satisfy functional equations of the form considered in Section I, with the characteristic function

$$\Psi(\mu) = \frac{1}{2}\varpi_0 = \text{constant}. \quad (174)$$

In considering the foregoing equations, it is of interest to establish, first, that equations (168) and (169) are really equivalent to the integrodifferential equations of theorem 1 (§ 3).

Thus, differentiating equation (170) with respect to τ_1 and using equation (168), we have

$$\frac{\partial X}{\partial \tau_1} = \frac{1}{2}\varpi_0 Y(\mu) \int_0^1 \frac{d\mu'}{\mu'} Y(\mu'). \quad (175)$$

Next, differentiating equation (171), we have

$$\frac{\partial Y}{\partial \tau_1} = -\frac{1}{\mu} e^{-\tau_1/\mu} + \frac{1}{2}\varpi_0 \int_0^1 \frac{d\mu'}{\mu - \mu'} \left[\frac{\mu}{\mu'} X(\mu) Y(\mu') - Y(\mu) X(\mu') \right]; \quad (176)$$

and, combining this with equation (173), we obtain

$$\frac{\partial Y}{\partial \tau_1} + \frac{Y}{\mu} = \frac{1}{2} \omega_0 X(\mu) \int_0^1 \frac{d\mu'}{\mu'} Y(\mu'). \quad (177)$$

It is seen that equations (175) and (177) are in agreement with equations (18) and (19) of theorem 1.

Finally, we may note that, according to equations (165)–(167) we can express the reflected and the transmitted intensities in the forms

$$I(0, \mu) = \frac{1}{4} \omega_0 F \frac{\mu_0}{\mu + \mu_0} [X(\mu) X(\mu_0) - Y(\mu) Y(\mu_0)] \quad (178)$$

and

$$I(\tau_1, -\mu) = \frac{1}{4} \omega_0 F \frac{\mu_0}{\mu - \mu_0} [Y(\mu) X(\mu_0) - X(\mu) Y(\mu_0)]. \quad (179)$$

8. The case $\omega_0 < 1$.—Comparing the expressions for the emergent intensities given in the preceding section (eqs. [178] and [179]) with those given in Paper XXI (Sec. I, eqs. [127] and [128]), we observe that we have here a confirmation and an illustration of the correspondence enunciated in theorem 9 between the functions X and Y occurring in the solutions of the equations of transfer in a finite approximation, and the functions defined in terms of the functional equations in the exact theory.

9. The ambiguity in the solution of the functional equations in the case $\omega_0 = 1$ and its resolution by an appeal to the K-integral.—When $\omega_0 = 1$, the equations (172) and (173) belong to the conservative class discussed in § 5, and, according to theorem 5, the solutions of these equations, in this case, are not unique, the general solutions being, in fact, expressible in the forms

$$X(\mu) + Q\mu [X(\mu) + Y(\mu)] \quad (180)$$

and

$$Y(\mu) - Q\mu [X(\mu) + Y(\mu)], \quad (181)$$

where Q is an arbitrary constant and $X(\mu)$ and $Y(\mu)$ are the standard solutions, having for the characteristic function $\frac{1}{2}$ the property

$$\alpha_0 = \int_0^1 X(\mu) d\mu = 2 \quad \text{and} \quad \beta_0 = \int_0^1 Y(\mu) d\mu = 0. \quad (182)$$

With solutions (180) and (181) of the equations

$$X(\mu) = 1 + \frac{1}{2} \mu \int_0^1 \frac{d\mu'}{\mu + \mu'} [X(\mu) X(\mu') - Y(\mu) Y(\mu')] \quad (183)$$

and

$$Y(\mu) = e^{-\tau_1/\mu} + \frac{1}{2} \mu \int_0^1 \frac{d\mu'}{\mu - \mu'} [Y(\mu) X(\mu') - X(\mu) Y(\mu')], \quad (184)$$

the expressions (178) and (179) for the emergent intensities take the forms

$$I(0, \mu) = \frac{1}{4} \omega_0 F \left\{ \frac{1}{\mu_0 + \mu} [X(\mu_0) X(\mu) - Y(\mu_0) Y(\mu)] + Q [X(\mu_0) + Y(\mu_0)] [X(\mu) + Y(\mu)] \right\} \quad (185)$$

and

$$I(\tau_1, -\mu) = \frac{1}{4}\mu_0 F \left\{ \frac{1}{\mu_0 - \mu} [Y(\mu_0)X(\mu) - X(\mu_0)Y(\mu)] - Q[X(\mu_0) + Y(\mu_0)][X(\mu) + Y(\mu)] \right\}. \quad (186)$$

Solutions (185) and (186) for the emergent intensities involve the arbitrary constant Q , and there is nothing in the framework of the equations of § 7, for the case $\omega_0 = 1$, which will remove this arbitrariness. We therefore conclude that the various invariances considered in Paper XVII are not sufficient to determine the physical solutions uniquely in conservative cases. We shall encounter further examples of this in Sections III and V. But it should be noted in the present context that a comparison of solutions (185) and (186) with those obtained in Paper XXI (Sec. II, eqs. [167]–[172]) provides a confirmation and an illustration of what is stated in theorem 9, namely, that the X - and Y -functions defined in terms of the reduced number of nonvanishing characteristic roots in conservative cases and which occur in the solutions of the equations of transfer in a finite approximation, are, in the framework of the exact theory, to be associated with the standard solutions of the corresponding functional equations.

We now turn to the matter of the arbitrariness in solutions (185) and (186) and the manner in which it is to be resolved.

The equation of transfer appropriate to the problem on hand is

$$\mu \frac{dI}{d\tau} = I(\tau, \mu) - \frac{1}{2} \int_{-1}^{+1} I(\tau, \mu') d\mu' - \frac{1}{4} F e^{-\tau/\mu_0}. \quad (187)$$

From this equation, two integrals which the problem admits can be derived. They are

$$F(\tau) = 2 \int_{-1}^{+1} I(\tau, \mu) \mu d\mu = \mu_0 F (e^{-\tau/\mu_0} + \gamma_1) \quad (188)$$

and

$$K(\tau) = \frac{1}{2} \int_{-1}^{+1} I(\tau, \mu) \mu^2 d\mu = \frac{1}{4} \mu_0 F (-\mu_0 e^{-\tau/\mu_0} + \gamma_1 \tau + \gamma_2), \quad (189)$$

where γ_1 and γ_2 are two constants. The first of these represents the flux integral. We shall refer to the second as the “ K -integral.”

Applying the integrals (188) and (189) at $\tau = 0$ and $\tau = \tau_1$, we have

$$F(0) = 2 \int_0^1 I(0, \mu) \mu d\mu = \mu_0 F (1 + \gamma_1), \quad (190)$$

$$F(\tau_1) = -2 \int_0^1 I(\tau_1, -\mu) \mu d\mu = \mu_0 F (e^{-\tau_1/\mu_0} + \gamma_1), \quad (191)$$

$$K(0) = \frac{1}{2} \int_0^1 I(0, \mu) \mu^2 d\mu = \frac{1}{4} \mu_0 F (-\mu_0 + \gamma_2), \quad (192)$$

and

$$K(\tau_1) = \frac{1}{2} \int_0^1 I(\tau_1, -\mu) \mu^2 d\mu = \frac{1}{4} \mu_0 F (-\mu_0 e^{-\tau_1/\mu_0} + \gamma_1 \tau_1 + \gamma_2). \quad (193)$$

On the other hand, we can also evaluate $F(0)$, $F(\tau_1)$, $K(0)$, and $K(\tau_1)$ according to the solutions (185) and (186) for $I(0, \mu)$ and $I(\tau_1, -\mu)$. In this manner we shall obtain four relations between the three constants γ_1 , γ_2 , and Q . However, it will appear that two of these four relations are equivalent and that, in fact, they just suffice to determine all the constants uniquely.

The integrals defining $F(0)$, $F(\tau_1)$, $K(0)$, and $K(\tau_1)$ in terms of $I(0, \mu)$ and $I(\tau_1, -\mu)$, given by equations (185) and (186), can all be evaluated by using the various relations valid for standard solutions and collected under theorem 8 (eqs. [81]–[86]). We find

$$F(0) = \mu_0 F \{ 1 + \frac{1}{2} Q (a_1 + \beta_1) [X(\mu_0) + Y(\mu_0)] \}, \quad (194)$$

$$F(\tau_1) = \mu_0 F \{ e^{-\tau_1/\mu_0} + \frac{1}{2} Q (a_1 + \beta_1) [X(\mu_0) + Y(\mu_0)] \}, \quad (195)$$

$$K(0) = \frac{1}{4} \mu_0 F \{ -\mu_0 + \frac{1}{2} a_1 X(\mu_0) - \frac{1}{2} \beta_1 Y(\mu_0) + \frac{1}{2} Q (a_2 + \beta_2) [X(\mu_0) + Y(\mu_0)] \}, \quad (196)$$

and

$$K(\tau_1) = \frac{1}{4} \mu_0 F \{ -\mu_0 e^{-\tau_1/\mu_0} + \frac{1}{2} \beta_1 X(\mu_0) - \frac{1}{2} a_1 Y(\mu_0) - \frac{1}{2} Q (a_2 + \beta_2) [X(\mu_0) + Y(\mu_0)] \}, \quad (197)$$

where a_n and β_n are the moments of order n of $X(\mu)$ and $Y(\mu)$, respectively (cf. eq. 11).

It is now seen that equations (190) and (194) and (191) and (195), in agreement with each other, determine

$$\gamma_1 = \frac{1}{2} Q (a_1 + \beta_1) [X(\mu_0) + Y(\mu_0)]. \quad (198)$$

From equations (192) and (196) we next find that

$$\gamma_2 = \frac{1}{2} a_1 X(\mu_0) - \frac{1}{2} \beta_1 Y(\mu_0) + \frac{1}{2} Q (a_2 + \beta_2) [X(\mu_0) + Y(\mu_0)]. \quad (199)$$

Finally, from equations (193) and (197) we obtain

$$\gamma_1 \tau_1 + \gamma_2 = \frac{1}{2} \beta_1 X(\mu_0) - \frac{1}{2} a_1 Y(\mu_0) - \frac{1}{2} Q (a_2 + \beta_2) [X(\mu_0) + Y(\mu_0)]. \quad (200)$$

Now, substituting for γ_1 and γ_2 in equation (200), according to equations (198) and (199), we find

$$\frac{1}{2} Q (a_1 + \beta_1) \tau_1 = -\frac{1}{2} (a_1 - \beta_1) - Q (a_2 + \beta_2). \quad (201)$$

Hence,

$$Q = -\frac{a_1 - \beta_1}{(a_1 + \beta_1) \tau_1 + 2(a_2 + \beta_2)}. \quad (202)$$

With this determination of Q in terms of the optical thickness, τ_1 , of the atmosphere and the moments of the standard solutions of equations (183) and (184), we have removed the arbitrariness left by the functional equations in the solutions for the emergent intensities. It is in some ways remarkable that an explicit appeal to the K -integral is necessary to resolve the arbitrariness left by the functional equations. We shall see later that similar appeals to the K -integrals are necessary in the two other cases of perfect scattering that we shall consider (namely, Rayleigh scattering and scattering in accordance with Rayleigh's phase function) to resolve the ambiguities in the solutions of the functional equations incorporating the various invariances of the problem.

10. The verification that Q satisfies the differential equation of theorem 7.—It is apparent that the quantity Q as introduced in § 9 must satisfy the differential equation of theorem 7. In our present context we can write this equation (eq. [70]) in the form

$$\frac{d}{d\tau_1} \left(\frac{1}{Q} \right) - \frac{\beta_{-1}}{Q} = -1, \quad (203)$$

since

$$y_{-1} = \frac{1}{2} \int_0^1 \frac{d\mu'}{\mu'} Y(\mu') = \frac{1}{2} \beta_{-1}. \quad (204)$$

We shall now show that Q as defined by equation (202) satisfies equation (203).

Making use of the relation (cf. theorem 8, eq. [82])

$$\alpha_1^2 - \beta_1^2 = 4 \int_0^1 \mu^2 d\mu = \frac{4}{3}, \quad (205)$$

we first re-write equation (202) in the form

$$\frac{1}{Q} = -\frac{3}{4} [(\alpha_1 + \beta_1)^2 \tau_1 + 2(\alpha_2 + \beta_2)(\alpha_1 + \beta_1)]. \quad (206)$$

From this equation we then obtain

$$\begin{aligned} \frac{d}{d\tau_1} \left(\frac{1}{Q} \right) = & -\frac{3}{4} \left[(\alpha_1 + \beta_1) \left\{ (\alpha_1 + \beta_1) + 2\tau_1 \frac{d}{d\tau_1} (\alpha_1 + \beta_1) \right\} \right. \\ & \left. + 2(\alpha_2 + \beta_2) \frac{d}{d\tau_1} (\alpha_1 + \beta_1) + 2(\alpha_1 + \beta_1) \frac{d}{d\tau_1} (\alpha_2 + \beta_2) \right]. \end{aligned} \quad (207)$$

To simplify equation (207) further, we observe that, according to equations (175) and (177), we now have

$$\frac{d}{d\tau_1} (X + Y) = \frac{1}{2} \beta_{-1} (X + Y) - \frac{Y}{\mu}. \quad (208)$$

Multiplying this equation by μ^n and integrating over the range of μ , we obtain

$$\frac{d}{d\tau_1} (\alpha_n + \beta_n) = \frac{1}{2} \beta_{-1} (\alpha_n + \beta_n) - \beta_{n-1}. \quad (209)$$

In particular,

$$\frac{d}{d\tau_1} (\alpha_1 + \beta_1) = \frac{1}{2} \beta_{-1} (\alpha_1 + \beta_1) \quad (210)$$

(since, according to eq. [182], $\beta_0 = 0$), and

$$\frac{d}{d\tau_1} (\alpha_2 + \beta_2) = \frac{1}{2} \beta_{-1} (\alpha_2 + \beta_2) - \beta_1. \quad (211)$$

Using the foregoing relations in equation (207), we find, after some minor reductions, that

$$\begin{aligned} \frac{d}{d\tau_1} \left(\frac{1}{Q} \right) = & -\frac{3}{4} [\beta_{-1} \{ (\alpha_1 + \beta_1)^2 \tau_1 + 2(\alpha_2 + \beta_2)(\alpha_1 + \beta_1) \} \\ & + (\alpha_1 + \beta_1)^2 - 2\beta_1(\alpha_1 + \beta_1)]. \end{aligned} \quad (212)$$

Hence (cf. eqs. [205] and [206])

$$\frac{d}{d\tau_1} \left(\frac{1}{Q} \right) = \frac{\beta_{-1}}{Q} - \frac{3}{4} (\alpha_1^2 - \beta_1^2) = \frac{\beta_{-1}}{Q} - 1. \quad (213)$$

This completes the verification.

(To be continued)

A PHOTOELECTRIC GUIDER FOR ASTRONOMICAL TELESCOPES*

HORACE W. BABCOCK

Mount Wilson Observatory

Received August 28, 1947

ABSTRACT

A new and simple method of optical scanning with a rotating knife-edge, in combination with the modern electron multiplier phototube, makes practicable for the first time an automatic device for guiding astronomical telescopes. A comparatively simple guider, working in both right ascension and declination and employing a single phototube, is performing satisfactorily in guiding the 100-inch reflector for high-dispersion spectrographic work. The instrument compensates for fluctuations in the apparent position of the star due to "seeing" and for residual errors in the driving mechanism of the telescope.

INTRODUCTION

An experimental guider for an astronomical telescope was designed by A. E. Whitford and G. E. Kron¹ and tested by them on the 60-inch reflector at Mount Wilson in 1936. This instrument employed one of the first developmental multiplier phototubes. Light of the guide star was split by a 90° roof-prism into two beams that were alternately chopped by a rotating sector disk and then reunited on the sensitive surface of the phototube. Although this guider performed well, it worked in only one co-ordinate (right ascension) and was a comparatively bulky piece of equipment. Whitford and Kron concluded that the conservative working limit of their guider was magnitude 8.6 at the focus of the 60-inch telescope (9.7 at the 100-inch or 11.2 at the 200-inch) but that it would be of doubtful usefulness in direct photography, owing to the scarcity of sufficiently bright guide stars.

In 1938 Whitford constructed a guider for the 65-foot solar tower telescope of the Mount Wilson Observatory. Owing to the large amount of light available, a solar guider naturally presents a much simpler problem than one for stellar work. This instrument controlled the position of the solar image in only one co-ordinate but was adequate to meet the demands. It has been in regular use since its completion. A more recent solar guider has been described by W. O. Roberts.² This instrument, employing four phototubes, works in two co-ordinates.

REQUIREMENTS

Observations with large astronomical telescopes are predominantly of two general types: (1) photography of the spectra of individual stars, which involves keeping the image of the star accurately on the slit of the spectrograph for the duration of the observation, and (2) direct photography, in which a photographic plate is exposed at the focus of the telescope while a guide star, off the optic axis (and hence subject to more or less severe coma), is followed in an eyepiece equipped with cross-hairs. In the latter case, guiding is usually done by the observer with a double-slide carriage actuated by hand-controlled screws; the carriage holds both the plateholder and the guiding eyepiece.

For the successful application of a photoelectric guider to direct photography, it is necessary that the phototube be sufficiently sensitive to follow with precision the average guide star that can be picked up in the limited area of the sky available close to the photographic plate. Even with the improved phototubes of today, this requirement remains rather difficult to meet. However, the requirements are much less stringent for a guider to be used with spectrographs of moderate or high dispersion, since such instru-

* Contributions from the Mount Wilson Observatory, No. 739.

¹ *Rev. Sci. Inst.*, **8**, 78, 1937.

² *Electronics*, **19**, 100, 1946.

ments are generally used only on stars brighter than the limit set by the sensitivity of the phototube. In spectrographic work, since the star under observation is on the optic axis of the telescope, coma is absent; furthermore, a considerable fraction (occasionally as much as 90 per cent) of the light does not pass through the slit but is reflected back from the polished slit jaws and is generally used in manual guiding. This same reflected light can equally well be used to actuate an automatic guiding device without any depletion of the light admitted to the spectrograph. It seems evident, then, that high-dispersion stellar spectroscopy is a type of astronomical work well adapted to an automatic guider, and this is particularly true because many of the exposures made in this type of work are of several hours' duration. The instrument to be described could, however, be adapted to direct photography and perhaps also to other uses involving the tracking of faint light-sources.

With a 12-inch telescope, accurate stellar photometry can be carried out on stars as faint as the tenth magnitude, using a 1P21 phototube³ (unrefrigerated). It is easily calculated from this that similar photometry should be feasible at the focus of the 100-inch reflector down to about magnitude 14, and hence it is estimated that a guider should function well with this telescope down to about the thirteenth magnitude, depending partly on the fraction of starlight reflected back at the slit.

When doing manual guiding at the coude focus of the 100-inch reflector, the observer makes use of a small auxiliary guiding telescope which is focused on the slit of the spectrograph. In this guiding telescope he sees a magnified image of the slit and of the star; by means of slight motions of the main telescope, which he actuates by a group of four push buttons, the observer corrects any deviations of the image of the star from the desired position on the slit. The motions are exceedingly slow and free from backlash, permitting corrections of a fraction of a second of arc in the pointing of the large telescope. The long equivalent focal length (250 feet) of the coude optical system necessitates nearly constant attention to guiding, except under such conditions of "seeing" that the image is large but steady in position. As a rule, guiding corrections are required every few seconds, partly because of random fluctuations in the position of the star due to atmospheric turbulence and partly to compensate for slight irregularities in the drive. The drive of the 100-inch telescope is nearly perfect, as the governor-controlled mechanical clock is exceedingly steady, and by means of a new transmission the rate can be adjusted over a continuous range of $1\frac{1}{4}$ per cent while an observation is in progress. Periodic error is almost, if not entirely, absent. In actual practice, in work at the coude focus, nearly as many corrections are made in declination as in right ascension; this indicates that any guider, to be satisfactory, must work in two co-ordinates. While for the 100-inch telescope the purpose of the guider is largely to overcome fluctuations in position due to imperfect seeing, it is perhaps worth pointing out that for some types of work a good guider could be expected to compensate satisfactorily the effects of larger errors in the driving system of a telescope, thus reducing the highly rigorous demands usually made on the drive.

DESCRIPTION

The guider that I designed and constructed in March, 1947, works at the focus of the fixed guiding telescope normally used for observing the star on the slit of the coude spectrograph. The ordinary eyepiece of the guiding telescope is replaced by an Huyghenian eyepiece, to which has been added a scanning device and a phototube. This scanning eyepiece forms one unit of the guider; the other is a small cabinet containing an amplifier, relays, controls, and a 2-inch cathode-ray tube used as an indicator of the star's exact position. A schematic diagram is shown in Figure 1, while Figures 2 and 3 show the scanner and amplifier.

³ G. E. Kron, *Bulletin of Panel on Orbits of Eclipsing Binaries*, No. 4 (panel held at Harvard College Observatory, 1946).

Inside the eyepiece of the scanner is mounted, in small ball bearings, a short coaxial brass tube, about 5 mm in inside diameter; and at the focal plane, inside the tube, is placed an orange gelatin filter, covering just half the field. The diametral edge of the filter, forming a "knife-edge," accurately intersects the optic axis, which is coincident with the axis of rotation of the tube. The orange filter only partially obstructs the visual light of the star, but it is essentially opaque as far as the phototube is concerned, since the 1P21 has little sensitivity to the red of $\lambda 6000$. On the outside of the brass tube a small worm gear is so mounted that the tube with its knife-edge can be rotated by a miniature electric motor at a rate of about 3 r.p.s.

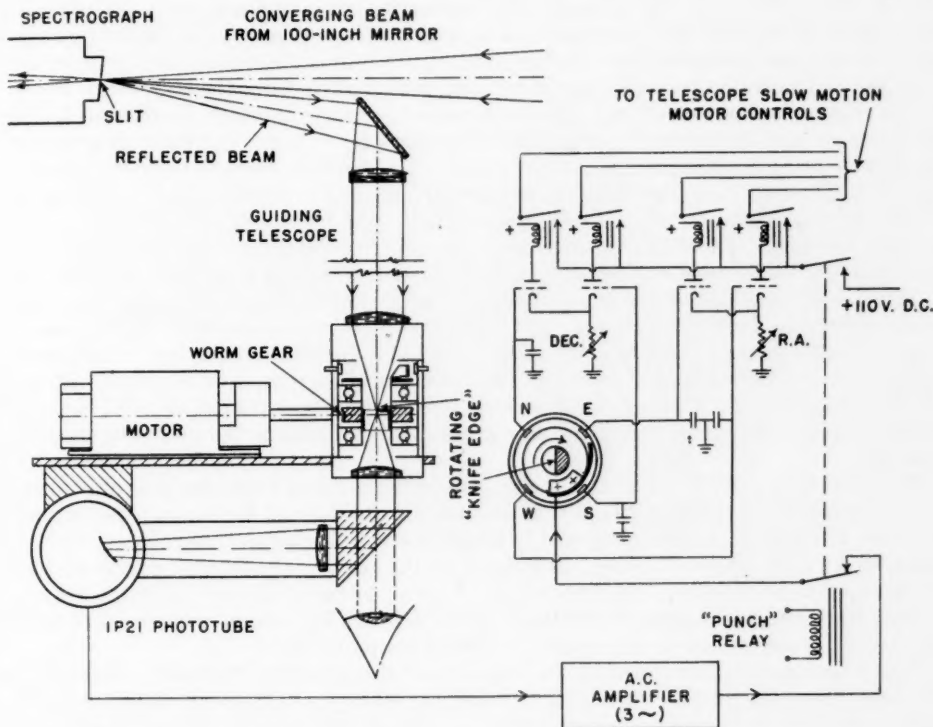


FIG. 1.—Schematic diagram of guider. The central tube in the eyepiece, carrying the knife-edge and the distributor brush, is rotated by the miniature motor through a worm and worm gear. The "punch" relay is briefly closed at regular intervals by a multi-vibrator circuit (not shown). The N, E, S, and W contacts of the distributor are connected to the corresponding deflecting plates of the cathode-ray tube shown in Fig. 3.

It is obvious that, if the image of the star lies on the optic axis, the flow of light past the rotating knife-edge will be constant but that, if the star position deviates, even by a small fraction of the diameter of the image, the intensity of the transmitted light will vary cyclically. The amplitude of the variations will be a measure of the deviation, if the deviation is small, while the phase of the fluctuating signal will indicate the direction in which the telescope must be moved to return the star to the desired axial position. For small deviations the error signal will be approximately sinusoidal, with a frequency equal to the rotation frequency of the knife-edge; for larger deviations, the error signal will approach a square wave. The guider now in use responds only to the fundamental fre-

quency of the error signal, but in a more elaborate system the higher-frequency components in the signal for large deviations could be employed to give a more rapid correction.

The scanner is so designed that the observer may look into the eyepiece for setting and for checking performance of the guider; when going to automatic control, a right-angle prism is swung into position behind the eyepiece, and this directs the light into a 1P21 phototube that is mounted in a shielded housing attached to the eyepiece assembly. The whole scanner, including motor, phototube, distributor, and optics is quite compact and weighs about 1 pound. The output current from the anode of the phototube is fed through a load resistor of several megohms, and the resulting signal voltage is amplified by a rather conventional amplifier of adjustable gain until the random low-frequency noise is of the order of a volt in amplitude. Higher-frequency noise is easily filtered out. The output of the amplifier is applied to a cathode-follower to give a low-impedance signal, which is then conducted back to the scanner, where it is distributed to four separate circuits by a brush that is carried on the rotating tube that contains the knife-edge. Phase discrimination is thus established. The four contacts of the miniature distributor, inside the eyepiece, are connected to capacitors that store up voltages corresponding to the amount of starlight transmitted by the scanner in the four directions—north, east, south, and west. The four capacitor voltages, in turn, are applied in opposing pairs to the grids of double-triode balance tubes, in the plate circuits of which are miniature relays, one for each direction. The cathode resistors of the double triodes are variable, so that the sensitivity, or "tightness" of guiding, may be adjusted separately in the two co-ordinates.

It is neither feasible nor necessary to have these small relays control the telescope slow motions directly. Instead, the contacts of the four control relays are fed through a heavy-duty "punching relay," which, by means of a multivibrator circuit, is intermittently closed at intervals of about 3 seconds. The duration of the punch is adjustable by the observer to match the quality of the seeing. This intermittent control permits the telescope to follow the excursions of the star image with sufficient speed and without overshooting.

The punching relay is one of the double-pole, double-throw type; one pair of contacts opens the amplifier circuit to the distributor for the duration of the punch; another pair supplies 110 V.D.C. to the contacts of the small control relays. Thus, the control circuits, which carry about 0.6 amp., are opened by the heavy-duty punching relay and not by the small control relays. The four control circuits, connected in parallel with the regular hand-operated telescope control buttons (which can be used at any time), actuate permanent power relays on the telescope control switchboard.

The four capacitors supplied by the contacts of the distributor are also connected to the four deflecting plates of a 2-inch cathode-ray tube. A single power supply provides about 800 volts D.C. (negative) for both the 1P21 phototube and the accelerating potential in the cathode-ray tube. While not really essential to the operation of the guider, the cathode-ray tube is of great convenience in making adjustments of the instrument and gives at a glance an indication of the performance. The spot on the screen of the tube, deflected by the unbalance in the co-ordinate voltages, shows in a greatly magnified way the microscopic deviations of the star image from the desired position and the correction of these deviations by the action of the guider. Symmetrically disposed about the screen of the cathode-ray tube are four small green pilot lights connected in series with the appropriate control relay circuits for the various directions. When the guider is working, any deviation of the indicating spot from its normal position in the center of the screen is closely followed by the flashing of one or two of the pilot lights on the side of the screen toward which the spot has moved, and the spot is quickly returned to the center.

If the star under observation is at a considerable zenith distance, atmospheric dispersion is encountered—the stellar image is no longer round but is spread out into a short spectrum. Under these conditions, the guider keeps the "photographic region" of



FIG. 2.—Photograph of the scanning eyepiece. The driving worm can be seen on the end of the motor shaft, and three of the distributor terminals are visible on the outside of the eyepiece. The right-angle prism at the left can be swung into position behind the eyepiece to direct the light into the 1P21 phototube.

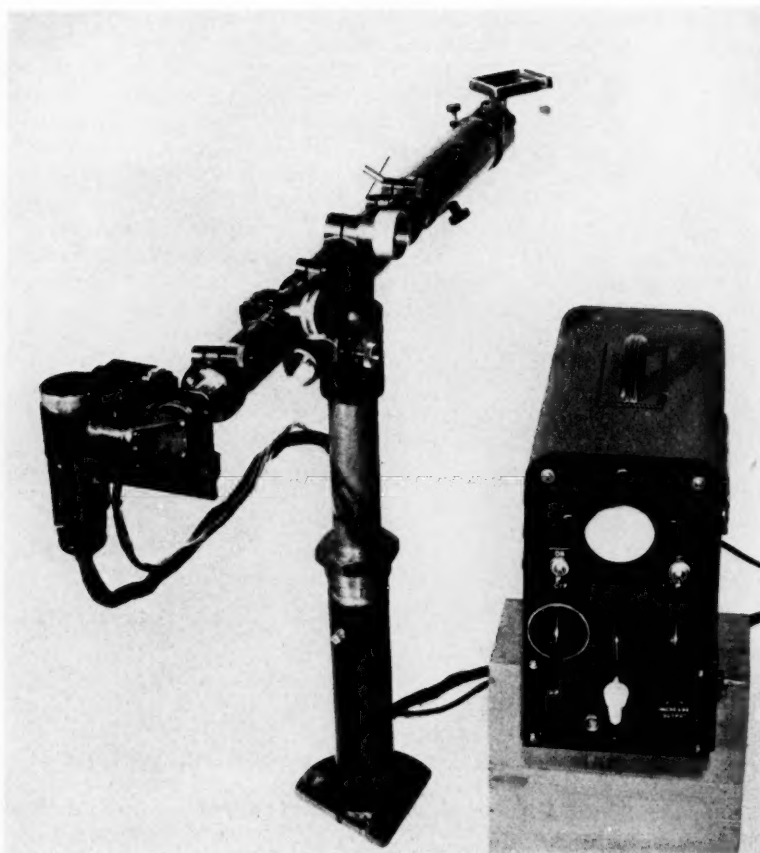


FIG. 3.—The scanning eyepiece mounted on the guiding telescope, together with the amplifier. A right-angle prism (not visible) on the far end of the guiding telescope receives light from the slit. The amplifier cabinet contains an 800-volt D.C. power supply for the phototube and the 2-inch cathode-ray tube, a separate 200-volt power supply, two-stage amplifier, and cathode-follower for the phototube signal, balance tubes, four miniature direction-control relays, "punch" relay with multivibrator, and rectifier for supplying D.C. to the scanning motor. The panel controls include potentiometers for adjusting the "tightness" of guiding in right ascension and declination, cathode-ray tube intensity, scanning speed, gain, and duration of punch. The four pilot lights around the cathode-ray tube show the direction in which the telescope is moved. Cable connections to the scanner and to the telescope switchboard are made at the back of the cabinet.

the image on the optic axis, since the 1P21 phototube has its maximum sensitivity at about λ 4000. This, of course, is the desired operating condition if the violet or blue region is being photographed by the spectrograph, as is usually the case. Visual guiding on this region of an atmospherically dispersed image is often rather inefficient.

When adjusting the guider on a star, the observer looks into the eyepiece of the scanner, having swung the deflecting prism to one side. He then sees the star on the slit; the rotating orange filter covering half the field is rather blurred except near the center. The point on the diametral edge of the filter that coincides with the axis of rotation appears as a stationary black dot, and the guider will center the star on this dot. By means of fine-pitch adjusting screws, the whole guiding telescope with the scanner may be moved so that the black dot falls on any desired point on or close to the slit. This feature enables the observer to apply "judgment" to the guider. If, for instance, the image is elongated by atmospheric dispersion and it is desired to photograph the red region of the spectrum, the black dot may be placed to one side so that the red part of the image falls on the slit. Or, if it is desired to observe one component of a close double star—in which case the guider brings the "center of light" of the pair to the axis of rotation—the dot may be displaced just enough to place the desired star on the slit.

At the coudé focus, the celestial field rotates with the telescope as it follows a star across the sky. In order that a deviation of the image in any given direction may be corrected by a motion of the telescope in the opposite direction, it is necessary that the hour-angle of the scanner be adjusted from time to time to maintain a rough correspondence with the hour-angle of the telescope. This adjustment is fortunately not at all critical, and a slight rotation of the whole scanning unit about every 2-hours is the only requirement. In case this adjustment is overlooked, the cathode-ray tube indicator will show the star moving in a rough loop or spiral path about the axis, under the action of the guider, instead of returning directly to the center.

PERFORMANCE

The guider has been in use each month since March, 1947, and I have employed it for practically all the plates that I have taken during this time. In addition to the obvious advantage of relieving the observer of many hours of rather tedious and exacting labor each night, the guider contributes to the efficiency of the work by permitting each plate to be developed while the next one is being taken and by facilitating the planning of the sequence of observations to match conditions. When properly adjusted, the automatic instrument has proved to be fully as efficient as an exacting human observer. To date, most of the observations with the guider have been on stars brighter than the eighth magnitude, and no definitive test has been made to determine how closely the theoretical limiting magnitude can be approached with satisfactory operation.

It will be recognized that the system of telescope, stellar image, guider, and control circuits is essentially a servomechanism of the intermittent-control type. This type of servo was used in the present case because it is quite adequate for the purpose and because it was easily adapted to the existing control circuits of the telescope. Various modifications of the basic system, by which it could be converted to one of the continuous-control type, are fairly obvious. For instance, if this type of scanner were to be adapted to direct photography, a double-slide carriage would be used, with two orthogonal screws driven by a pair of two-phase servomotors. The double-triode balance tubes following the distributor would drive balanced modulator circuits, supplying the motors, through amplifiers, with the appropriate A.C. error voltages. With proper damping, such a system would respond rapidly and continuously to errors, and the observer would still be able to apply "judgment corrections" from time to time by offsetting the scanner with respect to fixed cross-hairs.

SUNSPOT GROUPS OF IRREGULAR MAGNETIC POLARITY*

ROBERT S. RICHARDSON

Mount Wilson Observatory

Received August 29, 1947

ABSTRACT

Of 7890 spot-groups observed at Mount Wilson from January 1, 1917, to December 31, 1946, 6387 were classified magnetically. Of those classified, 5814, or 91.0 per cent, showed bipolar characteristics. Of the remaining groups, 24, or 0.4 per cent, were complex, with mixed polarities; 549, or 8.6 per cent, were unipolar. Among the 5814 bipolar groups were 180, or 3.1 per cent, which did not conform to the laws of sunspot polarity. Such spot-groups are said to be of *irregular magnetic polarity*. *The purpose of the investigation was to determine whether the groups of irregular polarity were irregular in other ways.*

Although irregular spot-groups may be of any size up to those visible to the unaided eye and may endure for several rotations, on the average they are slightly smaller and less stable than regular bipolar groups.

The axes of irregular groups seem to be inclined at larger angles to the solar equator than are the axes of regular groups. Such large inclinations might be expected on the hypothesis of the origin of sunspots proposed by V. Bjerknes.

The frequency and mean latitude of regular and irregular groups were examined for the cycles 1922-1935 and 1933-1945. No differences were revealed exceeding those between regular groups in different cycles and in opposite hemispheres. At the beginning of a cycle the mean latitude of the irregular groups was from 2° to 4° higher than that of the regular groups but decreased more rapidly, so that, when the cycle was about three-quarters over, the latitudes of the regular and the irregular groups were essentially the same.

The ratio of irregular to regular groups in different cycles does not appear to be constant, the percentage of irregular groups in the cycle 1922-1935 being about 30 per cent higher than in the cycles 1913-1924 and 1933-1945.

Mount Wilson Group No. 7732, first seen on March 24, 1945, in latitude 31° S., was a large stable spot of irregular polarity, exceptionally well suited for individual study. Investigation for magnetic field, Wilson effect, and Evershed effect failed to reveal abnormal characteristics. The vortex-structure of the surrounding hydrogen flocculi showed a counterclockwise distribution, opposite to that in 75 per cent of the regular spot-groups studied.

Thirteen recurrent spot-groups which were irregular in polarity during part of their lifetime were examined during the transition period. In five groups the behavior during transition was closely similar.

During some state of their life-history, sunspot groups usually consist of two members of opposite magnetic polarity so situated that a line joining them would be inclined at a small angle to the solar equator. The western member of the group is called the "leading spot," since it precedes or leads the eastern or following member as the two are carried across the sun's disk by the solar rotation. The arrangement in magnetic polarity of spot-groups is opposite in the northern and southern hemispheres and remains unchanged during the eleven-year cycle. The entire arrangement of polarities changes sign at the beginning of each new cycle.¹ These characteristics of spot-groups are so persistent that they can be expressed as definite laws of sunspot polarity.

Among the thousands of spot-groups that conform to these laws, however, a few constitute definite exceptions. Such groups are said to be of irregular magnetic polarity. Irregular spot-groups are so rare that one's natural tendency is to dismiss them as casual interlopers or sports among the horde of regular groups. But since in science exceptional objects often turn out to be surprisingly profitable upon closer investigation, a preliminary discussion of the available data on irregular spot-groups may later prove of value. Certainly, these rare groups must receive consideration in any theory of the origin of sunspots.

* Contributions from the Mount Wilson Observatory, Carnegie Institution of Washington, No. 740.

¹ Hale and Nicholson, *Mt. W. Contr.*, No. 300; *Ap. J.*, 62, 270, 1925.

Since January 1, 1917, a regular program of solar observations has been carried on at the 60- and 150-foot sun towers on Mount Wilson. A continuous record is therefore available which covers the last eight years of the cycle 1913-1923, the two complete cycles 1922-1935 and 1933-1945, and the first three years of the cycle which began in 1943. The methods of observation and of magnetic classification have previously been discussed in detail.²

A preliminary list of irregular spot-groups was formed from the notes to the *Magnetic Observations of Sunspots 1917-1924*,³ and from the *Magnetic Observations of Sunspots* in the *Publications of the Astronomical Society of the Pacific*. Each irregular group was re-examined on the original records, and a few whose bipolar characteristics were poorly defined were rejected.

Of 7890 spot-groups of all kinds observed at Mount Wilson from January 1, 1917, to December 31, 1946, 6387 were classified magnetically. Of those classified, 5814, or 91.0 per cent, were either definitely bipolar (β , β_p , β_f) or incompletely bipolar (α_p , α_f , $\beta\gamma$).⁴ Among these groups that displayed bipolar characteristics, 180, or 3.1 per cent, were irregular in polarity during most of their lifetime or, in the case of recurrent groups, irregular during the major portion of at least one transit. Of the remaining 573 classified groups, 24, or 0.4 per cent, were complex with mixed polarities (γ), and 549, or 8.6 per cent, were unipolar (α). Of the 7890 groups observed, 1503, or 19.0 per cent, were so small or the observations so fragmentary that the magnetic classification was unknown or uncertain.

The question that one would most like to have answered about irregular spot-groups is whether they are also irregular in other ways. In an attempt to find the answer, a list was made of ways in which spot-groups may differ among themselves:

STATISTICALLY

- Area
- Duration or stability
- Inclination to the equator
- Change in mean latitude with progress of the cycle
- Change in frequency with progress of the cycle

INDIVIDUALLY

- Strength and distribution of magnetic field
- Wilson effect
- Evershed effect
- Hydrogen vortex

Other characteristics could be added, such as intensity of umbra and penumbra relative to the surrounding photosphere, spectral peculiarities, etc.; but they are omitted because the necessary data would require a long program of special observations.

I. STATISTICAL COMPARISONS

AREA

The areas of sunspots corrected for foreshortening are customarily expressed in millionths of a solar hemisphere. The smallest spots certainly observable have an area of about 5; that is, they cover five-millionths of the visible solar surface. The largest spot-

² Hale, Ellerman, Nicholson, and Joy, *Mt. W. Contr.*, No. 165; *Ap. J.*, **49**, 153, 1919; Hale and Nicholson, *Mt. W. Contr.*, No. 300; *Ap. J.*, **62**, 270, 1925.

³ Hale and Nicholson, *Carnegie Institution of Washington Publication* 498, Part I; *Papers of the Mount Wilson Observatory*, Vol. V, Part I (1938).

⁴ Since the form of a spot-group differs from day to day, its classification as α_p or β_p , for example, depends upon its predominating magnetic characteristics. Other workers would doubtless obtain slightly different figures from those quoted here.

group for which we have reliable observations was that of April, 1947, which had a maximum area of 5400.⁵

The areas and positions of sunspots for each day in the year from 1878 to 1936 have been published in the *Greenwich Photoheliographic Results*. Since January, 1927, the areas and positions of spots have been published also in the *Monthly Weather Review* from data obtained principally from the Naval Observatory, with the aid of several co-operating institutions.

Since there is a systematic difference between the area of spots measured at Greenwich and the area measured at the Naval Observatory, it seemed safer not to combine results obtained from the two sources but to compare areas taken only from the same series of measurements. Table 1A shows the distribution in area obtained for 3496 spot-groups of regular polarity and 115 groups of irregular polarity, classified from 1917 to 1936, inclusive. The first column contains the ranges into which the spots were grouped;

TABLE 1A
COMPARISON OF NUMBER OF IRREGULAR SPOT-GROUPS OBSERVED WITH THE NUMBER
EXPECTED FROM DISTRIBUTION OF REGULAR SPOT-GROUPS
1917-1936 INCLUSIVE (GREENWICH)

Areas	Irreg. (No. Obs.)	Reg. (%)	Irreg. (Obs. - Expec.)	Reg. (%)	Irreg. (Obs. - Expec.)	Reg. (%)	Irreg. (Obs. - Expec.)	Reg. (%)	Irreg. (Obs. - Expec.)
0-50.....	80	51.6	+20.7						
50-100.....	15	15.5	-2.8	32.1	+3.8				
100-150.....	8	8.8	-2.1	18.2	+1.6	26.8	+2.6		
150-200.....	5	5.8	-1.7	12.1	+0.8	17.8	+1.4	24.3	+2.1
200-250.....	1	4.2	-3.8	8.7	-2.0	12.8	-1.6	17.5	-1.1
250-300.....	1	2.8	-2.2	5.8	-1.0	8.5	-0.7	11.6	-0.4
300-350.....	1	2.1	-1.4	4.3	-0.5	6.4	-0.3	8.7	0.0
350-400.....	0	1.5	-1.7	3.2	-1.1	4.7	-0.9	6.4	-0.8
400-450.....	1	1.2	-0.4	2.4	+0.2	3.5	+0.3	4.8	+0.4
450-500.....	0	1.0	-1.2	2.1	-0.7	3.1	-0.6	4.3	-0.5
500.....	3	5.4	-3.2	11.1	-0.9	16.4	-0.3	22.4	+0.3

the second, the number of irregular spots observed in each area group; the third, the percentage of regular spots in each area group; and the fourth, the difference between the number of irregular spots observed in the second column and the number that would be expected if the distribution were identical with that of the regular spots. Table 1B contains corresponding data for 2138 regular spot-groups and 65 irregular spot-groups, recorded from 1937 to 1946, inclusive.

Both tables show that the number of irregular groups of area 0-50 is significantly larger than would be expected if the distribution were similar to that of the regular groups, the excess amounting to three times the standard deviation. That irregular groups are smaller, on the average, than regular groups may also be shown by successively eliminating groups in the ranges 0-50, 50-100, etc., and then comparing the number of irregular groups remaining with the number expected, corresponding to the new distributions of the regular groups. The results shown in the fifth to tenth columns indicate that the percentage of irregular groups is generally greatest among the groups of smallest area considered.

DURATION

The relative stability of regular and irregular groups was studied by comparing the number that endured for 1, 2, 3, . . . days up to half a synodic rotation of 13 or 14 days.

⁵ *Nature*, 159, 549, 1947.

The length of time that a spot-group is visible depends partly, of course, upon its longitude when first seen. A group first seen at the east or approaching limb may remain visible for 13 or 14 days, whereas a group born near the central meridian cannot be seen for more than 6 or 7 days.

An ideal study would involve dividing the visible solar hemisphere into lunes—say, 15° of longitude wide—and comparing the duration of groups first seen within the same lune. Unfortunately, the limited number of irregular groups makes such a comparison

TABLE 1B

COMPARISON OF NUMBER OF IRREGULAR SPOT-GROUPS OBSERVED WITH THE NUMBER EXPECTED FROM DISTRIBUTION OF REGULAR SPOT-GROUPS
1937-1946 INCLUSIVE (*Monthly Weather Review*)

Areas	Irreg. (No. Obs.)	Reg. (%)	Irreg. (Obs. - Expec.)	Reg. (%)	Irreg. (Obs. - Expec.)	Reg. (%)	Irreg. (Obs. - Expec.)	Reg. (%)	Irreg. (Obs. - Expec.)
0-50.....	33.5	41.6	+6.5						
50-100.....	12.5	21.5	-1.5	36.9	+0.9				
100-150.....	4.5	10.4	-2.3	17.8	-1.1	28.2	-0.9		
150-200.....	2.5	7.1	-2.1	12.2	-1.3	19.4	-1.2	27.0	-1.4
200-250.....	7.0	5.1	+3.7	8.7	+4.3	13.8	+4.4	19.2	+4.2
250-300.....	0.0	2.8	-1.8	4.7	-1.5	7.5	-1.4	10.4	-1.5
300-350.....	2.0	2.4	+0.4	4.0	+0.7	6.4	+0.8	8.9	+0.7
350-400.....	0.0	1.8	-1.2	3.2	-1.0	5.0	-1.0	7.0	-1.0
400-450.....	0.0	1.2	-0.8	2.1	-0.7	3.4	-0.6	4.7	-0.7
450-500.....	1.0	1.5	0.0	2.6	+0.2	4.1	+0.2	5.7	+0.2
500.....	2.0	4.5	-0.9	7.8	-0.5	12.3	-0.3	17.2	-0.5

TABLE 2

COMPARISON OF NUMBER OF IRREGULAR SPOT-GROUPS OBSERVED WITH NUMBER EXPECTED FROM DISTRIBUTION OF REGULAR GROUPS 1917-1946 INCLUSIVE

No. Days Duration	Irreg. (No. Obs.)	Reg. (%)	Irreg. (Obs. - Expec.)	Reg. (%)	Irreg. (Obs. - Expec.)	Reg. (%)	Irreg. (Obs. - Expec.)	Reg. (%)	Irreg. (Obs. - Expec.)
1, 2.....	50	20.0	+14.1						
3, 4.....	40	16.8	+ 9.8	20.9	+12.8				
5, 6.....	20	14.2	- 5.6	17.8	- 3.1	22.5	-0.2		
7, 8.....	20	12.5	- 2.6	15.7	- 0.4	19.8	+2.2	25.6	+2.1
9, 10.....	15	12.2	- 7.1	15.3	- 4.9	19.4	-2.5	25.0	-2.5
11, 12.....	19	14.0	- 6.2	17.5	- 3.8	22.1	-0.9	28.9	-1.0
13, 14, 15.....	16	10.3	- 2.5	12.8	- 0.6	16.2	+1.4	20.9	+1.4

impracticable. The durations given in Table 2 are, therefore, for the whole disk, regardless of where a group originated. The first column contains the number of days' duration into which the groups were divided; the second, the number of irregular groups observed in each division; the third, the percentage of regular groups observed; and the fourth, the difference between the number of irregular groups observed, given in the second column, and the number expected on the basis of the regular distribution. For groups of short duration the excess of irregular groups observed over the number expected is clearly evident. Successive elimination of groups enduring from 1 to 6 days, shown in the fifth to

tenth columns, reveals that, in general, there is an excess in the percentage of irregular groups in the range of shortest duration.

Thus, although the results indicate that irregular spot-groups may be of any size up to naked-eye visibility and may endure for half a synodic rotation, on the average they appear to be slightly smaller and less stable than regular groups. This conclusion differs from that announced earlier, which was based on less material, less carefully selected.⁶

Long-lived spot-groups.—The relative stability of irregular spot-groups may also be studied by listing those that endured for one or more rotations. The results of such a comparison are given in Table 3 for the 5634 regular and 180 irregular spot-groups that appeared from 1917 to 1946. In compiling a sunspot catalogue it is customary to number each spot-group in the order of its appearance, regardless of whether it was seen before or not. Thus a spot-group that survives two rotations will be recorded under three different numbers and will be counted three times in computing the total number of spots observed. In Table 3, however, the figures all refer to *individual spot-groups*; that is, if a

TABLE 3
COMPARATIVE DURATION OF REGULAR AND
IRREGULAR SPOT-GROUPS

No. Times Obs.	No. Reg. Groups	Percentage Regular	No. Irreg. Groups	Percentage Irreg.
1.....	2961	70.2	142	90.5
2.....	1131	26.8	10	6.4
3.....	96	2.3	2	1.3
4.....	20	0.5	3	1.9
5.....	5	0.12	0	0.0
6.....	3	0.07	0	0.0

group survived three rotations, it has been counted only *once* and has not been included among the groups that survived one and two rotations.

The fact that the percentage of recurrent regular groups is three times the percentage of recurrent irregular groups furnishes additional evidence for the greater stability of groups of regular polarity. Also, since 12 of the 15 recurrent irregular groups were regular in polarity only during a portion of their lifetimes, the superior stability of the regular groups is probably even greater than appears from the table.

INCLINATION

The inclination of the axis of a spot-group to the solar equator is considered positive if the leading spot is the one nearer the equator. Measures by A. H. Joy⁷ and W. Brunner⁸ show that for the majority of spot-groups the inclination is positive and increases with increasing latitude. The relationship is poorly defined, so that the points fail to lie along a smooth curve even when formed from a large number of means.

Among the 180 irregular spot-groups were 114 with measurable inclinations. To serve as a standard of comparison, I measured the inclinations of 1007 bipolar spot-groups of regular polarity taken from the years 1918, 1923–1927 inclusive, 1929, 1930, 1939, and 1943, which covered periods of maximum, minimum, and intermediate sunspot activity. The average inclinations for different latitudes, together with the results obtained by Joy and Brunner, are shown in Table 4A. In assessing the results it must be borne in

⁶ *Annual Report Mt. W. Obs., 1945–1946*, p. 8.

⁷ Hale, Ellerman, Nicholson, and Joy, *Mt. W. Contr.*, No. 165; *Ap. J.*, **49**, 153, 1919.

⁸ *Astr. Mitt. Eidgenöss. Obs., Zürich*, **13**, 67, 1930.

mind that the leading and following members of many bipolar groups consist of loose collections of spots whose center of gravity is difficult to estimate. But, when measuring for inclination, one naturally selects bipolar groups whose members are exceptionally regular and compact. Owing to the limited number of irregular groups available, however, this material was less satisfactory than that used to determine inclinations for the regular groups.

In contrast to the regular groups, the irregular groups show a wider range of inclination to the equator and a more erratic increase in inclination with latitude and include more groups with negative inclinations (Table 4B). The mean inclination for the 1007

TABLE 4A
INCLINATION OF AXIS OF BIPOLAR SPOT-GROUPS

LATITUDE	JOY	BRUNNER	RICHARDSON	
			Reg.	Irreg.
0°- 9°.....	+ 3.0	+ 2.1	+ 5.1	- 5.8
10-14.....	+ 5.6	+ 5.4	+ 5.9	+ 0.7
15-19.....	+ 5.8	+ 7.2	+ 9.6	+ 0.2
20-24.....	+ 8.7	+ 9.9	+ 9.4	+15.5
25-29.....	+ 9.3	+14.4	+11.7	+ 2.1
≥ 30.....	+10.8	+19.0	+12.4	+16.6

TABLE 4B
DISTRIBUTION IN INCLINATION FOR REGULAR AND
IRREGULAR SPOT-GROUPS

INCLINATION	PERCENTAGE	
	Regular	Irregular
Positive.....	55.0	47.4
Negative.....	17.6	31.6
Approx. 0°.....	27.4	19.3
Approx. 90°.....	0.0	1.8

regular groups is +7.8, with a standard deviation of ± 20.2 . For 112 irregular groups the mean inclination is +2.1, with a standard deviation of ± 31.6 . (Two irregular groups with inclinations of 90° were omitted, since their sign is unknown.) The difference in the mean of the inclinations is 5.7, with a standard error in the difference of ± 1.1 . A difference in the mean of twice its standard error is generally considered significant; and, since in this case the difference is nearly five times its standard error, the greater deviation in the inclinations of the irregular groups may be real. On the other hand, it may arise entirely from the larger errors in the measurements on the irregular groups.

V. Bjerknes⁹ assumed that sunspots are produced by intersection of the solar surface with great subphotospheric vortices which lie nearly parallel to the equator. The position of a vortex can be traced by connecting the positive and negative members of spot-groups

⁹ *Mt. W. Contr.*, No. 312; *A p. J.*, 64, 93, 1926.

in the succession, positive-negative-positive, etc., inserting a hypothetical invisible spot of proper polarity whenever a link is missing in the chain. Irregular spot-groups are supposed to arise from abrupt S-shaped turns in the infinitely flexible vortex tube. On this basis, one would expect the axes of irregular groups to be distributed at a wide variety of angles to the solar equator instead of being nearly parallel to it, as with regular groups.

LATITUDE AND FREQUENCY VARIATION

Investigation of the distribution of regular and irregular spot-groups observed at Mount Wilson from 1917 to 1946, inclusive, was based upon the data given in Table 5. The spot-groups were carefully sorted with respect to hemisphere and cycle, with care being taken to avoid mixing low-latitude groups of an old cycle with the high-latitude groups of a new cycle. The first column gives the year; the second column, the phase θ_1 at mid-year corresponding to the length of the cycle determined by the interval between the appearance of the first and last groups; and the third column the phase θ_2 at mid-year corresponding to the length of the cycle determined by the interval between successive minima as fixed by Zürich. It is hard to say which method of determining the length of the cycle is the better, as both are open to criticism on several points.

The obvious objection to determining the length of the cycle from the interval between the first and last spots is that it depends solely upon two spots, completely disregarding the thousands of others that made up the cycle. The first and last spots of a cycle are usually small groups of short lifetime that might be easily missed because of cloudy weather or poor seeing. Moreover, since we are aware only of spots on the side of the sun turned toward the earth, we can never be sure that these really *are* the first and last groups. It should be noticed, also, that this method gives an interval corresponding to the duration of *one complete solar outburst* rather than to the length of a cycle regarded as a continuous function from one phase to the next similar phase.

The principal objection to determining the length of the cycle by the interval between successive minima fixed by Zürich from their relative sunspot numbers is that no discrimination is made between low-latitude groups of the old cycle and high-latitude groups of the new cycle. The minimum is arbitrarily fixed as the lowest point on a thirteen-month running chain of relative sunspot numbers regarded as continuous through minimum. Thus it is seen that the "length of a sunspot cycle" is a more uncertain quantity than is perhaps generally realized, the values given depending to a large extent upon chance or upon formal definition (see Table 6 and accompanying notes).

The figures in the fourth, fifth, eighth, and ninth columns of Table 5 are equal to the number of spot-groups actually counted at Mount Wilson during a year, multiplied by a factor equal to 365 divided by the number of days of observation. Although the number of spot-groups counted in an interval is probably not directly proportional to the number of days that the sun is observed, it is believed that this reduction should give a closer approximation to the true distribution than if it were disregarded. The figures in the sixth, seventh, tenth, and eleventh columns were obtained simply by taking the sum of the latitudes of the spot-groups observed and dividing them by their total number without further reduction.

One of the most characteristic features of the solar cycle is the progressive decrease in the average latitude of the spots with phase, known as Spörer's¹⁰ law of latitudes. About a year before spots of the old cycle disappear in low latitudes, a few groups of the new cycle break out between latitudes 25° and 35°. The zones of activity in both hemispheres rapidly widen toward the equator, so that their mean latitude steadily decreases, until at maximum it is around $\pm 16^\circ$, with spots occurring over practically the whole region from 0° to 30°. Activity in high latitudes then begins to decline, causing the zones to shrink on their outer edge. As minimum approaches, the spots of the waning cycle are

¹⁰ *A.N.*, 96, 23, 1879.

TABLE 5
NUMBER AND MEAN LATITUDE OF SPOT-GROUPS OBSERVED AT MOUNT WILSON

YEAR	θ_1	θ_2	REGULAR SPOT-GROUPS				IRREGULAR SPOT-GROUPS			
			No. of Groups		Mean Latitude		No. of Groups		Mean Latitude	
			N.	S.	N.	S.	N.	S.	N.	S.
Cycle 1913-1924										
1917.....	+0.39	+0.39	288	247	13°9	16°2	3.5	2.3	13°0	24°8
1918.....	+0.47	+0.49	253	273	12.2	14.6	6.4	7.7	13.8	5.6
1919.....	+0.56	+0.59	162	199	10.9	12.1	0.0	3.5	10.3
1920.....	+0.64	+0.69	118	104	11.7	10.8	0.0	2.5	8.6
1921.....	+0.73	+0.79	88	77	9.8	12.0	1.2	2.4	4.4	5.8
1922.....	+0.81	+0.89	50	36	8.2	8.9	2.4	1.2	8.2	7.5
1923.....	+0.90	+0.99	17	8	7.6	5.2	0.0	0.0
1924.....	+0.98	+1.09	3	1	6.0	4.0	3.2	0.0	5.3
Total.....	979	945	16.7	19.6
Cycle 1922-1935										
1922.....	+0.00	-0.11	2	0	30.0	0.0	0.0
1923.....	+0.08	+0.01	8	8	29.5	25.5	0.0	1.2	25.0
1924.....	+0.16	+0.09	61	25	24.5	26.2	1.1	0.0	18.0
1925.....	+0.23	+0.19	204	131	21.1	21.4	8.1	4.6	26.6	21.8
1926.....	+0.31	+0.28	209	214	19.2	17.3	7.0	3.5	16.8	31.3
1927.....	+0.39	+0.38	213	270	15.3	15.2	4.7	7.5	27.5	18.5
1928.....	+0.47	+0.48	181	203	12.8	14.2	4.5	10.1	16.2	12.5
1929.....	+0.54	+0.58	188	185	10.9	11.4	2.2	4.4	14.5	8.5
1930.....	+0.62	+0.68	131	103	11.0	9.5	9.0	6.8	9.9	10.0
1931.....	+0.70	+0.77	111	65	8.6	9.6	0.0	1.2	12.0
1932.....	+0.78	+0.87	42	45	8.8	7.5	3.3	1.1	11.7	9.0
1933.....	+0.85	+0.97	37	7	8.1	8.0	1.1	1.1	1.0	1.0
1934.....	+0.93	+1.07	12	3	4.5	2.0	0.0	0.0
1935.....	+1.01	+1.17	4	1	2.3	6.0	0.0	0.0
Total.....	1403	1260	41.0	41.5
Cycle 1933-1945										
1933.....	-0.02	-0.03	1	1	26°	32°	0.0	0.0
1934.....	+0.06	+0.07	18	39	23.6	26.2	1.1	0.0	29°9
1935.....	+0.15	+0.16	111	133	24.2	23.0	3.4	0.0	21.0
1936.....	+0.23	+0.26	261	280	19.2	20.4	4.7	5.9	23.5	21°6
1937.....	+0.31	+0.36	320	285	15.9	17.3	4.6	2.3	15.2	23.5
1938.....	+0.40	+0.45	341	286	15.5	15.0	7.1	11.8	15.5	20.6
1939.....	+0.48	+0.55	233	260	14.4	13.5	6.5	6.5	13.8	13.6
1940.....	+0.57	+0.64	197	240	12.9	10.8	9.7	2.4	13.1	4.5
1941.....	+0.65	+0.74	172	137	10.2	8.5	0.0	3.7	11.7
1942.....	+0.74	+0.84	98	98	10.3	8.5	2.1	3.2	9.5	9.0
1943.....	+0.82	+0.93	58	37	8.1	5.8	3.4	2.3	8.7	6.5
1944.....	+0.91	+1.03	9	14	5.2	8.1	0.0	0.0
1945.....	+0.99	+1.12	1	7	8.0	5.5	0.0	1.1	5.0
Total.....	1820	1817	42.6	39.2

TABLE 5—*Continued*

YEAR	θ_1	θ_2	REGULAR SPOT-GROUPS				IRREGULAR SPOT-GROUPS			
			No. of Groups		Mean Latitude		No. of Groups		Mean Latitude	
			N.	S.	N.	S.	N.	S.	N.	S.
	Cycle 1943—									
1943			0	5	32.2	0.0	0.0
1944			22	38	27.0	24.1	0.0	0.0
1945			80	156	23.8	21.8	0.0	3.4	25.3
1946			214	235	20.2	20.2	4.4	24.0

confined mostly within two belts located between 2° and 12° on either side of the equator. Thus, when the latitude covered by sunspot activity is plotted against time, the graph for a given hemisphere roughly resembles a blunt wedge inclined toward the equator with its narrow end in latitude 7° . It seemed possible that, if irregular sunspots originate in some unusual way, they may not conform to the pattern reproduced so faithfully each cycle by the regular groups.

The relation between the mean latitude, L , and the phase of the cycle, θ , was expressed by

$$L = A + B\theta + C\theta^2, \quad (1)$$

where θ is 0 at the beginning of the cycle and 1 at the end. The constants A , B , and C , obtained by least squares for the two complete cycles 1922–1935 and 1933–1945, are given in Table 7.

Comparison of the change in latitude with phase of the regular and the irregular spot-groups reveals some features of interest (Fig. 1). At the beginning of a cycle the irregular groups are from 2° to 4° farther from the equator than are the regular groups. But the mean latitude of the irregular groups decreases more rapidly than does that of the regular groups; hence, when the cycle is about three-quarters over, their distance from the equator is nearly the same. The higher latitude of the irregular groups during the early portion of the cycle might also be regarded as a difference in phase of the latitude variation. From this viewpoint, the irregular groups are about a year behind in phase at the beginning of the cycle but gain steadily, until toward the end the phase difference is negligible.

The relation between the number of spot-groups observed in an interval, R , and the phase, θ , has been expressed by

$$R = F\theta^a e^{-b\theta}, \quad (2)$$

an equation of Type III in Pearson's empirical family of curves. Stewart and Panofsky¹¹ in 1938 found that this equation represents, "to a good first approximation," the sixteen apparently widely dissimilar hump-shaped cycles from 1755 to 1933; later Stewart and Eggleston¹² concluded that it was doubtful if the form could be improved. The

¹¹ *A. J.*, **88**, 385, 1938.

¹² *A. J.*, **91**, 72, 1940.

TABLE 6
DATA USED TO DETERMINE DURATION OF SOLAR CYCLES

	SERIAL NUMBER		LAT.	DATE OF OBSERVATION	MINIMA (ZÜRICH)
	Gr.	Mt. W.			
First group* Last group Duration of sunspot pe- riod First group† Last group Duration of sunspot pe- riod First group‡ Last group Duration of sunspot pe- riod First group§ Last group	Cycle 1912-1924				
	7007 9570 2101	20° N. 7 N.	1912 Dec. 16-18 (1912.956) 1924 Sept. 24-Oct. 5 (1924.730)	1913.6 1923.6
				4311 days 11.774 years	10.0 years
	Cycle 1922-1935				
	919d 1092b	1976 4547	31 N. 4 N.	1922 June 24 (1922.477) 1935 May 24 (1935.392)	1923.6 1933.8
				4714 days 12.915 years	10.2 years
	Cycle 1933-1945				
	1071a	4427 7814	26 N. 8 N.	1933 Oct. 10 (1933.773) 1945 Aug. 8 (1945.600)	1933.8 1944.2
				4320 days 11.827 years	10.4 years
	Cycle 1943-—				
	7579	41 S.	1943 May 16-19 (1943.370)	1944.2	

* The following sunspot might be considered as the first group of the new cycle: Gr. No. 6974, seen 1911 Dec. 18-19 at +23°.

† The following sunspot might be considered as the first group of the new cycle: Gr. No. 910a, seen 1921 Oct. 1 at +34°.

‡ The following sunspot might be considered as the first group of the new cycle: Gr. No. 1047h, seen 1932 Jan. 15 at +48°.

§ The following sunspot might be considered as the first group of the new cycle: Mt. W. No. 7614, seen only on 1942 Dec. 20, was a small bipolar group in latitude +32°. Its polarities were like those of the cycle supposed to have begun in 1943, but the inclination of the members of the group to the equator was so great, about 75°, that its polarities had low weight in the decision as to which cycle it belonged.

shape of the curve is determined by a and b , F being merely a scale factor. The curve rises rapidly, owing to the quantity θ^a ; but damping by $e^{-b\theta}$ produces a maximum and decline. Features of particular interest in connection with equation (2) are:

$$v = \text{Time of maximum} = \frac{a}{b};$$

$$V = \text{Sunspot number at maximum expressed in arbitrary units} = \frac{F a^a e^{-a}}{b^a};$$

$$\sigma = \text{Standard deviation} = \frac{\sqrt{(a+1)}}{b};$$

$$M_0 = \text{Area under the curve or zero moment} = \frac{F \Gamma(a+1)}{b^{a+1}}.$$

Values of a , b , and $\log F$ for regular and irregular spot-groups were calculated by least squares from the data in Table 5. The values of these three constants, together with

TABLE 7
COMPARISON OF CONSTANTS IN EQUATION $L = A + B\theta + C\theta^2$ EXPRESSING
RELATION BETWEEN LATITUDE AND PHASE OF CYCLE

CYCLE	HEM.	POLARITY	CONSTANTS		
			A	B	C
1922-1935	Length of Cycle from First to Last Groups				
	{ N.	{ Reg.	32.1	-50.6	24.2
		{ Irreg.	32.1	-32.6	1.1
	{ S.	{ Reg.	32.0	-50.5	24.0
		{ Irreg.	38.6	-66.8	31.0
	{ N.	{ Reg.	26.0	-29.4	9.1
		{ Irreg.	30.2	-48.2	27.0
	{ S.	{ Reg.	29.9	-48.7	25.6
		{ Irreg.	37.3	-65.5	36.6
	Length of Cycle from Zürich Minima				
1922-1935	{ N.	{ Reg.	28.9	-43.6	23.3
		{ Irreg.	30.1	-30.0	4.8
	{ S.	{ Reg.	27.6	-38.3	18.1
		{ Irreg.	32.6	-44.6	15.0
1933-1945	{ N.	{ Reg.	27.8	-35.8	17.0
		{ Irreg.	28.9	-36.5	15.2
	{ S.	{ Reg.	29.1	-37.5	14.2
		{ Irreg.	27.1	-23.3	5.1

those of v , V , σ , and M_0 derived from them, are given in Table 8. No obvious relationships appear among the constants for the frequency distribution, although the fact that the standard deviation, σ , which measures the frequency distribution of the sunspot numbers around their mean value, is persistently larger for the irregular groups, may be of significance.

It is noteworthy that the percentage of irregular spot-groups was quite different in the two cycles. Thus, although the total area under the curve for the regular groups of cycle 1933–1945 was 66 per cent larger than that for the cycle 1922–1935, the total area under the curve for the irregular groups was the same in both cycles. If we compare the total number of regular and irregular groups that appeared in a cycle, including the data for the latter half of the cycle 1913–1924, an alternation is indicated in the percentage of

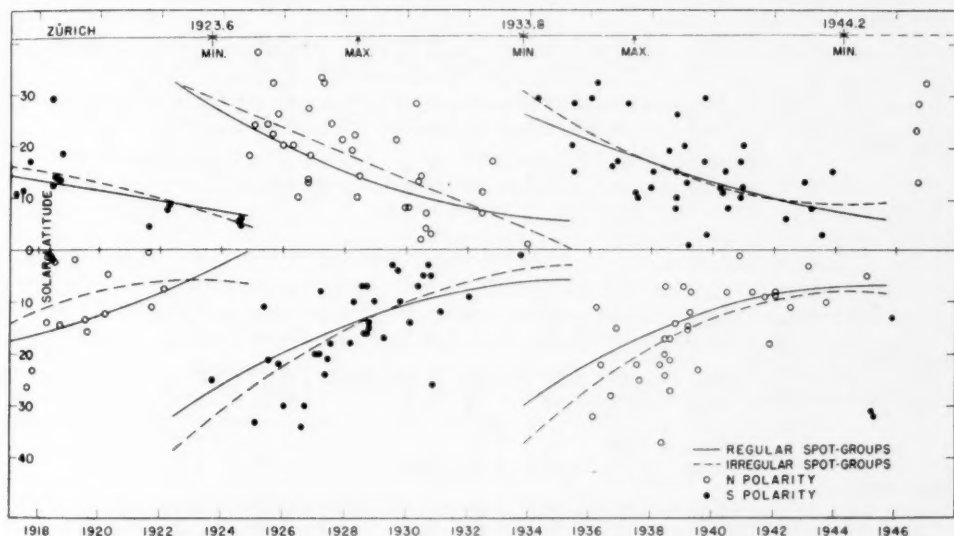


FIG. 1.—Spot-groups of irregular magnetic polarity observed at Mount Wilson from 1917 to 1946, inclusive. Continuous and broken curves show the change in latitude of regular and irregular groups, respectively, obtained by least-squares solution from the equation $L = A + B\theta + C\theta^2$.

irregular groups of the three successive cycles (Table 9). It will be of interest to see whether there is an increase in the percentage of irregular groups in the cycle that began in 1943.

II. INDIVIDUAL COMPARISONS

Although several irregular spot-groups have attained naked-eye visibility, they seem not to have been examined for the purpose of determining whether they are irregular in other respects besides their polarity.

A spot-group exceptionally well suited for individual study was first seen at Mount Wilson on March 24, 1945, at 31° S., 50° E. This happened to be the first irregular spot-group of the cycle that began about May, 1943, and is one of the finest examples on our records. It survived two rotations as Nos. 7732 and 7739 of the Mount Wilson series and was irregular both times. The average area of No. 7732, from March 24, when it was 50° east of the central meridian, until April 1, when it was 54° west, was 670. During this time the sunspot consisted chiefly of a penumbra inclosing a single large umbra.

TABLE 8
CONSTANTS EXPRESSING RELATION BETWEEN NUMBER OF SPOT-GROUPS
AND PHASE OF CYCLE

Cycle	Hem.	Pol.	Log <i>F</i>	<i>a</i>	<i>b</i>	<i>v</i>	<i>V</i>	<i>σ</i>	<i>M</i> ₀	$\frac{M_0 \text{ (Irreg.)}}{M_0 \text{ (Reg.)}} \times 100$
Length of Cycle from First to Last Group										
1922-1935 . . .	N.	{ Reg. Irreg.	5.57 4.32	3.54 3.90	10.21 10.91	0.35 0.36	256.5 7.6	0.21 0.20	121.3 3.5	2.9
		{ Reg. Irreg.	6.40 3.29	4.35 2.45	13.35 8.51	0.33 0.29	245.6 8.0	0.17 0.22	98.2 3.8	
	S.	{ Reg. Irreg.	6.64 3.28	4.25 2.57	13.32 8.18	0.32 0.31	478.0 7.4	0.17 0.23	189.4 3.8	2.0
		{ Reg. Irreg.	5.70 4.18	3.24 4.10	10.71 10.11	0.30 0.41	407.1 6.2	0.19 0.22	175.8 3.2	
Length of Cycle from Zürich Minima										
1922-1935 . . .	N.	{ Reg. Irreg.	4.13 1.94	1.96 1.25	6.00 4.25	0.33 0.30	210.0 5.4	0.29 0.35	127.9 3.8	3.0
		{ Reg. Irreg.	4.89 2.77	2.73 2.10	8.64 6.73	0.32 0.31	218.8 6.2	0.22 0.26	108.1 3.6	
	S.	{ Reg. Irreg.	4.99 2.01	2.93 1.52	7.93 3.83	0.37 0.40	282.3 5.5	0.25 0.42	157.3 4.7	3.0
		{ Reg. Irreg.	4.90 3.45	2.69 3.32	7.93 8.02	0.34 0.41	292.9 5.4	0.24 0.26	156.6 3.2	

TABLE 9
PERCENTAGE OF IRREGULAR GROUPS BY CYCLES

CYCLE	TOTAL NO. GROUPS		PERCENTAGE IRREG.	RATIO
	Reg.	Irreg.		
1913-1924	1923.3	36.3	1.89	0.61
1922-1935	2664.1	82.5	3.10	1.00
1933-1945	3637.3	81.8	2.25	0.72

MAGNETIC FIELD

The magnetic-field strength in the central umbra of No. 7732 was 3100 gauss, which is normal for a spot of this size. The photosphere was examined for invisible spots with the nicol prism and quarter-wave plate out to a distance of about ten times the radius of No. 7732. No magnetic fields were found strong enough to be detected by this method (about 200 gauss).

WILSON EFFECT

In November, 1769, A. Wilson¹³ noticed that, as a round stable spot approached the western limb, the umbra appeared to be gradually displaced toward the center of the disk with respect to the penumbra. He interpreted the displacement of the umbra to mean that spots are shallow depressions in the photosphere, the penumbra forming walls sloping down to the umbra. Many observations have since been made on the Wilson effect, but its nature is still in dispute. P. Chevalier¹⁴ found that 88 per cent of the spots which he selected for study showed displacements corresponding to an average depth of 1" or 750 km; but other spots showed displacements toward the limb as if elevated above the photosphere. E. Pettit¹⁵ attributes the Wilson effect to a ring of bright faculae surrounding the penumbra at an elevation of 1000–2000 km above the photosphere.

Spot-group No. 7732 was investigated for Wilson effect by making tracings of the umbra and penumbra, which had been enlarged eight times from direct photographs of the sun that were 17 cm in diameter. The contours of the penumbra and the umbra were rather irregular when the group was near the meridian but became more nearly symmetrical as it approached the west limb. On March 31 and April 1, when the spot was 0.74 and 0.78 radii, respectively, from the center of the disk, the umbra showed a Wilson effect of approximately 1". Part of this displacement may have been due to the eccentric position of the umbra within the penumbra. Although No. 7732 was not an ideal spot for study of the Wilson effect, it was probably about as good as the average selected for this purpose. Its appearance when near the limb was certainly not abnormal.

EVERSHED EFFECT

If a spot about 30°–50° from the meridian is observed with a radial slit, the lines in the spectrum of the penumbra on the side toward the center of the disk will usually show a distinct displacement shortward, while lines in the opposite side of the penumbra will show a displacement longward.¹⁶ The effect is readily explained as a Doppler shift due to currents flowing outward from the center of the spot parallel to the solar surface.

C. E. St. John¹⁷ found that iron lines of Rowland intensity 00–10 show velocities of outflow of from 1 to 0.1 km/sec, respectively; lines of intensity 15–40 show no displacements; and very strong lines such as H2 and K2 of Ca II, which originate high in the chromosphere, show velocities of inflow amounting to 1.3 km/sec. According to G. Abetti,¹⁸ the velocities of outflow often vary widely from one spot to another, ranging from practically zero to a maximum of 6 km/sec.

Spectrograms of No. 7732 were taken for the Evershed effect on March 31 and April 1 in the third order of the 75-foot spectrograph, where the dispersion is 0.2 Å/mm. Six iron lines in the region λ 6300 of intensity 3–7 were selected for measurement, together with a dozen atmospheric lines of about the same average intensity. Photographs of H2 and K2 were taken on April 2 in the first order.

The displacements of the iron lines, which are readily apparent from inspection of the plates, closely resemble those in the diagram of Evershed's original paper. The displacement increases from the inner to the outer edge of the penumbra, where it ceases

¹³ *Phil. Trans. R. Soc.*, **64**, 1, 1774.

¹⁶ J. Evershed, *M.N.*, **69**, 454, 1909.

¹⁴ *Ann. Zô-Sé*, **11**, 10, 1919.

¹⁷ *Mt. W. Contr.*, No. 69; *Ap. J.*, **37**, 322, 1913.

¹⁵ *Annual Report Mt. W. Obs.*, 1938–1939, p. 12.

¹⁸ *Atti R. Accad. dei Lincei*, Ser. 6, **4**, 242, 1926.

abruptly. The velocities in the λ 6300 region, corrected for apparent displacements shown by the atmospheric lines, are given in Table 10. The plus and minus signs indicate motion outward and inward, respectively. The third-order plates gave a much larger standard deviation than did those taken in the first order, the increase in scale evidently failing to compensate for the much broader and more diffuse appearance of the lines in the higher order. The different velocities found on the three days are attributed to differences in seeing rather than to actual changes in the rate of flow.

The Evershed effect found in No. 7732 agrees about as closely as can reasonably be expected with the results obtained by other observers on spots presumably regular in polarity.

HYDROGEN VORTEX

Spectroheliograms taken in the center of *H α* show long filaments around large spot-groups, often closely resembling the arrangement of iron filings around a bar magnet or the lines of flow in a vortex. If the magnetic field in a spot is due to the rotation of charged particles, we should expect to find a relation between magnetic polarity and the direction of rotation indicated by the filaments. Investigations by Hale and others¹⁹ have failed to disclose such a relationship. But if spots are grouped according to hemi-

TABLE 10
RADIAL MOTION IN PENUMBRA OF SPOT-GROUP NO. 7732
(Evershed Effect)

Date	Region	No. Lines	Mean Int.	Order	Velocity \pm Standard Dev.
1945 March 31....	λ 6300	16	4	3	$+0.92 \pm 0.34$ km/sec
April 1....	λ 6300	16	4	3	$+0.57 \pm 0.18$
April 1....	λ 3900	12	8	1	$+1.18 \pm 0.05$
April 2....	H2, K2	2	1	-0.83 ± 0.06

sphere, then 75 per cent show a curvature in the same direction as terrestrial cyclones, favoring the view that they are vortices produced by the solar rotation.

The vortex structure surrounding No. 7732 is clearly revealed on several hydrogen spectroheliograms taken with a 7-inch solar image. From experience gained in examining spectroheliograms for vortex structure, I considered the pattern formed by the filaments to be unusually well marked and definitely counterclockwise in direction. Since determination of the direction of rotation is solely a matter of personal judgment rather than of objective measurement, twelve persons at Mount Wilson were shown the plate correctly oriented and asked for their opinion. Eleven thought that the direction of rotation shown by the filaments was predominantly counterclockwise, although some were undecided at first. One thought the direction was clockwise.

Since No. 7732 was in the southern hemisphere, where the prevailing direction of rotation is clockwise, it constitutes an exception to the rule. But since about 25 per cent of the spot-groups for which the direction of rotation can be determined also fail to obey this "law," little significance can be attached to a single case. Hydrogen spectroheliograms of the other irregular spot-groups were examined, but none showed vortex structure sufficiently well marked to determine the direction of rotation.

LONG-LIVED SPOT-GROUPS WHICH HAVE BEEN RECLASSIFIED MAGNETICALLY

Although most of the spot-groups studied were irregular in polarity during their entire lifetime, some were classified originally as regular and then changed to irregular or vice

¹⁹ G. E. Hale, *Mt. W. Comm.*, No. 95; *Proc. Nat. Acad.*, 11, 691, 1925; *Nature*, 119, 708, 1927; R. S. Richardson, *Mt. W. Contr.*, No. 639; *A. J.*, 93, 24, 1941.

versa. Change in classification occurred most often among long-lived groups that endured several rotations. Among thirteen groups which were reclassified, eight displayed no characteristics that seemed especially significant. The process of transformation in the other five, however, was along closely similar lines. The general sequence of events in these five cases was about as follows:

Before transformation the spot-group consisted of a single round stable spot, which looked as if it would soon diminish and disappear. Instead, there occurred an outburst of activity usually in slightly higher latitude and a little to the east of the stable spot. Both Greenwich and Mount Wilson regarded these outbursts as a revival of activity in the old group, but it is quite possible that they were new groups that appeared in the same region as the old one. The activity continued during the next two or three days, the new spots eventually developing into a distinct bipolar group, opposite in polarity to the classification of the original stable spot. After this brief outburst the spot-group seemed to be declining when last seen.

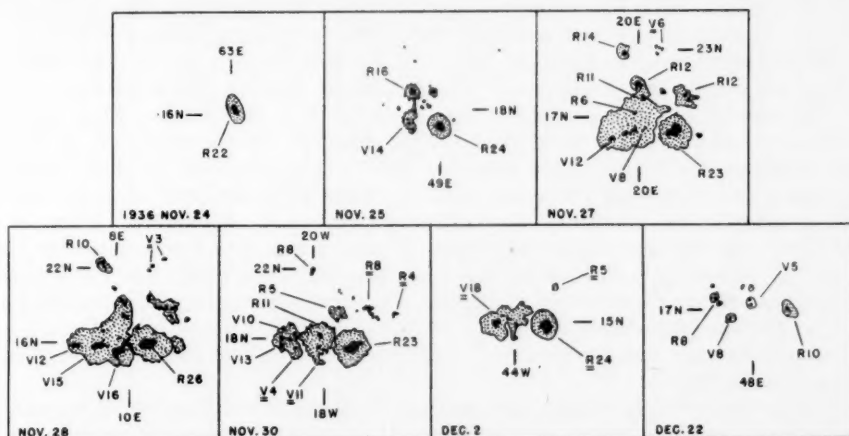


FIG. 2.—Steps in the transformation of a spot-group from regular to irregular polarity. On November 23, 1936, group No. 5127 consisted of a unipolar spot of regular polarity. The region became suddenly active, and by December 2 the spot had become an irregular bipolar group. After a solar rotation, No. 5127 was observed again on December 22 as a small bipolar group of regular polarity.

The behavior of No. 5127 was especially interesting (Fig. 2). When first seen on November 23, 1936, this group consisted of a single round spot of regular (positive) polarity at 16° N., 76° E. Sometime between November 24 and 25 it became active, spots of both positive and negative polarity appearing to the north of the single spot. By November 27, a naked-eye group had developed where four days before only a small spot existed. The new group could not be classified as either regular or irregular; for, although distinctly bipolar, the two members were north and south of each other, so that it was impossible to say which was the leading spot. By November 28 the portion of the group of south polarity had definitely become the leader, thus making the group irregular in the southern hemisphere for the cycle 1935–1945. Four days later the group consisted of a single huge penumbra, elongated parallel to the equator, in which the preceding and following umbrae were of south and north polarity, respectively.

Flares estimated at Mount Wilson to be of intensity 3 were observed in the spot-group on November 26 at $17^{\text{h}}49^{\text{m}}$ G.C.T., and on November 29 at $16^{\text{h}}08^{\text{m}}$. A magnetic storm began on November 28 at $23^{\text{h}}37^{\text{m}}5$, which continued through November 29.

Fe II EMISSION LINES IN α HERCULIS AND α SCORPII*

G. HERZBERG

Yerkes and McDonald Observatories

Received September 16, 1947

ABSTRACT

A number of fairly strong emission lines are found in the spectra of α Her and α Sco below 3300 Å. Most of these are due to Fe II. They have excitation potentials up to 5.6 volts.

In a program of investigations of the spectra of late-type stars, spectrograms near the limit of atmospheric transmission were obtained of α Bootis, β Ursae Minoris, α Scorpii, and α Herculis with the 500-mm quartz spectrograph of the McDonald telescope (dispersion 16 Å/mm at 3200 Å). Somewhat unexpectedly, emission lines were found in the spectra of α Her and α Sco in the region 3300–3150 Å. Spectrograms of α Boo, α Sco, and α Her are reproduced in Figure 1. The emission lines are particularly prominent for α Her and are readily recognized as such even without detailed measurement.

The first column of Table 1 contains the wave lengths of the emission lines measured in the spectrum of α Her and corrected for radial velocity, the second column gives estimated intensities, and the third and following columns give the identifications, multiplet designations, and excitation potentials. The numbers in parentheses after the laboratory wave lengths are laboratory intensities as given by C. E. Moore.¹ A few of the weaker lines have not been identified. Most of these are doubtful emission lines (indicated by “?” following the observed wave length). With one exception, the identified emission lines belong to three Fe II multiplets whose excitation energies range from 4.75 to 5.6 e.-v. The exception is the Fe I line λ 3164.3; it belongs to a multiplet of which even in the laboratory only one component has been found. This last identification must be considered as tentative.

Both α Her and α Sco have faint companions, of magnitudes 5.4 and 6.5, respectively. If these companions had strong emission lines, they might conceivably account for the observed spectra in Figure 1. However, during the exposures of α Her the companion was clearly separated from the main component, and the spectrograph slit was at right angles to the line joining the two components, so that a contamination of the spectrum by the component was exceedingly slight, even considering that at 3200 Å the companion might well be brighter than the main component. Moreover, the spectrum of α Her B was kindly taken more recently by D. M. Popper, with the result that no emission lines are present.

The companion of α Sco, because of poor seeing, was not clearly separated from the main component when the present exposures were taken. However, its spectrum has been studied in some detail by Struve and Swings.² It was classified as B4n. Moderately strong emission lines of [Fe II] were found in the ordinary photographic region, all of very low excitation (about 3 e.-v.). But no emission lines near 3200 Å were found. A re-examination of Struve and Swings's plates showed that these emission lines would have been visible had they been present with an intensity stronger than the continuous spectrum of the star.

It must therefore be concluded that in both cases— α Her and α Sco—the emission lines observed here are due to the main component. It appears that the only emission

* Contributions from the McDonald Observatory, University of Texas, No. 143.

¹ Multiplet Tables of Astrophysical Interest (Princeton, 1945).

² O. Struve and P. Swings, *Ap. J.*, **92**, 316, 1940.

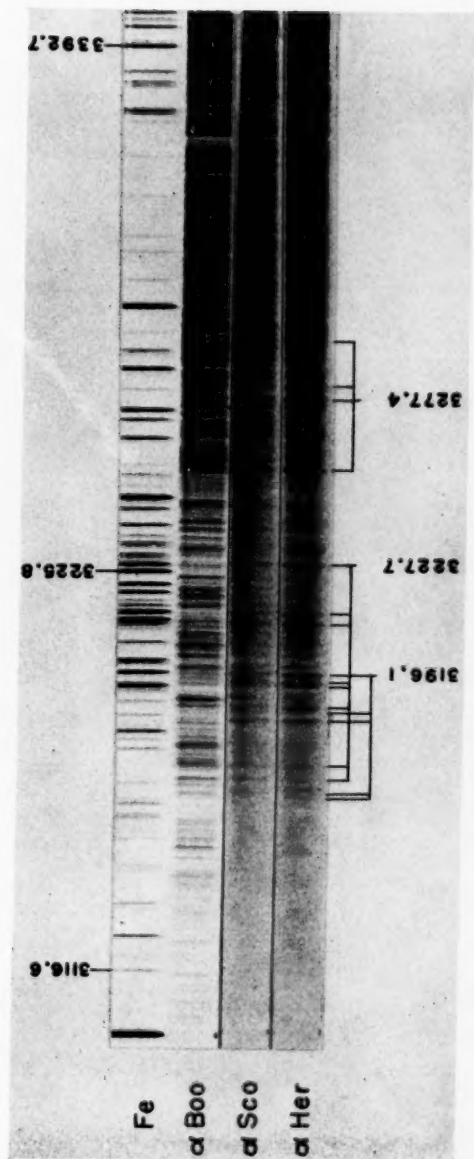
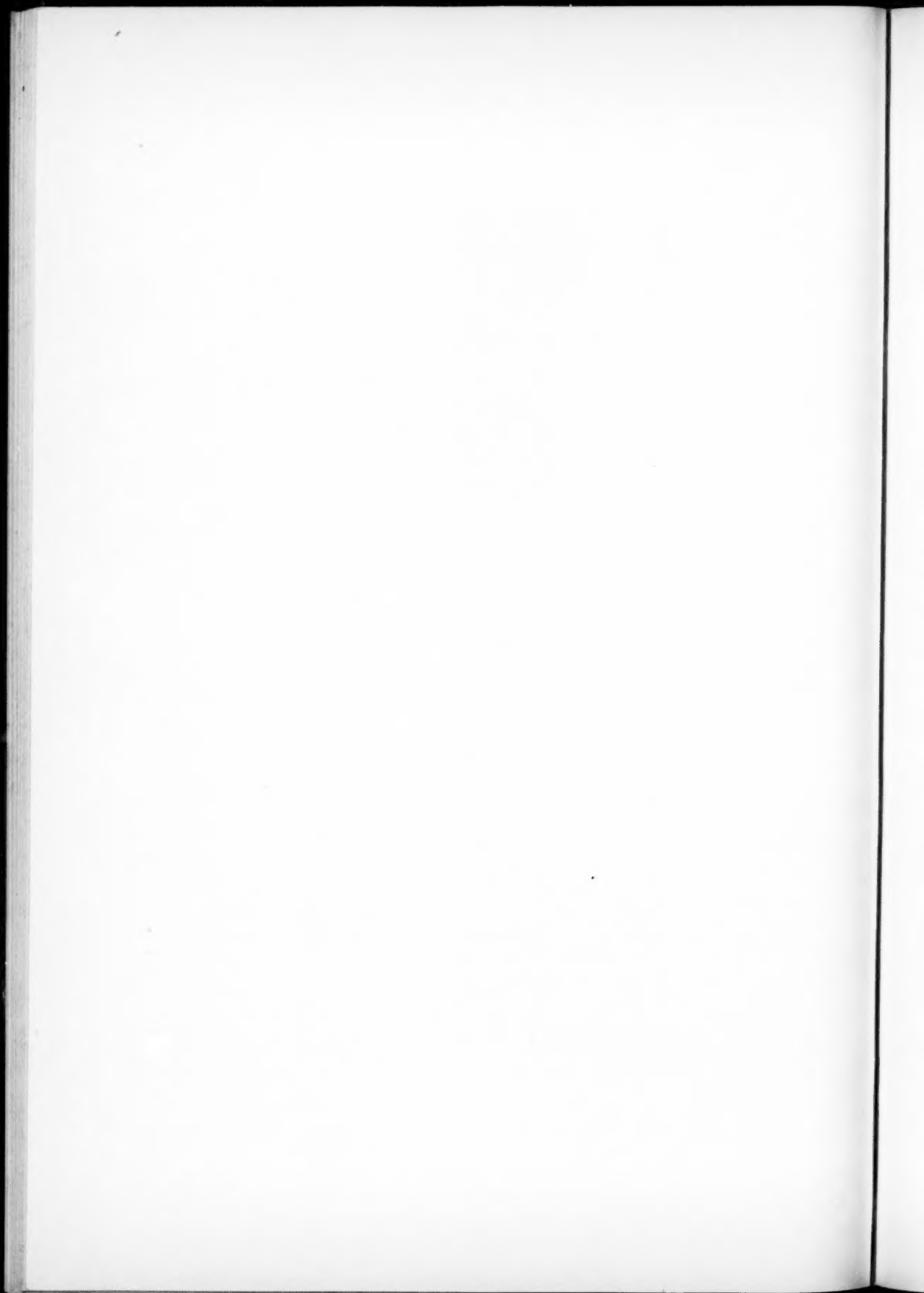


FIG. 1.—Ultraviolet spectra of α Boo, α Sco, and α Her. All were taken on May 22, 1946



lines previously found in these stars are the H and K lines.³ Both stars are typical irregular variables.

It seems probable that the appearance of Fe II emission lines requiring fairly high excitation in low-temperature stars is due to a corona-like nebulosity surrounding these stars. Indeed, if one were to investigate the solar spectrum in the far ultraviolet, where the intensity of the continuous spectrum corresponding to the temperature of the photosphere is negligible, it seems certain that one would find it to consist of coronal emission lines of rather high excitation. In stars like α Her the corona would be expected to have

TABLE 1
EMISSION LINES IN α HERCULIS

λ (Obs.)	Int.	Identification	Multiplet	J''	J'	Excit. Pot. (e.-v.)
3162.06	0	Fe II 3161.95(5)	$a^4P-z^4F^0$	3/2	3/2	5.59
3162.97	1	Fe II 3163.09(5)	$a^4P-z^4F^0$	5/2	5/2	5.57
3164.37	2	Fe I 3164.31(1)	$z^4D^0-g^4D$	3	4	6.34
3166.69	0	Fe II 3166.67(4)	$a^4P-z^4D^0$	5/2	3/2	5.56
3170.34	1	Fe II 3170.34(6)	$a^4P-z^4D^0$	3/2	1/2	5.58
3183.10	3	Fe II 3183.12(8)	$a^4P-z^4F^0$	3/2	5/2	5.57
3185.48	1	Fe II 3185.32(5)	$a^4P-z^4F^0$	1/2	3/2	5.59
3186.83	3	Fe II 3186.74(11)	$a^4P-z^4D^0$	3/2	3/2	5.56
3192.75	2	Fe II 3192.92(9)	$a^4P-z^4D^0$	5/2	5/2	5.53
3193.81	3	Fe II 3193.81(11)	$a^4P-z^4D^0$	1/2	1/2	5.58
3196.08	4	Fe II 3196.07(10)	$a^4P-z^4F^0$	5/2	7/2	5.52
3204.63?	1					
3208.01	1					
3210.37	4	Fe II 3210.45(10)	$a^4P-z^4D^0$	1/2	3/2	5.56
3213.41	4	Fe II 3213.31(13)	$a^4P-z^4D^0$	3/2	5/2	5.53
3223.74?	1					
3227.72	4	Fe II 3227.73(13)	$a^4P-z^4D^0$	5/2	7/2	5.49
3245.07	1					
3246.78	1					
3253.60?	0					
3255.87	4	Fe II 3255.88(8)	$a^4D-z^4D^0$	7/2	7/2	4.77
3266.37?	0					
3269.00	0					
3277.35	5	Fe II 3277.35(9)	$a^4D-z^4D^0$	7/2	9/2	4.75
3281.34	3	Fe II 3281.29(7)	$a^4D-z^4D^0$	5/2	5/2	4.80
3284.05?	1					
3285.68?	1					
3290.15	1					
3295.84	2	Fe II 3295.81(6)	$a^4D-z^4D^0$	3/2	3/2	4.82

a much lower temperature than that of the sun, so that Fe II lines (rather than Fe x) might become prominent. In addition, on account of the lower temperature of the photosphere, the coronal emission becomes visible at longer wave lengths than it would for the sun.

I am indebted to Drs. W. W. Morgan and W. Bidelman for discussions on the subject of this paper and to Dr. Morgan for preparing the enlargements.

NOTE ADDED IN PROOF.—It seems significant that the same Fe II emission lines have recently been observed by Merrill⁴ in the long-period variables R Leo, R And, and χ Cyg.

³ A. H. Joy and W. S. Adams, *Pub. A.S.P.*, **43**, 407, 1931.

⁴ P. W. Merrill, *A.p. J.*, **103**, 275, 1946; **105**, 360, 1947; **106**, 274, 1947.

SPECTROGRAPHIC OBSERVATIONS OF THE ECLIPSING BINARIES OF THE W URSAE MAJORIS TYPE AH VIRGINIS AND TZ BOOTIS*

Y. C. CHANG¹

McDonald Observatory

Received September 22, 1947

ABSTRACT

A number of spectrograms of each of these eclipsing binaries have been obtained at the McDonald Observatory, with a dispersion of 76 Å/mm at $H\gamma$. The spectral lines of AH Vir break up into components at quadrature. The difference in intensity of the components is greatest at phase 0.75 P and is least at phase 0.25 P. On the assumption of a circular orbit, it is found from the velocity-curve that $\gamma = +10$ km/sec; $K_b = 105$ km/sec; $K_f = 250$ km/sec. In many respects the spectroscopic behavior of this binary bears a close resemblance to that of YY Eri, another eclipsing variable of the W Ursae Majoris type. The mass functions are $m_b \sin^3 i = 1.33$ and $m_f \sin^3 i = 0.56$. It appears to be fairly general that the mass ratio as given by K_b/K_f differs from unity by an amount greater than can be reconciled with the mass-luminosity relation.

From the light-curve given by Lause, the photometric elements have been derived on the assumption of uniform disks and similar ellipsoidal shapes for the components of the binary. It is found that $P = 0.407$ day, $L_b = 0.65$, $r_b = 0.44$, $k = 1.67$, $i = 82^\circ.9$, $\gamma = 0.67$. The spectral lines of TZ Boo do not become double at quadrature. Although the range of variation is about 60 km/sec, there does not seem to be any correlation between the radial velocity and phase as calculated from the period of light-variation. The mean velocity is -58 km/sec.

The star AH Vir was announced as an eclipsing variable of the W Ursae Majoris type by Guthnick and Prager.² Both Prager³ and Kukarkin⁴ derived a period of about 0.339 day; but Lause⁵ obtained a new period of about 0.407 day. He pointed out that the reason why the shorter period had been adopted erroneously by the former workers is the fact that

$$6P' = 5P = 2 \text{ days ,}$$

where P' denotes the erroneous period. With further observations he later confirmed his own result⁶ and gave the formula for primary minimum:

$$\text{Min.} = 2425003.495 + 0^d.4075191 E ,$$

with photographic magnitudes at maxima and minima as follows:

$$\begin{aligned} M_1 &= 10^m.26 , & M_2 &= 10^m.30 , \\ m_1 &= 10^m.74 , & m_2 &= 10^m.58 . \end{aligned}$$

* Contributions from the McDonald Observatory, University of Texas, No. 144.

¹ On leave from the Institute of Astronomy, Academia Sinica, Nanking, China.

² *Beob.-Zirk.*, No. 13, p. 32, 1929.

³ *Kl. Veröff. Berlin-Babelsberg*, No. 6, p. 36, 1929.

⁴ *Ver. d. Freund. d. Phys. Nishni-Novgorod*, No. 11, 1929.

⁵ *A.N.*, 254, 376, 1934.

⁶ *Ibid.*, 257, 212, 1935.

In the table of eclipsing binaries of the Gaposchkins' book,⁷ the light-elements of this star are derived with Prager's period of 0.339 day. The elements are in contradiction with the results of our spectrographic observations; therefore, it has been considered worth while to compute rough elements with the light-curve and the observations given in Lause's paper.⁵ The quantity l^2 was plotted against $\cos^2 \theta$ in order to obtain the value of $\epsilon^2 \sin^2 i$ and to rectify the curve.⁸ The photometric elements are as follows:

$A_1 = 0^m.44$	$A_2 = 0^m.28$
$L_b = 0.65$	$L_f = 0.35$
$a_b = 0.50$	$a_f = 0.30$
$b_b = 0.44$	$b_f = 0.26$
$c_b = 0.40$	$c_f = 0.24$
$a_1 = 0.95$	$a_2 = 0.35$

$$k = \frac{r_b}{r_f} = 1.67$$

$$i = 82^\circ.9$$

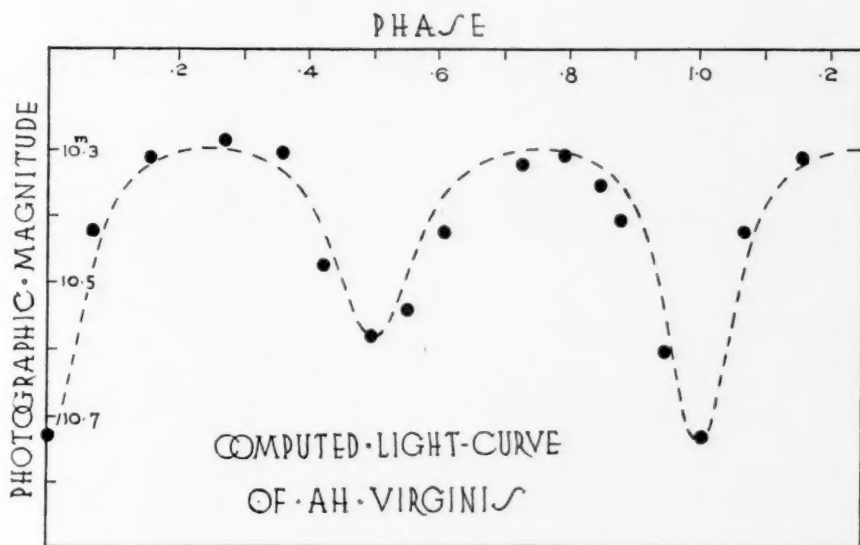


FIG. 1

The ratio of the surface intensity of the brighter component to the fainter is:

$$\gamma = 0.67,$$

and the eccentricity of the meridian section of the ellipsoidal star is

$$\epsilon = 0.60.$$

Figure 1 shows the computed light-curve in relation to the observations. Both components have a spectral type of K0.

⁷ *Variable Stars* ("Harvard Obs. Monographs"), p. 77.

⁸ *A. J.*, **36**, 64, 1912.

The spectrograms were obtained on 103a-O film, with the Cassegrain spectrograph attached to the 82-inch reflector, with the f/2 Schmidt camera and glass prisms used. The dispersion is 76 Å/mm at $H\gamma$. Phases of the spectrograms were computed with the epoch and period given by Lause. Near quadrature the spectral lines of both components could be measured separately. A set of about ten lines was chosen for radial velocity. The results of the measurements reduced to the sun are given in Table 1.

TABLE 1
RADIAL VELOCITIES OF AH VIRGINIS

Date	JD 243	Heliocentric Phase	Vel. of Brighter Comp. (Km/Sec)	Vel. of Fainter Comp. (Km/Sec)
1945 Mar. 9*	1523.829	0.071	+ 69
9*	1523.846	.112	+ 67
Mar. 9*	1523.861	.149	+104
1947 Mar. 2.	2246.899	.394	+ 52
2.	2246.929	.467	- 1
2.	2246.961	.546	+ 26
3.	2247.881	.803	- 68	+226
4.	2248.881	.257	+126	-242
8.	2252.851	.999	+ 28
8.	2252.876	.061	+ 53
8.	2252.901	.122	+ 40
8.	2252.925	.181	+155	-197
8.	2252.951	.245	+106	-229
10.	2254.838	.875	- 70	+203
10.	2254.868	.949	- 2
11.	2255.797	.228	+112	-206
11.	2255.828	.304	+124	-233
11.	2255.858	.378	+ 29
11.	2255.885	.444	+ 21
11.	2255.908	.501	+ 30
11.	2255.933	.562	- 24
11.	2255.981	.680	-105
12.	2256.813	.721	- 78	+301
12.	2256.838	.783	-103	+223
12.	2256.868	.856	- 29
12.	2256.892	.915	- 16
13.	2257.740	.996	+ 38
13.	2257.782	.099	+ 60
13.	2257.904	.399	+ 32
Mar. 31.	2275.869	.482	+ 22
Apr. 11.	2286.820	0.355	+ 15

* The spectrograms taken in 1945 were kindly loaned to me by Dr. W. A. Hiltner.

When the velocities were plotted (Fig. 2), it became evident that the observations have the run of a sine-curve. Assuming zero eccentricity for the orbit, we may pass velocity-curves through the observations for both components of the binary; from these curves the following spectroscopic elements were found for AH Vir:

$$\begin{aligned}
 P &= 0.4075191 \text{ (Lause)} & a_b \sin i &= 590,000 \text{ km} \\
 e &= 0.0 \text{ (assumed)} & a_f \sin i &= 1,400,000 \text{ km} \\
 \gamma &= +10 \text{ km/sec} & m_b \sin^3 i &= 1.33 \\
 K_b &= 105 \text{ km/sec} & m_f \sin^3 i &= 0.56 \\
 K_f &= 250 \text{ km/sec}
 \end{aligned}$$

Introducing the light-elements determined above, we obtain from the last four expressions the following values:

$$\begin{aligned}
 a_b &= 595,000 \text{ km} & r_b &= (abc)^{1/3} = 876,000 \text{ km} \\
 a_f &= 1,410,000 \text{ km} & r_f &= (abc)^{1/3} = 532,000 \text{ km} \\
 m_b &= 1.36\odot & d_b &= 0.68\odot \\
 m_f &= 0.57\odot & d &= 1.27\odot \\
 a &= a_b + a_f = 2,005,000 \text{ km}
 \end{aligned}$$

Paradoxically, the brighter and the more massive component is eclipsing the fainter one at the primary minimum. In the case of the eclipsing binary, YY Eri, Struve also found that the velocity-curve of the more massive component has a maximum at phase

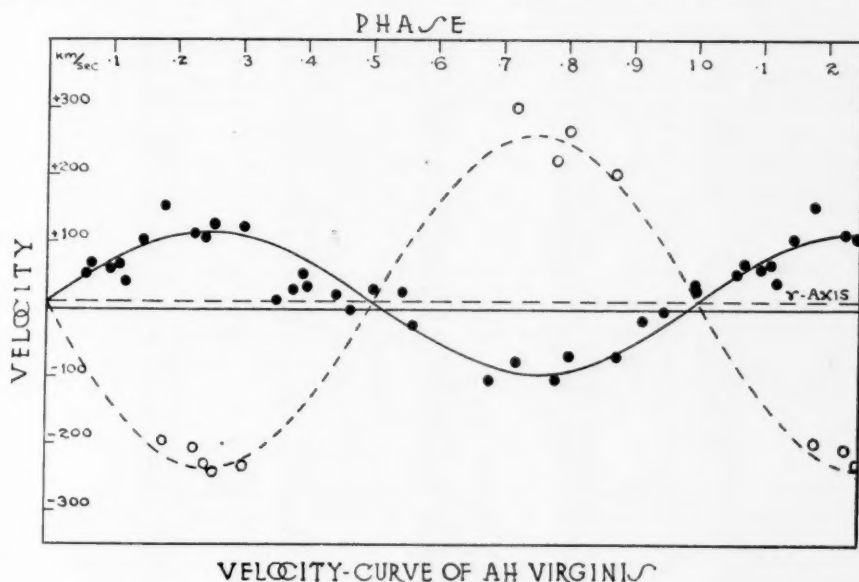


FIG. 2

0.25 P, and not a minimum.⁹ We may therefore conclude that the fainter component has the greater surface brightness.

The spectral lines are broadened on account of the rapid rotation. In Figure 3 the spectrum of α Boo, (which is K0 according to the *Henry Draper Catalogue* and is reclassified as K2 in Morgan, Keenan, and Kellman's *Atlas of Stellar Spectra*) is shown, together with that of AH Vir. The broadening is at once evident upon inspection. On the assumption of spherical shape for the stars, calculation shows that lines due to the brighter component should have a width corresponding to a Doppler shift of 312 km/sec and that the fainter component should have a width corresponding to 190 km/sec. The line-widths in the spectrograms seem to be of this order of magnitude.

The spectral lines become double when the components of AH Vir are at quadrature. The relative intensity of the components varies in a way that cannot be readily explained. The intensities are very similar at phases near 0.25 P, while the difference in intensities is greatest at phase 0.75 P. This variation is most striking for the strong line

⁹ *Ap. J.*, 105, 92, 1947.

λ 4045, which does not have faint lines in its near neighborhood. Perhaps the nearest line is λ 4041 but it is probably too faint and a little too far to the violet to be effective in forming a blend. The phases of the spectrograms and the components due to the brighter and fainter stars are marked in Figure 3. The line λ 4227 also shows this variation in the relative intensity of the components. Several possible mechanisms to account for this phenomenon have been suggested by Struve in his discussion of α Vir.¹⁰ From the observations plotted in Figure 1, the maximum at phase 0.25 P is higher than that at phase 0.75 P. This fact, as well as the difference in intensity of the spectral compo-

TABLE 2
RADIAL VELOCITIES OF TZ BOOTIS

Date	JD 243	Heliocentric Phase	Velocity (Km/Sec)
1947 Mar. 8.....	2253.010	0.732	- 30
10.....	2254.906	.112	- 39
10.....	2254.949	.257	- 75
10.....	2254.993	.405	- 77
12.....	2256.929	.920	- 31
12.....	2256.975	.075	-114
14.....	2258.879	.482	- 73
14.....	2258.915	.603	- 44
14.....	2258.955	.738	- 39
19.....	2263.849	.207	- 76
19.....	2263.923	.456	- 78
19.....	2263.960	.581	- 63
19.....	2263.997	.705	- 57
20.....	2264.866	.629	-104
20.....	2264.902	.751	- 88
20.....	2264.938	.872	- 95
21.....	2265.891	.079	- 91
24.....	2268.837	.993	- 46
24.....	2268.879	.134	- 33
24.....	2268.922	.279	- 29
25.....	2269.827	.324	- 52
25.....	2269.870	.469	- 51
25.....	2269.911	.607	- 21
25.....	2269.952	.745	- 74
26.....	2270.885	.884	- 30
Mar. 26.....	2270.925	.019	+ 17
Apr. 1.....	2276.835	.907	- 78
1.....	2276.915	.177	- 58
Apr. 9.....	2284.850	0.879	- 52

nents, may be explained qualitatively by assuming a brighter advancing hemisphere for the fainter star of the eclipsing system.

When the spectral lines of both components can be observed at the same time, it is obvious that the ratio of the brightnesses of the components does not differ very much from unity. But, using the masses as obtained here and applying the mass-luminosity relation as empirically determined by Kuiper,¹¹ we find that the components should differ by at least 3 mag., or sixteen times, in brightness. This result is in contradiction to the spectrographic and photometric observations. It probably means that the mass-luminosity relation breaks down when dealing with the close components of binaries of the W UMa type.

¹⁰ *Ap. J.*, **80**, 365, 1934.

¹¹ *Ap. J.*, **88**, 489, 1938.

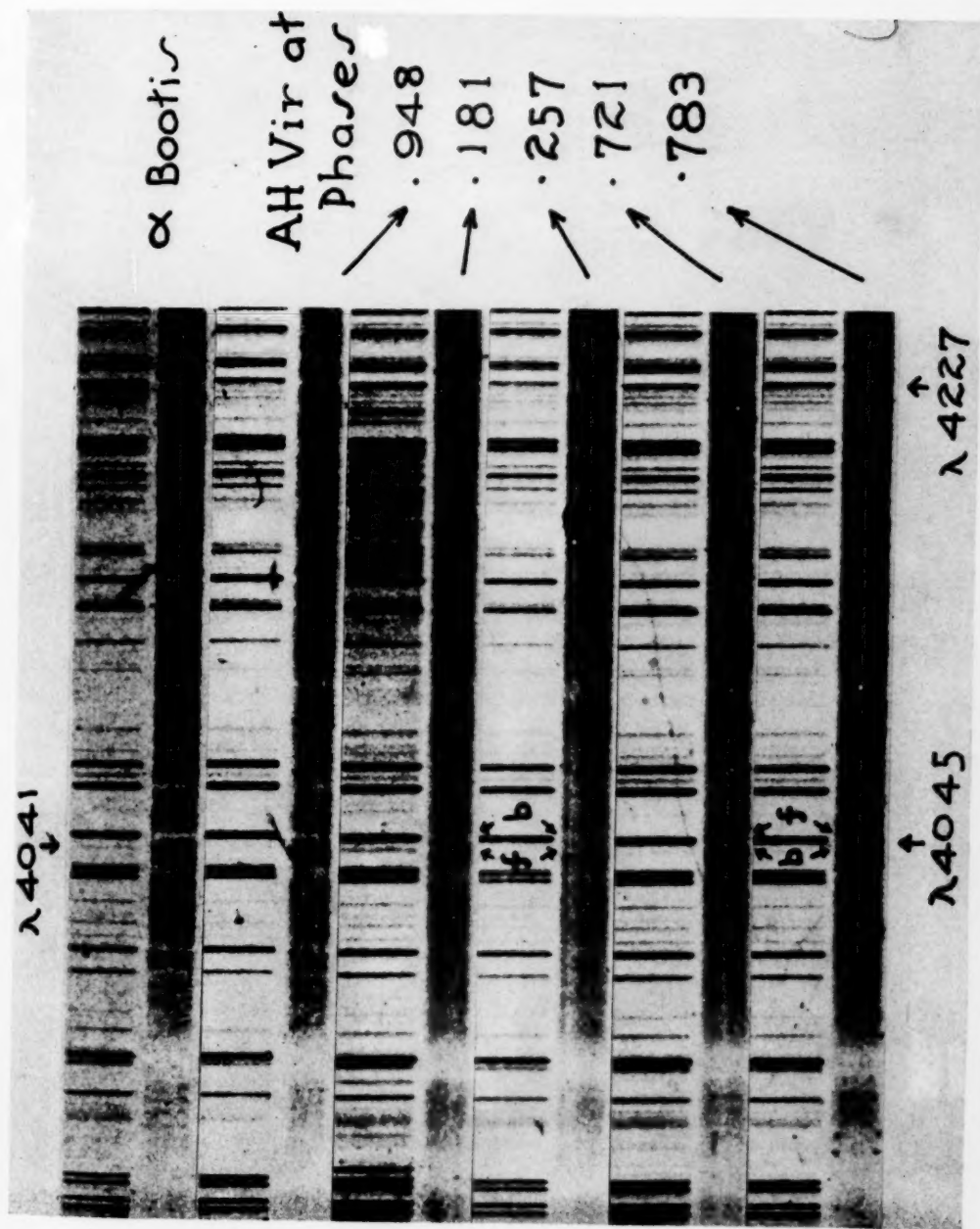
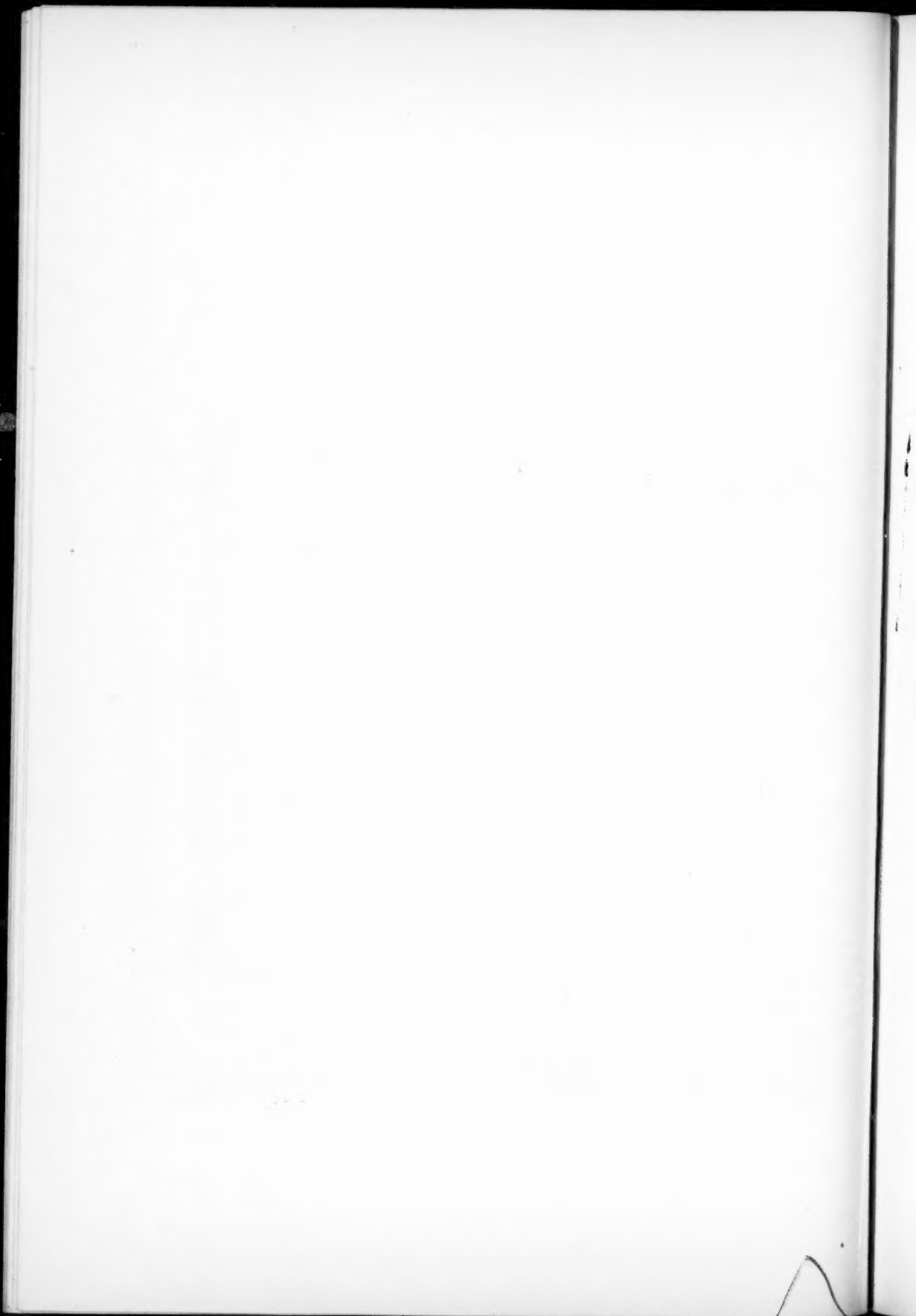


FIG. 3



The star TZ Boo was found to be an eclipsing binary of W UMa type by Guthnick and Prager¹² in 1926. They later obtained a light-curve and gave the following elements:¹³

$$\text{Min.} = 2424609.241 + 0^d29716 \text{ E}$$

$$M_1 = M_2 = 10^m.6$$

$$m_1 = 11^m.1$$

$$m_2 = 11^m.05$$

The observations made near the time of discovery may be represented equally well by $P' = 0^d25865$ and $P = 0^d29716$, where P' and P are related by

$$\frac{2}{P} = \frac{2}{P'} - 1.$$

Observations made in 1927 confirmed the period $P = 0^d29716$. Prager considered it possible that this star might be a variable of the RR Lyr type. The true period would then be only half the value given here.¹⁴

Twenty-nine spectrograms were obtained with the same instrument and the same dispersion as in the case of AH Vir. The spectral type is K. The lines do not appear to become double at quadrature. Table 2 gives the results of radial-velocity determinations.

No correlation could be found between phase and velocity when the data were plotted; and the other period, P' , does not improve the result. An average value of -58 km/sec may perhaps be considered as the velocity of the center of mass of the system.

It is a great pleasure to acknowledge here my indebtedness to Professor Struve for the use of the McDonald and Yerkes equipment, for his suggestion of the problem, and for his constant interest and encouragement during the progress of the work.

¹² *A.N.*, 228, 331, 1926.

¹³ *Kl. Veröff. Berlin-Babelsburg*, No. 4, p. 8, 1927.

¹⁴ *Geschichte und Literatur* (Berlin, 1934).

NOTES

AN EXTENSION OF THE INTERSTELLAR ABSORPTION-CURVE*

In order to extend the previous study¹ of the variation of interstellar absorption with wave length beyond the former limit of $1.03\ \mu$, the infrared radiation of four space-reddened stars has been measured with a lead sulphide photoconductive cell at the focus of the 100-inch telescope. The cell was very generously furnished by R. J. Cashman, of Northwestern University, to whom the writer is indebted for much helpful advice. The

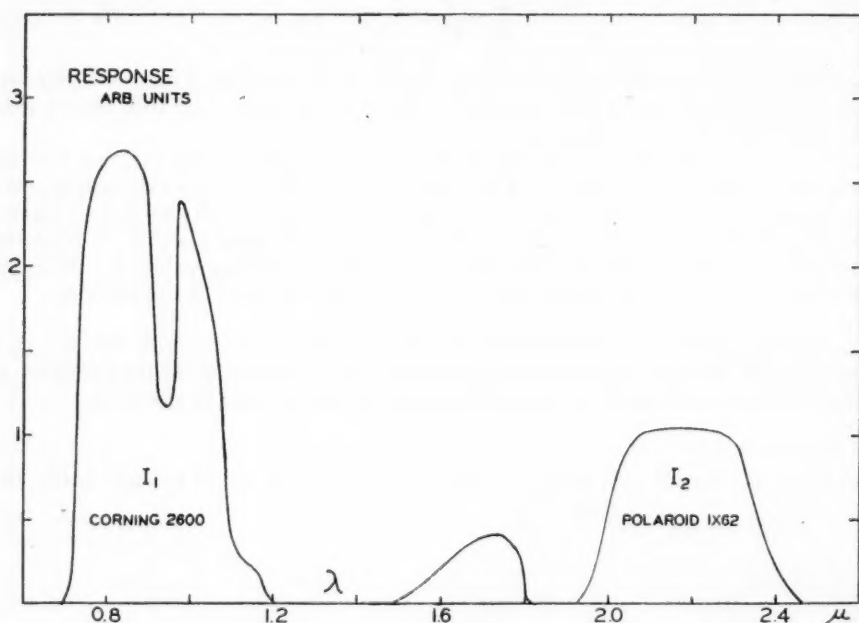


FIG. 1.—Response of the lead sulphide cell through the filters used to an equal-energy source, assuming 5 mm of precipitable water in the atmosphere. The gap in the I_2 band is caused by the Ω -band of water vapor.

amplifier uses a synchronous detector, which, though worked out independently, is quite similar to that described by Palevsky, Swank, and Grenchik.² It has the advantage of strict linearity in the vicinity of the zero and also the advantage of being phase-sensitive, so that sources emitting less infrared than the chopper vanes give a negative response. Details will be published elsewhere.

Suitable filters isolated two spectral regions, as shown in Figure 1. The computed effective wave lengths are $0.90\ \mu$ ($1.11\ \mu^{-1}$) and $2.1\ \mu$ ($0.48\ \mu^{-1}$); these are designated I_1 and I_2 , respectively. The isolation of the I_2 band was made possible by an organic-dye

* Report based on observations made at the Mount Wilson Observatory, August, 1947.

¹ Stebbins and Whitford, *Ap. J.*, **98**, 20, 1943; **102**, 318, 1945; *Mt. W. Contr.*, Nos. 680 and 712.

² *Rev. Sci. Inst.*, **18**, 298, 1947.

film,³ furnished through the courtesy of E. R. Blout, of the Polaroid Corporation. The effective wave length of the bands depends not only on cell response and filter transmission (both measured by the writer) but, in addition, on the water-vapor bands of the atmosphere. These play a large role in defining the edges of the I_2 band. Fortunately, as first pointed out by C. L. Pekeris,⁴ there is a curve-of-growth effect which makes the total absorption of these bands not very sensitive to water mass. A layer of 5 mm of precipitable water was adopted as the average of the conditions on the nights in question. Since the measures were differential between stars not too far apart in the sky, variations in water absorption will tend to cancel out if the effective wave length is not changed. Calculations with various assumed amounts of water vapor show that such is indeed the case.

The six stars observed are listed in Table 1. The new measures with lead sulphide give for each star the relative intensity through the two filters, expressed as a color index,

TABLE 1
STARS OBSERVED WITH LEAD SULPHIDE

HD	Name	Mag.	Spectrum	$V-I$
24398.....	ζ Per	2.91	cB1	-1 ^m 57
24760.....	ϵ Per	2.96	B2	-2.47
198478.....	55 Cyg	4.89	cB2e	-0.66
206165.....	9 Cep	4.78	cB2	-1.06
20902.....	α Per	1.90	cF4	-0.49
195593.....	44 Cyg	6.30	cF5	+1.06

TABLE 2
REDUCTION OF LEAD SULPHIDE OBSERVATIONS

Stars Compared	$(V-I)$	Observed $\Delta(I_1-I_2)$	Average Deviations	Interpo- lated I_1	I_2	Reduced I_2	Devia- tion from λ^{-1}
ζ Per— ϵ Per.	0 ^m 90	+0.23	$\pm 0^m00 \pm 0^m05$	-0 ^m 43	-0.66	-0.14	+0.21
9 Cep— ϵ Per.	1.43	+ .34:	$\pm .13 \pm .05$	- .69	-1.03	- .12	+ .23
55 Cyg— ϵ Per.	1.83	+ .71	$\pm .00 \pm .05$	- .89	-1.60	- .28	+ .07
44 Cyg— α Per.	1.55	+0.62	$\pm 0.02 \pm 0.02$	-0.73	-1.35	-0.29	+0.06

$I_1 - I_2$. Then reddened and unreddened stars are compared, to get an infrared color difference, $\Delta(I_1 - I_2)$. The observed values are shown in the third column of Table 2. Each is the mean of observations on two nights, except for 9 Cephei, for which three nights were combined. The fourth column gives the average deviations for the reddened and the unreddened stars, respectively. In order to use these data to extend the interstellar reddening-curve, they must be fitted onto the existing difference-curve defined for each pair of stars by the six-color observations.¹ This is done by a linear interpolation between the R and I points, and the results are shown in the fifth column. The I_1 point at $1.11\mu^{-1}$ comes at just a third of the distance from $I(0.97\mu^{-1})$ to $R(1.37\mu^{-1})$. Then the infrared color difference, $\Delta(I_1 - I_2)$ defines a new point, I_2 , at $0.48\mu^{-1}$ (sixth col.) about halfway between the previous limit and $\lambda^{-1} = 0$ (infinite wave length). For inter-comparison the results for the four pairs of stars are reduced in the seventh column to

³ Blout, Amon, Shepherd, Thomas, West, and Land, *J. Opt. Sci. Amer.*, **36**, 40, 1946; see esp. Fig. 8.

⁴ *Ap. J.*, **79**, 441, 1934.

a common basis of a color excess of $(V - I) = 1^m00$.⁵ The eighth column gives the departure of the reduced I_2 points from a straight-line λ^{-1} law fitted at the V and I points.

There is room for an extension of the absorption-curve to the ultraviolet between the U point at 0.353μ ($2.83 \mu^{-1}$) and the ozone limit at about 0.295μ . Dr. Stebbins has very kindly permitted the inclusion in this report of an observation of the pair ζ and ϵ Persei taken by him in 1941, with the six-color photometer and a silver filter. The measured transmission agreed with that found by E. Pettit⁶ for this type of film in showing a sharp maximum at 0.320μ ($3.12 \mu^{-1}$); this was adopted as the effective wave length. Table 3 shows the complete absorption-curve for this pair of stars reduced to the baseline $V - I = 1^m00$. In it are combined the six-color data (revised very slightly, following additional unpublished measures), the 1941 measures through the silver filter, and the new infrared result at 2.1μ .

The mean curve for all four pairs of stars is shown in Figure 2. While the scatter of the I_2 points is considerable, all stars show an S-shaped curve of the type predicted theoretically by Oort and van de Hulst.⁷ The mean of the I_2 points is $0^m14 \pm 0.04$ (p.e.) fainter than would be predicted from a strict λ^{-1} relation passing through the V and I points. A point 0^m22 below the straight line would lie on the theoretical curve.

TABLE 3
INTERSTELLAR ABSORPTION FROM ζ AND ϵ PERSEI

Filter	S	U	V	B	G	R	I	I_2
$1/\lambda (\mu^{-1})$	3.12	2.83	2.37	2.05	1.75	1.39	0.97	0.48
Δ mag.	+1.30	1.18	1.00	0.81	0.64	0.35	0.00	-0.14

The results here reported are preliminary and need to be strengthened by further observations. In all the measurements at 2.1μ , except those of α Persei and ζ Persei, the signal-to-noise ratio was uncomfortably small. It is hoped that improvements in the lead sulphide cell will permit higher accuracy and will bring into the range of observation several B stars with about twice the color excess of those thus far attempted. The B stars are, of course, intrinsically very weak in the infrared. Possibly, additional favorable cases of reddened stars of later type can be found, but measures on a few calibration stars indicate that the cool supergiants seem to be ruled out by an intrinsic weakness in the infrared, which is quite sensitive to spectral type.

The present observations, while of limited accuracy, show a trend which warrants the following conclusions:

1. The type of size-distribution function postulated by Oort and van de Hulst, showing a rapid decline in the number of particles with radius larger than a certain critical value, is confirmed.
2. As pointed out by J. L. Greenstein,⁸ only dielectric particles can show the transition toward Rayleigh (λ^{-4}) scattering indicated by the reverse curvature in the infrared. The observations argue, then, for dielectric rather than for metallic particles.
3. The total absorption of reddened stars in the visible and photographic regions has

⁵ The I point is arbitrarily assigned the value 0^m00 , and V point $+1^m00$. In the previous discussion (cf. n. 1) of reddened B stars a reduced baseline, $U - I = 1^m00$, was used. Greenstein (n. 8) re-examined the data with a baseline $V - I = 1^m00$, in order to eliminate any doubts about the effect of Balmer absorption on the U point but found the conclusions unchanged. The $V - I$ baseline is adopted here to permit inclusion of reddened stars of later type in which Balmer absorption is stronger and more variable.

⁶ *Ap. J.*, **66**, 43, 1927; *Mt. W. Contr.*, No. 336.

⁷ *B.A.N.*, **10**, 187, 1946.

⁸ *Ap. J.*, **104**, 403, 1946.

a value compatible with stellar-density arguments rather than the inadmissibly high value derived⁸ by extrapolation of the previously existing curve. The wave lengths of the C_1 filters used in the original survey⁹ of B stars are shown in Figure 2. A straight line through these points cuts the vertical axis, $\lambda^{-1} = 0$, close to the probable extrapolated intersection of the observed curve. The ratios between total absorption and color excess, $A_{pg}/E_1 = 9$ and $A_{vis}/E_1 = 7$, previously derived⁹ on the assumption of a λ^{-1} law, therefore appear to be fairly close to the correct values, after all. In view of the remaining uncertainties, they may be allowed to stand for the present.

4. A reverse curvature in the infrared makes the residual absorption at 2μ an even smaller fraction of the total absorption in the visible or photographic regions than that

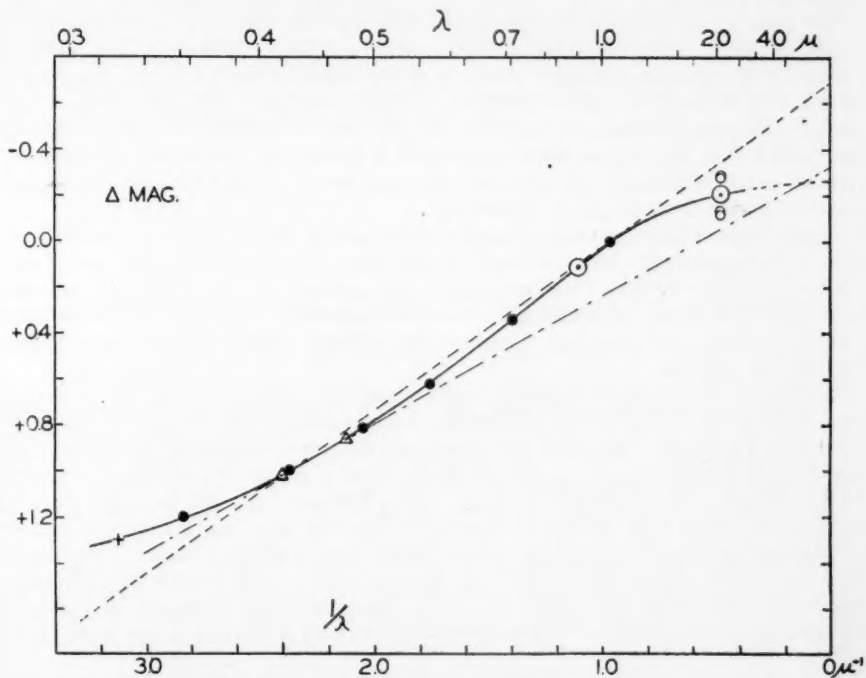


FIG. 2.—Mean interstellar absorption-curve from four pairs of stars, reduced to $V - I = 1^m00$. Filled circles are six-color observations; small open circles are individual lead sulphide observations, with large open circles showing the mean; and the cross is the silver-filter observation on one pair only. The triangles show the baseline of the C_1 colors.

predicted by a λ^{-1} law.¹⁰ The hope that infrared surveys may show objects previously hidden by the dust clouds is therefore strengthened.

Grateful acknowledgment is made to Dr. I. S. Bowen and the staff of the Mount Wilson Observatory for the facilities extended. This research was supported in part by the Research Committee of the Graduate School, from funds supplied by the Wisconsin Alumni Research Foundation.

A. E. WHITFORD

WASHBURN OBSERVATORY
UNIVERSITY OF WISCONSIN
November 1947

⁹ Stebbins, Huffer, and Whitford, *Ap. J.*, **90**, 209, 1939; **91**, 20, 1940; *Mt. W. Contr.*, Nos. 617 and 621.

¹⁰ Stebbins and Whitford, *Ap. J.*, **106**, 235, 1947; *Mt. W. Contr.*, No. 734.

NOVAE AND PLANETARY NEBULAE

The close correspondence between the spectra of planetary nebulae and the spectra of novae in the nebular stage, as well as the apparent similarity of planetary nebulae to the shells expanding about novae during a certain interval after the outburst, have led to the suggestion that planetary nebulae are the final products of novae outbursts. Since such an assumption has been accepted by some authors as an established basis for theoretical speculations, it seems necessary to emphasize that the merely descriptive similarity is deceptive. Actually, two strong arguments contradict the assumption of an evolutionary connection between the outburst of an ordinary nova and the formation of a planetary nebula.

1. The velocity of expansion of planetary nebulae is of the order of 20 km/sec with moderate dispersion, the maximum velocity observed being 55 km/sec for NGC 2392. The velocity of expansion of nova shells is of the order of 1000 km/sec, ranging from about 300 to 1700 km/sec. Since velocities in this range are observable even with low dispersion, it is certain that such velocities do not occur in planetary nebulae. The Crab nebula, which has sometimes been considered a planetary, shows a high velocity of expansion; but it is actually the remnant of a supernova, differing markedly in appearance and behavior from a typical planetary.

Different lines in the spectrum of a planetary nebula show different velocities of expansion. The highest velocities are found for the lines of lowest ionization, which appear on the outside of the nebula. This contradicts the assumption that planetary nebulae are nova shells slowed down by interaction with the interstellar medium. The separation of the velocity ranges for novae and for planetary nebulae creates an additional difficulty for such an assumption.

2. The linear diameters of typical bright planetary nebulae are of the order of 0.1 parsecs. The electron densities, and therefore the densities of protons, are of the order of $5 \cdot 10^{-3} \text{ cm}^{-3}$. The mass contained in a planetary nebula exclusive of the stellar nucleus is thus of the order of 0.1 solar masses, while the mass of most nova shells is of the order of 10^{-4} solar masses. This difference in mass is very obvious from the fact that most nova shells fade out when they attain an apparent diameter of a few seconds of arc, while many planetaries have apparent diameters larger than a minute of arc. The difference in velocity, together with the difference in mass, is responsible for the very obvious difference in lifetime; with few exceptions, nova shells fade out in about 20 years, while planetary nebulae are apparently permanent objects with a lifetime of the order of 30,000 years.

Although the ejection of a planetary nebula and the outburst of a nova are distinctly different phenomena, they belong, nevertheless, in the same class of events, the kinetic energy of a planetary nebula being of the same order as that of a nova shell. But, beyond the fact that both processes are the results of instabilities of possibly similar orders of magnitude, no direct relationship seems to exist.

R. MINKOWSKI

MOUNT WILSON OBSERVATORY
December 1947

THE PARALLAX OF SS CYGNI

A series of parallax plates of SS Cygni was started by J. Titus in 1940 with the 40-inch Yerkes refractor. On each observing night the star was reduced to its minimum magnitude (12) by means of a sector with a variable opening. The series was completed in July, 1947. Twenty stars in the field were measured for differential proper motion over the seven years' interval. From these, three comparison stars, showing small peculiar motions and with magnitudes between 11.5 and 12.0, were chosen.

The relative parallax of SS Cygni was found to be $+0''.030 \pm 0''.007$ (p.e.), which gives an absolute parallax of $0''.032$. The value for the proper motion was $0''.115 \pm 0''.002$ (p.e.), with a position angle of 69° .

In order to check on possible systematic errors in the derived parallax, an 11.5-mag. star, $100''$ preceding and $67''$ south of SS Cygni, was measured simultaneously. The parallax of this star relative to the same comparison stars was found to be $-0''.002 \pm 0''.006$ (p.e.).

The parallax of SS Cygni determined here contradicts the value of $-0''.012 \pm 0''.008$ (p.e.) derived by van Maanen¹ with the 60-inch Mount Wilson reflector, but it is in close agreement with a parallax of $0''.038$ suggested by Parenago and Kukarkin² from a discussion of the proper motion.

The present parallax gives an absolute magnitude for SS Cygni of 9.5 at minimum or normal light, with periodic increases to an absolute magnitude of 5.7 at maximum. Since the spectrum has been classified as dG5 or later at minimum by C. T. Elvey and H. W. Babcock from the distribution of intensity in the continuous spectrum,³ the star is several magnitudes below the main sequence.

K. AA. STRAND

YERKES OBSERVATORY
DEARBORN OBSERVATORY
December 5, 1947

THE CLASSIFICATION OF THE "METALLIC-LINE" STARS

The group of A stars whose spectra indicate conspicuous differences from the normal are difficult to describe and, unless the descriptions and distinctions are made with the greatest care, there is danger of not separating the various kinds of peculiarities. This is particularly true in the case of the so-called "metallic-line" stars, and it is important to define this class as precisely as possible. Work leading toward a catalogue of metallic-line stars is now in progress at Yerkes, and the following description of the class and list of standard members is intended to aid in the segregation of this interesting group.

The criteria distinguishing the metallic-line stars are: (1) The K line is considerably weaker than would be expected for the average metallic-line type. (2) There is no possibility of explaining the spectrum in terms of one or two normal stars; the metallic lines near K indicate a type as late as do the features farther toward the red. In the spectroscopic binaries in the group it has been found that the K line and other lines have the same velocity. (3) The metallic-line stars show no obvious similarity to recognized "shell-spectrum" types and are readily distinguishable from the "silicon", "strontium", "europium" groups.¹ In these latter groups the lines of one or several of a small number of elements (*Mn* II, *Si* II, *Eu* II, *Cr* II, *Sr* II, and an unidentified group of lines) are strikingly strong compared with the spectra of normal stars. The K line also tends to be weak in some of the "manganese," "silicon," and "europium" stars.

Table 1 lists data concerning 13 of the bright metallic-line stars which have been in use as standards. Owing to the spurious absolute-magnitude effect in these spectra and the weakness of *Ca* I 4226, some of the later metallic-line stars match either ζ Leo (F0 II-III) or α CMi (F5 IV) almost equally well; this is indicated in the table by F5 IV = F0 II-III. A similar effect is also present for some of the other stars in the table.

¹ *Ap. J.*, **87**, 424, 1938.

² *Veränderliche Sterne*, **4**, 249, 1934.

³ *Ap. J.*, **97**, 412, 1943.

¹ W. W. Morgan, *Ap. J.*, **73**, 104, 1931; **74**, 24, 1931; **75**, 46, 1932; **77**, 77, 330, 1933; Morgan, Keenan, and Kellman, *An Atlas of Stellar Spectra* (Chicago, 1943), pp. 17-20; and Armin J. Deutsch, *Ap. J.*, **105**, 283, 1947.

From the objects listed, the following facts are evident: (1) The K-line type ranges from A1 to A6 on the Yerkes *Atlas* system. (2) The hydrogen-line type ranges from A5 to F2, with some correlation between this and the K-line type. (3) The metallic-line type ranges from A5 to F6. No strong correlation exists between this type and the K-line type; that which is present is partly due to the method of selection. (4) The absolute magnitudes of the eight stars in the table for which accurate values are available range from +2.0 to +3.0; the absolute magnitudes of the cluster members are from Smart's papers on the Hyades and Ursa Major clusters.² (5) Six of the thirteen stars are spectroscopic binaries with orbits, and others may be binary in nature. The percentage of binaries is

TABLE 1
STANDARD METALLIC-LINE STARS

Star	α (1900)	δ (1900)	m	Ca II K	H- Lines	Metallic Lines	M_{vis}	Pe- riod	K (Km/Sec)
α Gem B.....	7 ^h 28 ^m 2	+32° 6'	2.85	A1	A5	A5	2.2	2 ^d 9	32
63 Tau.....	4 17.7	+16 33	5.68	A1	F0	F5 IV = F0 II-III	2.8	8.4	38
ζ UMa (ft).....	13 19.9	+55 27	3.96	A2	A8	A7	2.0		
HR 1519 (Tau)....	4 40.5	+11 31	5.43	A2	A7	F0 IV	2.2		
16 Ori.....	5 3.8	+9 42	5.42	A2	A9	F2 IV	2.6		
15 UMa.....	9 1.8	+52 0	4.54	A2	F0	F5 IV = F0 II-III			
ζ Lyr A.....	18 41.3	+37 30	4.29	A4	A7	F0		4.3	51
60 Tau.....	4 16.4	+13 50	5.76	A5	F0	F2	3.0		46*
HR 1403 (Tau)...	4 22.1	+21 24	5.74	A5	F0	F2	2.7		
HR 4646.....	12 7.5	+78 10	5.12	A5	F2	F5 IV		1.3	63
τ UMa.....	9 2.7	+63 55	4.74	A5	F0	F6 II			
δ Cap.....	21 41.5	-16 35	2.98	A6	F2	F5 IV = F0 II-III	2.5	1.0	66
δ^2 Vir.....	12 40.6	+8 13	(5.6)†	A6	F2	F6 IV		(38)‡	41

* Observed range in velocity.

† Magnitude corrected 0.4 mag. for secondary.

‡ Period may be near 1 day?

TABLE 2

Star	C_1	K-Line Type	Normal C_1	E_1	H-Line Type	Normal C_1	E_1	Metallic- Line Type	Normal C_1	E_1
ζ UMa (ft).....	+0.06	A2	-0.06	+0.12	A8	+0.08	-0.02	A7	+0.06	0.00
15 UMa.....	+ .12	A2	- .06	+ .18	F0	+ .09	+ .03	F5 IV	+ .18	- .06
HR 4646.....	+ .14	A5	+ .03	+ .11	F2	+ .13	+ .01	F5 IV	+ .18	- .04
τ UMa.....	+0.16	A5	+0.03	+0.13	F0	+0.09	+0.07	F6 II	+0.23	-0.07

very high in the group, inasmuch as, for all stars brighter than 5.0 mag., both in the classes A0-F0 and F0-F5, only about one star in ten has a spectroscopic orbit.

Colors on the C_1 scale for four of the metallic-line stars listed in Table 1 are given in Table 2, together with the spectral classification according to the K line of Ca II, the hydrogen lines, and the metallic lines, the normal color, and the apparent color excess. The colors were obtained by Stebbins, Huffer, and Whitford and were reduced to the C_1 scale by Stebbins.

From Table 2 it is clear that the K-line types do not indicate the relative color temperatures of the stars but introduce a systematic spurious reddening of +0.14 mag.

² *M.N.*, 99, 168, 441, 1938-1939.

There is apparently little choice between the type from the metallic lines and that from the hydrogen lines; the indeterminateness in the metallic-line type, depending on the luminosity of the comparison star, complicates the problem of assigning normal colors for these objects. It may be that a similarity to earlier-type giant stars is indicated by the colors as well as by the general line spectrum, in spite of the low absolute magnitudes of the metallic-line group; it is definite, however, that the metallic-line stars behave like F stars as far as their colors are concerned.

The six-color observations of Stebbins and Whitford for the two metallic-line stars, NPS 4 and ζ Lyr A, were discussed by Morgan and Bidelman.³ The range between the K-line types and metallic-line types for these two stars is not so extreme as for some of the objects listed in Table 1.

Since the intrinsic colors correspond to class F and the absolute magnitudes are similar to main-sequence objects of early F type, the standard metallic-line stars are of about the same size as the main-sequence F stars. The rotational velocities of the metallic-line group are lower than the average for A stars; they may be fairly normal for classes F2-F5.

NANCY G. ROMAN
W. W. MORGAN
OLIN J. EGGEN

YERKES AND WASHBURN OBSERVATORIES
November 1, 1947

THE HIGHER MEMBERS OF THE ($2^3P^0-n^3D$) SERIES OF $He\ I$ IN THE SPECTRUM OF 55 CYGNI

The higher members of the diffuse triplets of $He\ I$ in the B3 supergiant, 55 Cygni, were previously measured as far as $\lambda\ 3465.89$ ($2^3P^0-17^3D$).¹ A new spectrogram, of better quality, was obtained on Process emulsion, with the Cassegrain quartz spectrograph of the McDonald Observatory, giving a linear dispersion of 27 Å/mm at $\lambda\ 3500$.

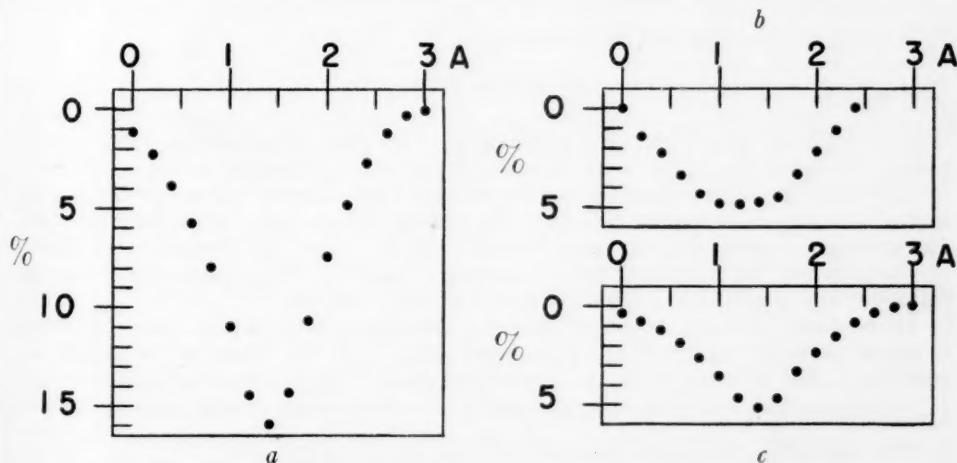


FIG. 1.—Profiles of $He\ I$ lines in 55 Cygni

The date was July 12, 1947, 8^h37^m U.T. On this spectrogram the $He\ I$ series can be seen as far as $\lambda\ 3450.22$ ($2^3P^0-21^3D$), beyond which the higher members are blended with

³ *Ap. J.*, 104, 245, 1946.

¹ *Ap. J.*, 90, 721, 1939.

the strong line $He\ I\ (2^1S-6^1P^0)\ 3447.59.^2$ Since the higher members of the diffuse $He\ I$ series must become hydrogenic in character and since the total intensities of these lines are moderate, the question arises as to whether the effect of Stark broadening (or of collisional broadening) might not be noticeable for these higher members. A suspicion that this might be the case has already been mentioned in a previous article.³ The highest members of the $He\ I$ series which are strong enough to be measured and which are not complicated by blends or by overlapping of wings are Nos. 15 and 16. The average profile of these two lines is shown in Figure I, *b*. For comparison, Figure I, *a*, gives the average profiles of Nos. 8 and 9.⁴ Finally, in Figure I, *c*, we have compressed the profile of Nos. 8 and 9 to give the same central depths as Figure I, *b*. We see that the two profiles are not alike: that of the higher members is less peaked than that of the lower members. This suggests that broadening by electrical fields is not entirely negligible, even for an early-type supergiant. Unsöld⁵ has shown that for a hydrogenic atom the absorption coefficient is approximately

$$a = \text{const.} \int \frac{\Delta\lambda_0^{3/2}}{\Delta\lambda^{5/2}} e^{-(\Delta\lambda_0/\Delta\lambda)^{3/2}}.$$

In the extreme wings, where $\Delta\lambda \gg \Delta\lambda_0$, the absorption coefficient is independent of the principal quantum number n , because $f \sim 1/n^3$ and $\Delta\lambda_0 \sim n^2$. Hence the profiles become flatter as we go to higher values of n , but they do not become appreciably broader.

O. STRUVE
H. CHUN

YERKES OBSERVATORY
December 13, 1947

ASTROPHYSICAL EVIDENCE FOR THE PROBABILITY OF A NUCLEAR REACTION

It was generally supposed that the reaction



was not allowed, on account of the difficulty which seemed to arise for the theory of energy production by white dwarfs. The discussion of β reactions by Konopinsky¹ would indicate that the reaction is an allowed one, though Oppenheimer² had suggested a rather improbable way to escape the difficulty. The present author had also³ adopted this view. Nevertheless, it seems that no astrophysical evidence has yet been found for or against this assumption. We shall show that, if we suppose reaction (1) to be allowed, it does not introduce any contradiction with the theory of white dwarfs.

I have shown³ that on account of the high gravitational field of white dwarfs, hydrogen is almost perfectly separated from the other elements and is "floating" in a shell surrounding a core of heavy elements. The energy production can occur in only two ways: (1) in the mixed layer, where hydrogen and heavy elements are mixed, the reaction with

² The same number of lines was measured in P Cygni (*Ap. J.*, **90**, 735, 1939).

³ Unsöld and Struve, *Ap. J.*, **91**, 366, 1940.

⁴ These profiles have not been corrected for instrumental broadening, but the correction is comparatively small.

⁵ *Zs. f. Phys.*, **59**, 366, 1929.

² *Phys. Rev.*, **51**, 908, 1941.

¹ *Rev. Mod. Phys.*, **15**, 209, 1943.

³ *Ann. d'ap.*, **8**, 143, 1945.

carbon and nitrogen, or (2) reaction (1) in the hydrogen shell. The energy production by reaction (1) was given, per gram, by Bethe and Critchfield⁴ and is

$$\epsilon = 410 \rho c_H^2 \tau^2 e^{-\tau}, \quad (2)$$

with

$$\tau = \frac{33.8}{T^{1/3}} \quad (T \text{ in million degrees}). \quad (3)$$

On account of the very rapid decrease of the energy production with the decrease of temperature, we may suppose a radiative equilibrium with shell source even when we consider reaction (1). When the hydrogen layer is very thin, this shell is a very thin one and is at the surface of the mixed layer.

We are considering very thin hydrogen layers, their maximum thickness being given by the following relation⁵

$$\frac{\Delta R}{R} \leq 10^{1.35} R L^{2/7} M^{-9/7}, \quad (4)$$

where R , L , and M are given in solar units. This condition implies that degeneracy appears inside the mixed layer.

In this hydrogen layer the temperature is given as a function of the depth, by

$$T = 10^{6.43} \frac{M}{R} \frac{\Delta R}{R}, \quad (5)$$

and the density by

$$\rho = 10^{0.116} R^{-13/4} L^{-1/2} M^{15/4} \left(\frac{\Delta R}{R} \right)^{13/4}. \quad (6)$$

From equations (2), (3), (5), and (6) it is possible to obtain the energy production due to reaction (1). We get the following result:

$$L = 10^{2.91} R^{-17/12} M^{41/12} \left(\frac{\Delta R}{R} \right)^{41/12} e^{-12(R/M)^{1/3} (\Delta R/R)^{-1/3}}. \quad (7)$$

If we try to determine from this equation the thickness, $\Delta R/R$, of the hydrogen layer for different white dwarfs, we must obtain a result in agreement with equation (4), and the energy production by the carbon cycle must be smaller.

In the case of α_2 Eridani B, no special difficulty arises. We get the following results:

$$\frac{\Delta R}{R} = 0.125.$$

Limiting value of $\Delta R/R$: 0.255. Energy production by carbon cycle to energy production of the star:

$$\frac{L_c}{L^*} = 10^{-4.40}.$$

It does not seem that any difficulty shows up for other stars, especially for the difficult one, van Maanen 2. It would therefore seem that no astrophysical difficulties arise if reaction (1) were an allowed one.

⁴ *Phys. Rev.* **54**, 248, 862 (L), 1938.

⁵ Schatzman, *op. cit.*, eq. (187).

E. SCHATZMAN

INSTITUT D'ASTROPHYSIQUE
PARIS, FRANCE
December 1947

REVIEWS

Time, Knowledge, and the Nebulae. By MARTIN JOHNSON. New York: Dover Press, 1947. Pp. 189. \$2.75.

The purpose of this little book is to give a survey of the way in which the concept of *time* appears in various current philosophic and scientific theories and, in particular, its position in the theories of the "expanding universe." It would be beyond the capacities of the reviewer to attempt a critical evaluation or summary of the author's treatment of the various philosophical speculations about the nature of time; and it must suffice to say that he has found it to be a very interesting, if often unconvincing, exposition of a wide variety of viewpoints. This unconvincing characteristic is not to be laid to the charge of the author, of course, but mostly to the scientist's natural tendency to agree with the dictum of Lord Kelvin that we begin to understand the physical world only as we are able to put our ideas about it into quantitative mathematical form. Nevertheless, since even the most strictly scientific theories are grounded in intuitive ideas, it is always of interest to see other viewpoints, even when one is not led to their adoption.

On the more strictly scientific side, which is assumed to be of the most immediate interest to the readers of this *Journal*, the book will be primarily of value as a popularized statement of the theory which has been proposed in recent years by Professor E. A. Milne and which has been developed at length in his book, *Relativity, Gravitation, and World-Structure* (Oxford University Press, 1935), as well as in more recent articles, which have appeared, for the most part, in the *Proceedings of the Royal Society* (London). As such, however, it seems to the reviewer to be distinctly unsatisfactory, since the discussion is limited almost entirely to Milne's own point of view and quite ignores the criticisms which have been raised by others. It is certainly true that Milne's theory has been of considerable value in stimulating a reconsideration of kinematical problems in connection with relativistic theories; but, in the form in which Milne has developed it, there are substantial difficulties which mitigate against its acceptance. The interested reader will find a more detailed account of the matter in the papers by H. P. Robertson (*Ap. J.*, **82**, 284, 1935; **83**, 187, 257, 1936). From the point of view of the physicist, the troubles which arise have their origins firmly imbedded in the differing natures of the electromagnetic field and of mechanical effects as time-measuring devices. While it would have been impracticable for the author to have given a full discussion of these matters in his book, it is difficult to forgive him for ignoring them so completely.

E. L. HILL

Department of Physics
University of Minnesota

John Couch Adams and the Discovery of Neptune. By SIR HAROLD SPENCER JONES. Cambridge: Cambridge University Press, 1947. Pp. 43. \$0.75.

The hundredth anniversary of the discovery of Neptune has brought renewed interest in the facts centering round this very remarkable episode in the history of science. Two attempts have recently been made to "sift and piece together the available evidence disinterestedly and dispassionately." One of these is the short pamphlet under review by the Astronomer Royal, Sir Harold Spencer Jones; and the other is by Professor W. M. Smart, published by the Royal Astronomical Society in its "Occasional Notes" for August, 1947 (Vol. 2, No. 11). Of these two studies, the one by Smart appears to the reviewer as distinctly the more satisfactory. All the essential facts mentioned by Sir Harold in his pamphlet are also to be found in Smart's account. But certain aspects of Airy's conduct, not particularly commendable in the Astronomer Royal, are omitted in Sir Harold's account: for example, it is not indicated that Airy's famous "Account of Some Circumstances Historically Connected with the Discovery of the Planet Exterior to Uranus" at the meeting of the Royal Astronomical Society on November 13, 1846, does less than full justice to Adams' share in the discovery, and it is not also mentioned that Airy wrote to Le Verrier "as the real predictor of the planet's place." However, as Smart justly concludes, "for all times the names of Adams and Le Verrier will be linked indissolubly with Neptune and each will be accorded an equal share of fame" in one of the most remarkable achievements of the human mind.

S. CHANDRASEKHAR

Yerkes Observatory